FREE-SPACE OPTICAL COMMUNICATION SYSTEMS USING ON-OFF KEYING IN ATMOSPHERIC TURBULENCE

by

Luanxia Yang

B.Eng., Beijing University of Chemical Technology, P. R. China, 2009
M.Sc., The University of Edinburgh, United Kingdom, 2010

A THESIS SUBMITTED IN PARTIAL FULFILLMENT OF
THE REQUIREMENTS FOR THE DEGREE OF

DOCTOR OF PHILOSOPHY

in

The College of Graduate Studies

(Electrical Engineering)

THE UNIVERSITY OF BRITISH COLUMBIA

(Okanagan)

July 2015

Abstract

In this thesis, we focus on the bit-error rate (BER) performance improvements for free-space optical (FSO) communication links operating over atmospheric turbulence channels using on-off keying (OOK). Laser beams employed in these links are subject to scintillation, during their propagation through atmospheric channels, and this can lead to significant BER performance degradation. Such systems can suffer from irreducible error floors that result from the use of demodulation with fixed and unoptimized detection thresholds. The resulting error floors are analyzed for the general case of low and high state offsets (i.e., nonzero extinction ratios). To improve the BER performance, there are three techniques developed in this thesis.

The first technique employs electrical signal-to-noise ratio (SNR) optimized detection. The system uses the electrical SNRs to implement adaptive detection thresholds and eliminate the error floors. The system can accommodate operation with nonzero extinction ratios, as it uses the method of moments and maximum likelihood estimation techniques to estimate the low and high state offsets and electrical SNR.

The second technique employs source information transformation. Using source information transformation can also eliminate error floors, and it can detect the OOK signal without knowledge of the instantaneous channel state information and probability density function of the turbulence model. It is shown that source information transformation can achieve comparable performance to the idealized adaptive detection system, with greatly reduced implementation complexity.

The third technique employs convolutional code. Using convolutional code can mitigate the effects of turbulence induced fading. The BER performance is analyzed for FSO systems using convolutional code and OOK. Through our analysis, it is shown that using convolutional code can improve the BER performance of an FSO system significantly.

Preface

This thesis is based on [J1-J2, SJ1, SJ2]. My supervisors, Dr. Julian Cheng and Dr. Jonathan F. Holzman, co-authored all of the publications and supervised all of my research work. I am responsible for all theories derived, as well as the manuscript preparation and revisions.

Refereed Journal Publications

J1. **L. Yang**, J. Cheng, and J. F. Holzman, "Performance of convolutional coded subcarrier intensity modulation over Gamma-Gamma turbulence channels," *IEEE Communications Letters*, vol. 17, pp. 2332-2335, December 2012.

J2. **L. Yang**, J. Cheng, and J. F. Holzman, "Maximum likelihood estimation of the lognormal-Rician FSO channel model," *IEEE Photonics Technology Letters*, Accepted for publication in *IEEE Photonics Technology Letters*, 2015.

Refereed Conference Publications

C1. **L. Yang**, J. Cheng, and J. F. Holzman,"Optical communications over lognormal fading channels using OOK," *Proceedings of the International Workshop on Optical Wireless Communications (IWOW)*, Newcastle Upon Tyne, UK, October, 2013.

C2. **L. Yang**, J. Cheng, and J. F. Holzman, "Electrical-SNR-optimized detection thresholds for OOK IM/DD optical wireless communications," *Proceedings of the IEEE Canadian Workshop on Information Theory (CWIT)*, pp. 186-189, Toronto, Canada, June, 2013.

C3. **L. Yang**, J. Cheng, and J. F. Holzman, "Performance of convolutional coded OOK IM/DD systems over strong turbulence channels," *Proceedings of the IEEE International Conference on Computing*, Networking and Communications (ICNC), pp. 35-39, San Diego, USA, January, 2013.

Refereed Journal Publications (submitted)

SJ1. **L. Yang**, J. Cheng, and J. F. Holzman, "Estimation of electrical SNR for FSO communications," *IEEE Photonics Technology Letters*, submitted for publication.

SJ2. **L. Yang**, J. Cheng, and J. F. Holzman, "Optical wireless communications over lognormal fading channels using OOK with nonzero extinction ratios," *IEEE/OSA Journal of Lightwave Technology*, submitted for publication.

Table of Contents

List of Tables

List of Figures

List of Acronyms

Acronyms	Definitions
AWGN	Additive White Gaussian Noise
BER	Bit-Error Rate
BPSK	Binary Phase-Shift Keying
CDF	Cumulative Distribution Function
CF	Characteristic Function
CRLB	Cramer-Rao Lower Bound
CSI	Chanel State Information
EM	Expectation-Maximization
FSO	Free-Space Optical
Gbit/s	Gigabit per Second
i.i.d.	Independent and Identically Distributed
IM/DD	Intensity Modulation with Direct Detection
MGF	Moment Generating Function
MLE	Maximum Likelihood Estimation
MoME	Method of Moments Estimation
MSE	Mean Squared Error

NMSE	Normalized Mean Squared Error
OOK	On-Off Keying
OWC	Optical Wireless Communications
pdf	Probability Density Function
PEP	Pairwise Error Probability
PPM	Pulse Position Modulation
RF	Radio Frequency
RV	Random Variable
SI	Scintillation Index
SIM	Subcarrier Intensity Modulation
SNR	Signal-to-Noise Ratio

List of Symbols

Symbols	Definitions
$\triangle f$	Effective noise bandwidth of a receiver
σ_R^2	The Rytov variance
C_n^2	The index of refraction structure parameter
σ_{si}^2	The scintillation index
$\ln(\cdot)$	The log function with base e
$\Gamma(\cdot)$	The Gamma function
$K_\nu(\cdot)$	The modified Bessel function of the second kind of order ν
$E[\cdot]$	The statistical expectation operation
$\mathrm{Var}[\cdot]$	The statistical variance operation
$\mathrm{Cov}[\cdot,\cdot]$	The statistical covariance operation
$\delta(\cdot)$	The Dirac delta function
$p!$	The factorial of a positive integer p
$\mathbb{Z}$	The set of all integers
$\mathrm{erfc}(\cdot)$	The complementary error function
$Q(\cdot)$	The Gaussian Q-function

$I_v(\cdot)$	The modified Bessel function of the first kind with order v
${}_mF_n(\cdots;\cdots;\cdot)$	The generalized Hypergeometric function
$B(\cdot,\cdot)$	The Beta function
$\binom{N}{n}$	The generalized binomial coefficient
$\mathbb{R}$	The set of all real numbers
$\Phi_R(\cdot)$	The CF of a RV R
$x * y$	The convolution of x and y
$x \oplus y$	The exclusive OR gate with inputs x and y
$\mathrm{Re}[\cdot]$	The real part of a number
$\mathrm{Im}[\cdot]$	The imaginary part of a number

Acknowledgements

I am deeply grateful to my supervisors Dr. Julian Cheng and Dr. Jonathan F. Holzman for their enthusiasm, guidance, advice, encouragement, support, and friendship. It is my honor to study and research under their supervision. I will continue to be influenced by their rigorous scholarship, clarity in thinking, and professional integrity.

I would like to thank Dr. Yunfei Chen from the University of Warwick in United Kingdom for serving as my external examiner. It is my great honor to have such an expert on my committee. I would also like to thank Dr. Thomas Johnson, Dr. Jahangir Hossian and Dr. Shawn Wang for their willingness to serve on the thesis examination committee. I really appreciate their valuable time and constructive comments on my thesis.

I owe many people for their generosity and support during my Ph.D. study at the University of British Columbia. I would like to thank my dear colleagues for sharing their academic experiences and constructive viewpoints generously with me during our discussions. I would also like to thank my dear friends for sharing in my excitement and encouraging me when I was frustrated during this journey.

Finally, I would like to thank my parents for their patience, understanding, support, and love over all these years. All my achievements would not have been possible without their constant encouragement and support.

Chapter 1

Introduction

1.1 Background and Motivation

Optical wireless communication (OWC) links have certain advantages over radio frequency links. Examples of such advantages include low deployment cost, high link security, and freedom of spectral license regulations. An outdoor OWC system, in particular, uses free-space as the transmission medium, and is also known as free-space optical (FSO) communication [1]. However, FSO communication can suffer from fog/cloud coverage and harsh weather conditions. These atmospheric effects can degrade the system reliability and performance [2]. Ultimately, rain, snow, sleet, fog, dust, heat, etc. can affect our viewing of distant objects, and these factors can also affect the transmission of laser beams through the atmosphere.

Absorption, scattering, and refractive-index fluctuations (i.e., optical turbulence[1]) are three primary atmospheric processes that affect optical wave propagation through the atmosphere. Typically, absorption and scattering are grouped together under the topic of extinction, which is defined by a reduction or attenuation in the amount of radiation passing through the atmosphere. Both effects are well characterized and can be effectively modeled and compensated for by software packages such as LOWTRAN, FASCODE, MODTRAN, HITRAN, and LNPCWIN as a function of wavelength λ [3]. On the other hand, optical turbulence is a random effect, which is generally considered to be the most serious optical effect on a propagating laser beam through the atmosphere.

It is well known that the performance of FSO systems can be significantly degraded by turbulence-

[1] Optical turbulence is a subset of atmospheric turbulence. However, we will not distinguish between these two terms and use them interchangeably in this thesis.

induced fading. Turbulence-induced fading can lead to power losses at the photodetector and random fluctuations of the received signal. The performance degradation is especially pronounced for FSO systems using irradiance modulation and direct detection (IM/DD) with on-off keying (OOK), and it is these systems that are the primary focus of this thesis.

In this thesis, we focus on bit-error rate (BER) performance improvements for FSO communication links operating with OOK over atmospheric turbulence channels. To improve the BER performance, there are three techniques developed in this thesis.

The first technique, for improving the BER performance of FSO links using OOK, employs electrical signal-to-noise ratio (SNR) optimized detection. The electrical-SNR-optimized detection requires the perfect knowledge of the probability density function (pdf) of the turbulence and electrical SNR. Such knowledge is often quantified by way of mathematical models for the turbulence-induced fading [4], [5]. Among the turbulence-induced fading[2] models introduced so far, it has been well accepted that the lognormal distribution characterizes FSO fading channels under weak turbulence conditions over several hundred meters, or longer, depending on the temperature, wind strength, altitude, humidity, and atmospheric pressure [6], [7]. The K-distribution characterizes FSO fading channels under strong turbulence conditions over several kilometres [8]. The negative exponential distribution characterizes FSO fading channels in the limiting case of saturated scintillation [9]. There also exist generalized models for use over a broad range of weak-to-strong turbulence conditions. The Gamma-Gamma distribution is used, but it can underestimate effects of small- and large-scale scintillations and can suffer from decreased accuracy [10]. The lognormal-Rician distribution can be used, and it has been found to offer two advantages. First, heuristic analyses of wave propagation through turbulence show that the lognormal-Rician fading distribution accurately characterizes experimental data [11]. Second, the lognormal-Rician fading distribution is highly adaptable over a wide range of weak-to-strong turbulence conditions through its parameters [12]. However, the application of the lognormal-Rician fading distribution has been limited, as it does not have a tractable closed-form pdf.

[2] In the rest of the thesis, turbulence-induced fading is referred as (atmospheric) turbulence for simplicity unless stated otherwise.

Given the potential of the lognormal-Rician distribution, for accurately characterizing FSO fading channels, there have been efforts to characterize this distribution with estimated shaping parameters. In [13], the authors applied a physical model of turbulence-induced scattering to estimate the shaping parameters of the lognormal-Rician fading distribution. It should be noted, however, that this approach depends heavily upon estimated parameters in a physical model of the turbulence-induced scattering, and such parameters are often either unavailable or lacking in accuracy. For computational simplicity, the authors applied the Tatarskii model to characterize refractive index fluctuations and geometrical optics to characterize turbulent eddies, but the underlying assumptions of this approach can lead to notable inaccuracies, as discussed in [11]. In [14], the authors introduced the generalized method of moments approach to estimate the shaping parameters of the lognormal-Rician distribution. It should be noted, however, that this approach demands a large number of data samples, on the order of 10^6 data samples, and this impedes its implementation in FSO communications. For a standard FSO link, experiencing quasi-static turbulence fading on a typical millisecond timescale, the system would exhibit latency on the order of 1×10^6 millisecond = 1000 seconds. This duration is unacceptably long for FSO communications, as typical FSO channels exhibit stationary statistics, i.e., constant channel model parameters, on the timescale of several minutes. Clearly, FSO systems applying channel estimation with a lognormal-Rician fading distribution need a more rapid estimation of the shaping parameters.

The above turbulence models can be used to characterize FSO channels, for the implementation of adaptive detection thresholds in OOK IM/DD systems. FSO systems operating without such adaptive detection thresholds would simply apply fixed detection thresholds, and such modulation is often adopted by current commercial FSO products. In [2], [15], the authors studied the performance of OOK IM/DD systems using fixed detection thresholds through atmosphere turbulence channels, and it was found that these unoptimized systems suffered from irreducible error floors. Existing commercial FSO communication systems have employed high transmission powers to overcome the effects of atmospheric turbulence, but this practice results in high cost. With this in mind, there have been many recent efforts to implement OOK IM/DD systems with

effective adaptive detection. In [2], [16], the authors applied adaptive detection with assumed perfect knowledge of the instantaneous channel state information (CSI), as the instantaneous SNR is used to detect each data symbol. In this case, the receiver merely requires computation of a simple mathematical expression, and the BER remains at a minimal value. However, perfect knowledge of CSI is challenging to realize in practice. In [17], the authors investigated blind detection, i.e., detection assuming the absence of instantaneous CSI and a statistical channel description at the receiver, for OOK in a FSO system. This method leads to a decision delay as the receiver is required to compute the detection threshold using all the received statistics. In [18], [19], the authors considered sequence detection for OOK in an FSO system, in which block-wise decisions are made using an observation window of N bit intervals. Unfortunately, such an algorithm had significant computational requirements. In general, the above methods have obvious practical concerns for OOK IM/DD operation with nanosecond data symbol durations (i.e., Gbps rates) and millisecond turbulence coherence times, as rapid detection threshold adjustments are needed on the timescale of the millisecond turbulence coherence times [2], [17], [19], [20].

To accommodate practical concerns for adaptive detection, the electrical-SNR-optimized detection system was proposed in [21], [22]. Such a system offers a compromise between the practical advantages of operation with fixed detection threshold, as only slow adaptations are needed to define the detection thresholds, and the performance advantages of operation with adaptive detection thresholds, as it avoids irreducible error floors [23]. The electrical-SNR-optimized detection thresholds only need to change over the especially long timescales, of seconds or minutes, over which a stationary turbulence channel assumption is applied (as the electrical SNR remains constant over these timescales) [6]. The electrical-SNR-optimized system can, therefore, reduce the implementation complexity, compared to that of the idealized system using adaptive threshold detection. Unfortunately, existing electrical-SNR-optimized systems make an assumption of perfect knowledge of the electrical SNR and turbulence pdf.

The second technique, for improving the BER performance of FSO links using OOK, is source information transformation. In [24], the authors introduced pilot-symbol (PS) assisted modulation

(PSAM) to mitigate the turbulence fading and improve the system performance. The PS provides the receiver with explicit turbulence fading references for detection and helps mitigate the fading effects. However, PSAM causes delays in the receiver as it is necessary to store the whole frame before decoding. In [25], it was demonstrated that an FSO system can use two laser wavelengths at the transmitter and two photodetectors at the receiver operating in a differential mode with excellent BER performance for an OOK IM/DD system with a detection threshold fixed at zero. Unfortunately, this scheme suffers from low throughput, as two lasers are used to transmit the same information in each symbol duration.

The third technique, for improving the BER performance of FSO links using OOK, employs error control coding. In particular, convolutional coding is considered here, as it can be effective in mitigating fading effects and improving the BER performance [26]. For such convolutional codes, error bounds are widely used to analyze the error rate performance. In [26], [27], the authors derived approximate upper bounds on pairwise error probability (PEP) as well as approximate upper bound expressions on the average BER for OOK IM/DD systems over the lognormal turbulence channels using various coding schemes (include convolutional code). In [28], the authors studied the PEP of OOK OWC systems within temporally correlated K-distributed turbulence. They derived an upper bound on the PEP for the channel and then applied the union-bound technique in conjunction with the derived PEP bound to obtain upper bounds on the BER performance. In [29], the authors extended their work on PEP for coded OOK OWC systems to the Gamma-Gamma turbulence channels. In [31], the authors also derived an approximate PEP expression for coded FSO links over the Gamma-Gamma turbulence channels. However, an accurate approximation of PEP was not obtained, and the computation of the upper bound for the average BER is complex.

1.2 Thesis Organization and Contributions

This thesis consists of seven chapters. A summary of each chapter and its contributions are given as follows.

In Chapter 1, we present background knowledge of FSO history and its development. The

motivation of the research in this thesis is justified. We also provide a comprehensive review of FSO literature related to the research topics of this thesis.

Chapter 2 presents essential technical background for the entire thesis. A brief description of an OOK IM/DD system is given. The additive noise at the receiver is also discussed. Then, some background knowledge on atmospheric turbulence channels is presented, and five atmospheric turbulence channel models are reviewed.

In Chapter 3, we investigate the BER of OOK IM/DD FSO systems employing various detection thresholds, as OOK IM/DD systems with fixed detection thresholds lead to irreducible error floors. The expressions of irreducible error loors are derived and expressed as comulative distribution functions (CDFs) of the channel irradiance. We apply the electrical-SNR-optimized detection system, as such a system can eliminate irreducible error floors without requiring perfect knowledge of the instantaneous CSI and turbulence pdf.

In Chapter 4, maximum-likelihood estimation (MLE) is applied to characterize the lognormal-Rician turbulence model parameters, and the expectation-maximization (EM) algorithm is used to compute maximum likelihood estimates of the unknown parameters. Electrical SNR estimation is also investigated for FSO communication systems using IM/DD over lognormal fading channels. Both method of moments estimation (MoME) and MLE are studied for electrical SNR estimation. The MSE is used to examine the performance of the estimators.

In Chapter 5, FSO communication using OOK and source information transformation is proposed. This system can detect the OOK signal without knowledge of the instantaneous CSI and pdf of the turbulence model. The pdf of the detection threshold and an upper bound on the average BER are derived. Numerical studies ultimately show that the proposed system can achieve comparable performance to the idealized adaptive detection system, with a greatly reduced level of implementation complexity and a SNR penalty factor of only 1.85 dB at a BER of 2.17×10^{-7} for a lognormal turbulence channel with a scintillation level of $\sigma = 0.25$.

In Chapter 6, we investigate IM/DD systems employing OOK and subcarrier intensity modulation (SIM) and binary phase-shift keying (BPSK) with convolutional code. We analyze the error

rate performance of OOK IM/DD systems operating over weak and strong turbulence conditions and compare the BER performance of OOK to that of SIM-BPSK systems. A highly accurate convergent series solution is derived for the PEP of the OOK IM/DD system. The solution establishes a simplified upper bound on the average BER. For quasi-static fading channels, we also study the BER performance of a convolutional coded system using block interleaving where each block experiences independent fading.

Finally, we summarize the thesis in Chapter 7 and suggest some future research topics for further study.

Chapter 2

OOK IM/DD System and Turbulence Channel Models

In this chapter, we present a brief description of the OOK IM/DD system and the additive noise model at the receiver. Background information on atmospheric turbulence channels is presented by way of five atmospheric turbulence channel models.

2.1 System Model

Figure 2.1 shows the block diagram of an FSO system operating through the atmosphere. The transmitter is composed of a source encoder, an optical modulator and a transmitting telescope. At the transmitter, the source information bits are input into the source encoder, and encoded into an electrical signal. After being properly biased, the electrical signal modulates a laser beam. At the end of transmitter, there is a telescope to control the direction and size of the laser beam. At the receiver, a telescope is used to collect and focus the received optical beam onto the photodetector for optoelectronic conversion. The electrical signal is then decoded.

For OOK IM/DD operation with the above system, the signal in the baseband to be transmitted can be written as

$$s(t) = \sum_i a_i g(t - iT_p) \tag{2.1}$$

where $a_i \in \{-1, 1\}$ is the data bit, and T_p is the symbol duration. In (2.1), the pulse shaping is defined as $g(t) = 1$ for $0 < t < T_p$, and $g(t) = 0$ otherwise. The transmitted intensity has a bias

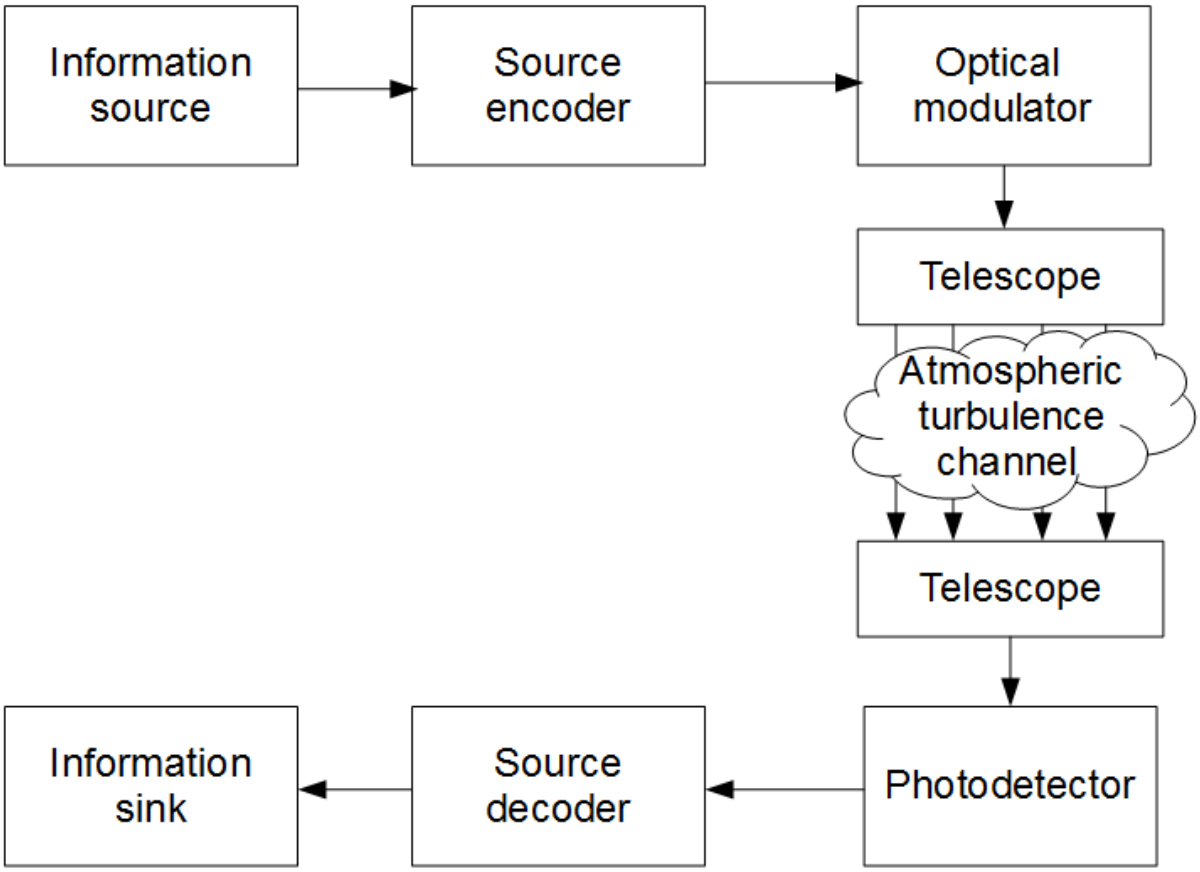

Figure 2.1: Block diagram of an FSO system through an atmospheric turbulence channels.

term of unity added to ensure non-negative values and it can be expressed as

$$\hat{s}(t) = 1 + \sum_i a_i g(t - iT_p). \tag{2.2}$$

The signal $\hat{s}(t)$ is transmitted through an atmospheric turbulence channel and is distorted by a multiplicative irradiance process $I(u,t)$, where u is used to describe the space. The received electrical signal after photodetection can be written as

$$r(t) = R[(1+\xi)I(u,t) + \sum_i I(u,t)a_i g(t - iT_p)] + n(t). \tag{2.3}$$

The photodetector responsivity, without loss of generality, is assumed to be $R = 1$. In (2.3), the positive parameter ξ is the low and high state offset that quantifies a nonzero extinction ratio [32]. Nonzero extinction ratios are due to practical considerations for semiconductor laser transmitters, which often operate with finite power levels for the low and high states. Typical values of ξ are between 0.1053 and 0.2857 [33]. When $\xi \neq 0$, the low and high states of the received electrical signal are affected by turbulence. When $\xi = 0$, the received electrical signal simplifies to the classical model discussed in [15].

In (2.3), $I(u,t)$ is assumed to be a stationary random process for signal scintillation caused by atmospheric turbulence, and $n(t)$ is additive white Gaussian noise (AWGN) due to thermal noise and/or ambient shot noise. Using a p-i-n photodiode and following [21], the shot noise is assumed to be dominated by the ambient shot noise. (Both ambient shot noise and thermal noise are statistically independent of the desired signal.) The total noise power is $\sigma_g^2 = \sigma_s^2 + \sigma_T^2$, where σ_s^2 and σ_T^2 denote the respective ambient shot noise power and the thermal noise power.

The received signal is sampled at time T_p. The sample $I(u, t = T_p)$ is a random variable (RV) I, and the sample $n(t = T_p)$ is a RV N having zero mean and variance $\sigma_g^2 = N_0/2$, where N_0 is the noise power spectral density. If "0" is transmitted, s_0 is true and the laser is in the low state, so the sample for demodulation is $r|_{s_0} = \xi I + N$. If "1" is transmitted, s_1 is true and the laser is in the high state, so the sample for demodulation is $r|_{s_1} = (2+\xi)I + N$. It is important to note that the

nonzero state offset ξ leads to turbulence dependence for the received signal when s_0 or s_1 is true.

2.2 Additive Noise at the Receiver

Optical receivers convert incident power into electric current through a photodetector. Besides turbulence effects, two major types of additive noise, thermal noise and shot noise can affect the received signal photocurrent. The additive noise at the receiver is related to the type of photodetector that is used, and we will focus on the p-i-n photodiode in this thesis. We will briefly review the two types of additive noise, and then discuss the resulting SNR for the optical receivers in the rest of this section.

2.2.1 Thermal Noise

Thermal noise (also known as Johnson noise [34] or Nyquist noise [35]) exists at a finite temperature. It is due to random thermal motion of electrons and atoms in a resistor, which creates a random voltage signal across its terminals. Mathematically, thermal noise can be modeled as a stationary Gaussian random process with a spectral density that is frequency independent well into the terahertz spectrum. Therefore, it is considered to be white noise. The spectral density of thermal noise is given by [32]

$$S_T(f) = \frac{2k_B T}{R_L} \tag{2.4}$$

where k_B is the Boltzmann constant, T is the absolute temperature in Kelvins, and R_L is the load resistance. The spectral density $S_T(f)$ is two-sided and the photocurrent noise variance can be obtained as by [32]

$$\sigma_T^2 = \int_{-\infty}^{\infty} S_T(f)|H(f)|^2 df = \int_{-\triangle f}^{\triangle f} S_T(f) df = \frac{4\triangle f k_B T}{R_L} \tag{2.5}$$

where $H(f)$ is the frequency reponse of the filter at the receiver and we assume $|H(f)| = 1$, and the $\triangle f$ is the effective noise bandwidth of the receiver. It is worth noting that the thermal noise

spectral density $S_T(f)$ and the resulting photocurrent noise variance do not depend on the received average photocurrent.

2.2.2 Shot Noise

Shot noise is due to photons and electron quantization (because light and electric current consist of quantized 'packets'). Contributions from signal photons lead to quantum noise, and contributions from electrons in the semiconductor lead to dark noise. Shot noise was first introduced in 1918 by Schottky [36] who studied fluctuations of current in vacuum tubes and has been thoroughly investigated since then [37], [38].

The energy associated with particles comes in discrete steps. A photon with a frequency ν will have an energy of $h\nu$ where h is the Planck's constant. It is therefore not possible to have a continuous flow of energy. Instead, the energy comes as bursts of particles that are witnessed as quantum noise fluctuations. Mathematically, quantum noise is a stationary random process following Poisson statistics, which in practice is often approximated by Gaussian statistics. For our purposes, quantum noise is assumed to be white noise with a constant spectral density due to the received average photocurrent, i.e., $S_q(f) = qI_p$, where q is the electronic charge and I_p is the received average photocurrent. The noise variance can be obtained as [32]

$$\sigma_q^2 = \int_{-\infty}^{\infty} S_q(f)|H(f)|^2 df = \int_{-\triangle f}^{\triangle f} S_T(f) df = 2\triangle f q I_p. \tag{2.6}$$

Dark noise is present when no light is incident on the photodetector. This dark noise current is due to the semiconductor material in the photodetector. Electrons and holes are liberated due to thermal effects in the semiconductor, as these carriers overcome the bandgap. This results in a time-averaged dark current I_d with spectral density $S_d(f) = qI_d$ and variance

$$\sigma_d^2 = \int_{-\infty}^{\infty} S_d(f)|H(f)|^2 df = \int_{-\triangle f}^{\triangle f} S_d(f) df = 2\triangle f q I_d. \tag{2.7}$$

Therefore, the total variance of shot noise can be obtained as

$$\sigma_s^2 = \sigma_q^2 + \sigma_d^2 = 2\triangle f q(I_p + I_d). \tag{2.8}$$

2.2.3 Signal-to-Noise Ratio

The performance of an optical receiver depends on the SNR which is defined as the ratio of signal power to total noise power. The SNR of a receiver with a p-i-n photodiode is considered here. The signal power is proportional to the photocurrent squared, while the noise contributions are from the thermal noise and shot noise, i.e., $\sigma_n^2 = \sigma_T^2 + \sigma_s^2$. Therefore, the SNR can be expressed as

$$SNR = \frac{I_p^2}{\sigma_n^2} = \frac{I_p^2}{2\triangle f q(I_p + I_d) + 4\triangle f K_B T / R_L}. \tag{2.9}$$

It is worth noting that in the p-i-n receivers for FSO systems, thermal noise tends to dominate because the incident signal power and the dark current are relatively low.

2.3 Atmospheric Turbulence Models

In an FSO system, the transmitted signals are typically subject to atmospheric turbulence over the atmospheric transmission links. The random variation in signal irradiance due to atmospheric turbulence caused by inhomogeneities in both temperature and pressure of the atmosphere is a major source of degradation of FSO system performances. To predict and mitigate such performance degradation caused by atmospheric turbulence, researchers have studied FSO channels extensively and proposed different atmospheric turbulence models [4].

The common statistical models that are used to characterize atmospheric turbulence channels are the lognormal, K, negative exponential, Gamma-Gamma, and lognormal-Rician models [4]. The lognormal distribution characterizes weak turbulence and is suitable for characterizing FSO communications in clear sky links over several hundred meters [39]. The K-distribution is suitable for describing strong turbulence over links that are several kilometres in length [8]. The negative

exponential distribution describes the limiting case of saturated scintillation [40]. The Gamma-Gamma distribution and lognormal-Rician are two generalized models that can be applied to a wide range of turbulence conditions [41], [11].

2.3.1 Lognormal Turbulence

For the lognormal channel model, the optical irradiance I is given by

$$I = \exp(X) \tag{2.10}$$

where X is a Gaussian RV with mean μ and variance σ^2. Consequently, I follows a lognormal distribution with a pdf given by [39]

$$f_I(I) = \frac{1}{\sqrt{2\pi}\sigma I} \exp\left(-\frac{(\ln I - \mu)^2}{2\sigma^2}\right), \quad I > 0. \tag{2.11}$$

Normalizing the mean, i.e., $E[I] = 1$, where $E[\cdot]$ is the expectation operation, the pdf of I can be written as

$$f_I(I) = \frac{1}{\sqrt{2\pi}\sigma I} \exp\left(-\frac{(\ln I + \sigma^2/2)^2}{2\sigma^2}\right), \quad I > 0. \tag{2.12}$$

The parameter σ is the scintillation level, and its value is typically less than 0.75 [15]. Turbulence effects on the performance are minimal when scintillation levels are below $\sigma = 0.1$, so the investigated electrical SNR in this thesis is characterized for typical scintillation levels ranging from 0.1 to 0.75 [21], [42].

2.3.2 K-distributed Turbulence

The K-distributed turbulence model is a widely accepted turbulence model, and it can be used to describe the irradiance fluctuations under strong turbulence conditions. It can be shown that the K-distributed RV I is a product of two independent RVs I_x and I_y, where I_x and I_y follow exponential

and Gamma distributions, respectively [43], with pdfs

$$f(I_x) = \exp(-I_x), \;\; I_x > 0 \tag{2.13}$$

and

$$f(I_y) = \frac{\alpha I_y^{\alpha-1}}{\Gamma(\alpha)} \exp(-\alpha I_y), \;\; I_y > 0 \tag{2.14}$$

where $\Gamma(\cdot)$ is the Gamma function, and α is the effective number of discrete refractive scatters and it takes a value in $(1,2)$ [44].

The K-distribution can be derived as follows. Conditioning on I_y and substituting $I_x = I/I_y$ into (2.13), we can obtain the conditional pdf of I as

$$f_{I|I_y}(I|I_y) = \frac{1}{I_y} \exp\left(-\frac{I}{I_y}\right), \;\; I > 0. \tag{2.15}$$

To obtain the pdf of I, we take the expectation of (2.15) with respect to the pdf of I_y. The pdf of I becomes [45]

$$\begin{aligned} f_I(I) &= \int_0^\infty f_I(I|I_y) f(I_y)\, dI_y \\ &= \frac{2}{\Gamma(\alpha)} \alpha^{\frac{\alpha+1}{2}} I^{\frac{\alpha-1}{2}} K_{\alpha-1}(2\sqrt{\alpha I}) \end{aligned} \tag{2.16}$$

where $K_{\alpha-1}(\cdot)$ is the modified Bessel function of the second kind with order $\alpha - 1$. The mth moment of I is given by [43]

$$E[I^m] = \frac{m!\Gamma(m+\alpha)}{\alpha^m \Gamma(\alpha)}. \tag{2.17}$$

The scintillation index of K-distributed turbulence is

$$\sigma_{SI}^2 \triangleq \frac{E[I^2]}{(E[I])^2} - 1 = 1 + \frac{2}{\alpha} \tag{2.18}$$

where σ_{SI}^2 is within $(2,3)$.

2.3.3 Negative Exponential Turbulence

In the limiting case of strong irradiance fluctuations (i.e., in the saturation regime and beyond) where the propagation distances span several kilometres, the number of independent scatterings becomes large [46], [47]. This saturation regime is also called the fully developed speckle regime. The amplitude fluctuation of the field traversing the random medium under this condition is experimentally verified to obey the Rayleigh distribution [48], [49]. Thus, the irradiance I follows the negative exponential distribution whose pdf is given as

$$f_{NE}(I) = \frac{1}{I_0}\exp\left(-\frac{I}{I_0}\right), \ I > 0 \tag{2.19}$$

where $I_0 = E[I]$ is the mean irradiance. Without loss of generality, we can normalize I by setting $E[I] = 1$. In the saturation regime, the value of the scintillation index approaches unity.

2.3.4 Gamma-Gamma Turbulence

The Gamma-Gamma distribution is a useful and flexible turbulence model because it can describe a wide range of turbulence conditions [41]. The pdf of the Gamma-Gamma distributed optical irradiance is

$$\begin{aligned} f_I(I) =& \frac{2}{\Gamma(\alpha)\Gamma(\beta)}(\alpha\beta)^{\frac{\alpha+\beta}{2}} I^{\frac{\alpha+\beta}{2}-1} \\ & \times K_{\alpha-\beta}\left(2\sqrt{\alpha\beta I}\right), \ I > 0. \end{aligned} \tag{2.20}$$

Assuming spherical wave propagation, the parameters α and β are related to the atmospheric conditions according to [29]

$$\alpha = \left[\exp\left(\frac{0.49\chi^2}{(1+0.18d^2+0.56\chi^{\frac{12}{5}})^{\frac{7}{6}}}\right) - 1\right]^{-1} \tag{2.21}$$

and

$$\beta = \left[\exp\left(\frac{0.51\chi^2(1+0.69\chi^{\frac{12}{5}})^{-\frac{5}{6}}}{(1+0.9d^2+0.62\chi^{\frac{12}{5}})^{\frac{5}{6}}}\right) - 1\right]^{-1} \tag{2.22}$$

where $\chi^2 = 0.5C_n^2 k^{\frac{7}{6}} L^{\frac{11}{6}}$ and $d = 0.5k^{1/2}DL^{-1/2}$. Here, the parameter C_n^2 is the altitude-dependent index of the refractive structure parameter that varies from $10^{-17}\mathrm{m}^{-\frac{2}{3}}$ for weak turbulence to $10^{-13}\mathrm{m}^{-\frac{2}{3}}$ for strong turbulence, λ is the optical wavelength and $k = 2\pi/\lambda$ is the wavenumber. The optical link distance is L, and D is the diameter of the receiver aperture.

2.3.5 Lognormal-Rician Turbulence

For the FSO system of interest, there is an assumption of perfect background noise rejection, from narrowband optical, electronic, and/or spatial filtering [39]. For the resulting lognormal-Rician channel model, the optical irradiance I can be obtained by $I = |U_C + U_G|^2 \exp(2\chi)$, where U_C is a real deterministic quantity, U_G is a circular complex Gaussian RV with zero mean, χ is a real Gaussian RV, $|U_C + U_G|$ is a Rician RV, $|U_C + U_G|^2$ is a noncentral chi-square RV with a degree of freedom of two, and $\exp(2\chi)$ is a lognormal RV. Consequently, I follows a lognormal-Rician distribution with a pdf given by [13]

$$\begin{aligned} f_I(I) = &\frac{(1+r)e^{-r}}{\sqrt{2\pi}\sigma_z} \int_0^\infty \frac{dz}{z^2} I_0\left(2\left[\frac{(1+r)r}{z} I\right]^{1/2}\right) \\ &\times \exp\left(-\frac{1+r}{z} I - \frac{1}{2\sigma_z^2}\left(\ln z + \frac{1}{2}\sigma_z^2\right)^2\right) \end{aligned} \tag{2.23}$$

where z represents $\exp(2\chi)$, $r = |U_C|^2/E[|U_G|^2]$ is the coherence parameter, σ_z^2 is the variance of the logarithm of the irradiance modulation factor z, and $I_0(\cdot)$ is the zero-order modified Bessel function of the first kind.

As noted in [4], it is not generally known how to directly relate the above two empirical parameters to the physical characteristics of atmospheric conditions, but it is possible to characterize trends in the two parameters, with respect to the Rytov variance, $\sigma_R^2 = 0.5k^{\frac{7}{6}} L^{\frac{11}{6}} C_n^2$. The characteristic trends in the two parameters are seen in [13], for variations in the Rytov variance, σ_R^2, i.e., variations in L and/or C_n^2. In the limit of zero inner scale, the parameter r decreases as σ_R^2 increases, while the parameter σ_z^2 is approximately equal to the Rytov variance for small σ_R^2, reaches a peak value of approximately 0.58 for $\sigma_R^2 \approx 8$, and decreases slowly to approximately 0.4 for large σ_R^2.

When the coherence parameter r approaches infinity, the lognormal-Rician distribution specializes to the lognormal distribution with a pdf of [13], [14]

$$f_I(I) = \frac{1}{\sqrt{2\pi}\sigma_z I} \exp\left(-\frac{1}{2\sigma_z^2} \left(\ln I + \frac{1}{2}\sigma_z^2 \right)^2 \right). \tag{2.24}$$

When r approaches 0, the lognormal-Rician distribution specializes to the lognormally modulated exponential distribution, characterizing strong scintillation, with a pdf of [13], [50]

$$f_I(I) = \frac{1}{\sqrt{2\pi}\sigma_z} \int_0^\infty \frac{dz}{z^2} \exp\left(-\frac{I}{z} - \frac{1}{2\sigma_z^2} \left(\ln z + \frac{1}{2}\sigma_z^2 \right)^2 \right). \tag{2.25}$$

The nth moment of the lognormal-Rician RV I is known to be [13]

$$E[I^n] = \frac{(n!)^2}{(1+r)^n} \exp\left(\frac{n(n-1)}{2}\sigma_z^2 \right) \sum_{k=0}^{n} \frac{r^k}{(n-k)!(k!)^2}. \tag{2.26}$$

2.4 Summary

In this chapter, we presented the essential background knowledge needed for technical content in the remainder of this thesis. A brief description of an OOK IM/DD system was provided. The additive noise at the receiver was also discussed. Then, some background knowledge on atmospheric turbulence channels was presented, according to five commonly-used atmospheric turbulence channel models.

Chapter 3

OOK IM/DD Systems with Nonzero Extinction Ratios and Electrical-SNR-Optimized Detection Thresholds

In this chapter, we study the error rate performance of OOK IM/DD FSO systems employing various detection thresholds. Such systems, when implemented with fixed detection thresholds, lead to irreducible error floors. The expressions for the reducible error floors are derived and expressed as cumulative distribution functions of the channel irradiance. We then investigate an electrical-SNR-optimized detection system, as such a system can eliminate irreducible error floors without requiring perfect knowledge of the instantaneous CSI and the turbulence pdf.

3.1 OOK with Fixed and Unoptimized Detection Thresholds

In the low state, the received signal ($r = \xi I + N$) is a sum of two RVs, N and I_s, where $I_s = \xi I$. Since N and I_s are assumed to be independent, the pdf of the received low state signal is the convolution

of the marginal pdfs of I_s and N, according to

$$\begin{aligned} f(r|s_0) =& \frac{1}{\xi} f_I\left(\frac{r}{\xi}\right) * f_N(r) \\ =& \int_0^{\infty} \frac{1}{\sqrt{2\pi}\sigma x} \exp\left(-\frac{\left(\ln\frac{x}{\xi}+\frac{\sigma^2}{2}\right)^2}{2\sigma^2}\right) \frac{1}{\sqrt{2\pi}\sigma_g} \exp\left(-\frac{(r-x)^2}{2\sigma_g^2}\right) dx \end{aligned} \tag{3.1}$$

where $*$ denotes the convolution operation, and $f_N(r) = \frac{1}{\sqrt{2\pi}\sigma_g} \exp\left(-\frac{r^2}{2\sigma_g^2}\right)$ denotes the noise pdf.

In the high state, the pdf of the received signal ($r = (2+\xi)I + N$) can be defined in a similar manner according to

$$\begin{aligned} f(r|s_1) =& \frac{1}{2+\xi} f_I\left(\frac{r}{2+\xi}\right) * f_N(r) \\ =& \int_0^{\infty} \frac{1}{\sqrt{2\pi}\sigma x} \exp\left(-\frac{\left(\ln\frac{x}{2+\xi}+\frac{\sigma^2}{2}\right)^2}{2\sigma^2}\right) \frac{1}{\sqrt{2\pi}\sigma_g} \exp\left(-\frac{(r-x)^2}{2\sigma_g^2}\right) dx. \end{aligned} \tag{3.2}$$

For a given fixed detection threshold T_{th}, the probability of false alarm P_F and probability of miss P_M can be written as the respective expressions

$$P_F = \int_{T_{th}}^{\infty} f(r|s_0)\, dr = \int_{T_{th}}^{\infty} \frac{1}{\xi} f_I\left(\frac{r}{\xi}\right) * f_N(r)\, dr \tag{3.3}$$

and

$$P_M = \int_0^{T_{th}} f(r|s_1)\, dr = \int_0^{T_{th}} \frac{1}{2+\xi} f_I\left(\frac{r}{2+\xi}\right) * f_N(r)\, dr. \tag{3.4}$$

Assuming that p_1 represents the *a priori* probability that "1" is sent, one can write the BER for

OOK using a fixed detection threshold T_{th} as

$$\begin{aligned}
P_e &= (1-p_1)P_F + p_1 P_M \\
&= \frac{(1-p_1)\exp\left(-\frac{\sigma^2}{8}\right)}{\sqrt{2\pi}\sigma}\int_0^{\infty}\frac{\sqrt{\xi}}{x^{3/2}}\exp\left(-\frac{\ln^2\frac{x}{\xi}}{2\sigma^2}\right)Q\left(\frac{T_{th}-x}{\sigma_g}\right)dx \\
&+ \frac{p_1\exp\left(-\frac{\sigma^2}{8}\right)}{\sqrt{2\pi}\sigma}\int_0^{\infty}\frac{\sqrt{2+\xi}}{x^{3/2}}\exp\left(-\frac{\ln^2\frac{x}{2+\xi}}{2\sigma^2}\right)Q\left(\frac{x-T_{th}}{\sigma_g}\right)dx \\
&= \frac{(1-p_1)\exp\left(-\frac{\sigma^2}{8}\right)}{\sqrt{2\pi}\sigma}\int_0^{\infty}\frac{\sqrt{\xi}}{x^{3/2}}\exp\left(-\frac{\ln^2\frac{x}{\xi}}{2\sigma^2}\right)Q\left(\sqrt{2\gamma}(T_{th}-x)\right)dx \\
&+ \frac{p_1\exp\left(-\frac{\sigma^2}{8}\right)}{\sqrt{2\pi}\sigma}\int_0^{\infty}\frac{\sqrt{2+\xi}}{x^{3/2}}\exp\left(-\frac{\ln^2\frac{x}{2+\xi}}{2\sigma^2}\right)Q\left(\sqrt{2\gamma}(x-T_{th})\right)dx
\end{aligned} \tag{3.5}$$

where $Q(x)=\frac{1}{\sqrt{2\pi}}\int_x^{\infty}e^{-\frac{t^2}{2}}dt$ is the Gaussian Q-function, and we have denoted the electrical SNR by $\gamma=(E[I])^2/N_0$ [21], or simply $\gamma=1/N_0$ under a normalized mean assumption.

In the large SNR regime, when γ approaches infinity or equivalently when $\sigma_g^2=N_0/2$ approaches zero, the Gaussian distribution approaches a Dirac delta function $\delta(\cdot)$. Hence, one can have

$$\lim_{\gamma\to\infty} f_N(r)=\delta(r) \tag{3.6}$$

and

$$\lim_{\gamma\to\infty}\frac{1}{a}f_I\left(\frac{r}{a}\right)*f_N(r)=\frac{1}{a}f_I\left(\frac{r}{a}\right) \tag{3.7}$$

where a is a constant taking either ξ or $2+\xi$. When the electrical SNR is asymptotically large, and we assume that limits and integrals are reversible, it follows that

$$\lim_{\gamma\to\infty}P_F=\int_{T_{th}}^{\infty}\frac{1}{\xi}f_I\left(\frac{r}{\xi}\right)dr=1-F_I\left(\frac{T_{th}}{\xi}\right) \tag{3.8}$$

and

$$\lim_{\gamma\to\infty}P_M=\int_0^{T_{th}}\frac{1}{2+\xi}f_I\left(\frac{r}{2+\xi}\right)dr=F_I\left(\frac{T_{th}}{2+\xi}\right) \tag{3.9}$$

Table 3.1: Error floor expressions for FSO systems employing fixed detection thresholds of $T_{th} = (1+\xi)E[I]$ over a lognormal fading channel with $\sigma = 0.25$.

ξ	0.15	0.18	0.2	0.25
Theoretical error floor	0.0044	0.0049	0.0054	0.0065
Simulated error floor	0.0045	0.0049	0.0054	0.0066

where $F_I(\cdot)$ represents the CDF of the irradiance I. Therefore, the false alarm probability and miss probability in a large SNR regime are determined by the CDF of the irradiance evaluated at T_{th}/ξ and $T_{th}/(2+\xi)$, respectively. Substituting (3.8) and (3.9) into (3.5) gives

$$\begin{aligned}\lim_{\gamma\to\infty} P_e &= \lim_{\gamma\to\infty}(1-p_1)P_F + p_1 P_M \\ &=(1-p_1)Q\left(\frac{\ln T_{th} - \ln\xi + \sigma^2/2}{\sigma}\right) + p_1 Q\left(\frac{\ln(2+\xi) - \ln T_{th} - \sigma^2/2}{\sigma}\right)\end{aligned} \tag{3.10}$$

which is the error floor for an OOK IM/DD system with a fixed detection threshold through lognormal turbulence channels. As seen from (3.10), the error floor depends on both T_{th} and ξ, and typically one chooses the fixed detection threshold as $T_{th} = (E[r|s_1] + E[r|s_0])/2$. When $\xi = 0$, $T_{th} = E[I]$ and the analytical error floor expression in (3.10) is equivalent to [15, eq. (20)], which was derived under an assumption of a normalized second moment, i.e., $E[I^2] = 1$. When $\xi \neq 0$, it is simple to show that $T_{th} = (1+\xi)E[I]$.

It is important to note that the error floor varies with the offset ξ. For a lognormal turbulence channel with $\sigma = 0.25$ and an equal *a priori* data symbol probability, the predicted error floors are shown in Table 3.1 for different values of ξ. It is seen that an increase of ξ results in a higher error floor. The theoretical error floors are verified with simulated BER limits with the results shown in Table 3.1.

Following the same approach, one can predict the error floors for different turbulence channel models based on the corresponding CDFs. The resulting error floors are summarized in Table 3.2,

Table 3.2: Error floor expressions for various turbulence channel models.

Turbulence Channel	Error Floors
Lognormal	$(1-p_1)Q\left(\frac{\ln T_{th}-\ln\xi+\sigma^2/2}{\sigma}\right)$ $+p_1 Q\left(\frac{\ln(2+\xi)-\ln T_{th}-\sigma^2/2}{\sigma}\right)$
K-distribution	$(1-p_1)\{1-\frac{1}{2}[h(1,\alpha,T_{th},\xi)+h(\alpha,1,T_{th},\xi)]\}$ $+p_1[h(1,\alpha,T_{th},2+\xi)+h(\alpha,1,T_{th},2+\xi)]/2$
Gamma-Gamma	$(1-p_1)\{1-\frac{1}{2}[h(\beta,\alpha,T_{th},\xi)+h(\alpha,\beta,T_{th},\xi)]\}$ $+p_1[h(\beta,\alpha,T_{th},2+\xi)+h(\alpha,\beta,T_{th},2+\xi)]/2$
Negative Exponential	$(1-p_1)\exp\left(\frac{T_{th}}{\xi\mu}\right)+p_1\left[1-\exp\left(\frac{T_{th}}{(2+\xi)\mu}\right)\right]$

where the function $h(x,y,z,w)$ is defined as

$$h(x,y,z,w)=\left(\frac{xyz}{w}\right)^x \frac{\Gamma(y-x)}{\Gamma(x+1)\Gamma(y)}\,{}_1F_2\left(x;x+1,x-y+1;\frac{xyz}{w}\right) \tag{3.11}$$

and where ${}_1F_2(\cdot;\cdot,\cdot;\cdot)$ is the generalized hypergeometric function [51].

3.2 OOK with Electrical-SNR-Optimized Detection Thresholds

A performance trade-off can be established between operation with fixed detection thresholds (which can suffer from irreducible error floors) and operation with adaptive detection thresholds (which requires knowledge of the instantaneous SNR for each data symbol). With this in mind, we consider a system with electrical-SNR-optimized detection thresholds, as it offers a compromise between the practical advantages of operation with fixed detection thresholds and the performance advantages of operation with adaptive detection thresholds. Our approach considers the optimization problem

$$\arg\min_{T_{th}} P_e = \arg\min_{T_{th}}[(1-p_1)P_F + p_1 P_M]. \tag{3.12}$$

From (3.5) and (3.12), it is clear that our electrical-SNR-optimized detection requires knowledge of T_{th}, ξ, and the underlying turbulence model. To find the detection threshold that minimizes the BER at a given electrical SNR, we take the derivative of (3.5) with respect to T_{th} and set it to zero, i.e., $\frac{d}{dT_{th}}P_e = 0$. This gives

$$-(1-p_1)f(T_{th}|s_0) + p_1 f(T_{th}|s_1) = 0 \tag{3.13}$$

where $f(T_{th}|s_0)$ and $f(T_{th}|s_1)$ are the likelihood functions evaluated at T_{th}.

3.2.1 Electrical-SNR-Optimized Detection Based on a Known Turbulence pdf

Assuming perfect knowledge of the pdf of the lognormal turbulence model, we substitute (3.1) and (3.2) into (3.13) and have

$$\begin{aligned} &-(1-p_1)\int_0^\infty \frac{\sqrt{\xi}}{x^{3/2}} \exp\left(-\frac{\ln^2 \frac{x}{\xi}}{2\sigma^2}\right) \exp\left(-\gamma(x^2 - 2xT_{th})\right) dx \\ &+ p_1 \int_0^\infty \frac{\sqrt{2+\xi}}{x^{3/2}} \exp\left(-\frac{\ln^2 \frac{x}{2+\xi}}{2\sigma^2}\right) \exp\left(-\gamma(x^2 - 2xT_{th})\right) dx = 0. \end{aligned} \tag{3.14}$$

For a given electrical SNR γ, the electrical-SNR-optimized detection threshold can be calculated numerically from (3.14). The location of the electrical-SNR-optimized detection threshold lies at the intersection of two scaled likelihood functions: $(1-p_1)f(r|s_0)$ and $p_1 f(r|s_1)$. As shown in Fig. 3.1, when the electrical SNR approaches infinity, the total area underneath the intersected pdfs, i.e., $(1-p_1)P_F + p_1 P_M$, will become infinitely small. The proposed electrical-SNR-optimized detection can therefore be used to eliminate the error floors caused by a receiver using fixed detection thresholds. Our numerical results in Section 3.3 will be used to support these analytical arguments.

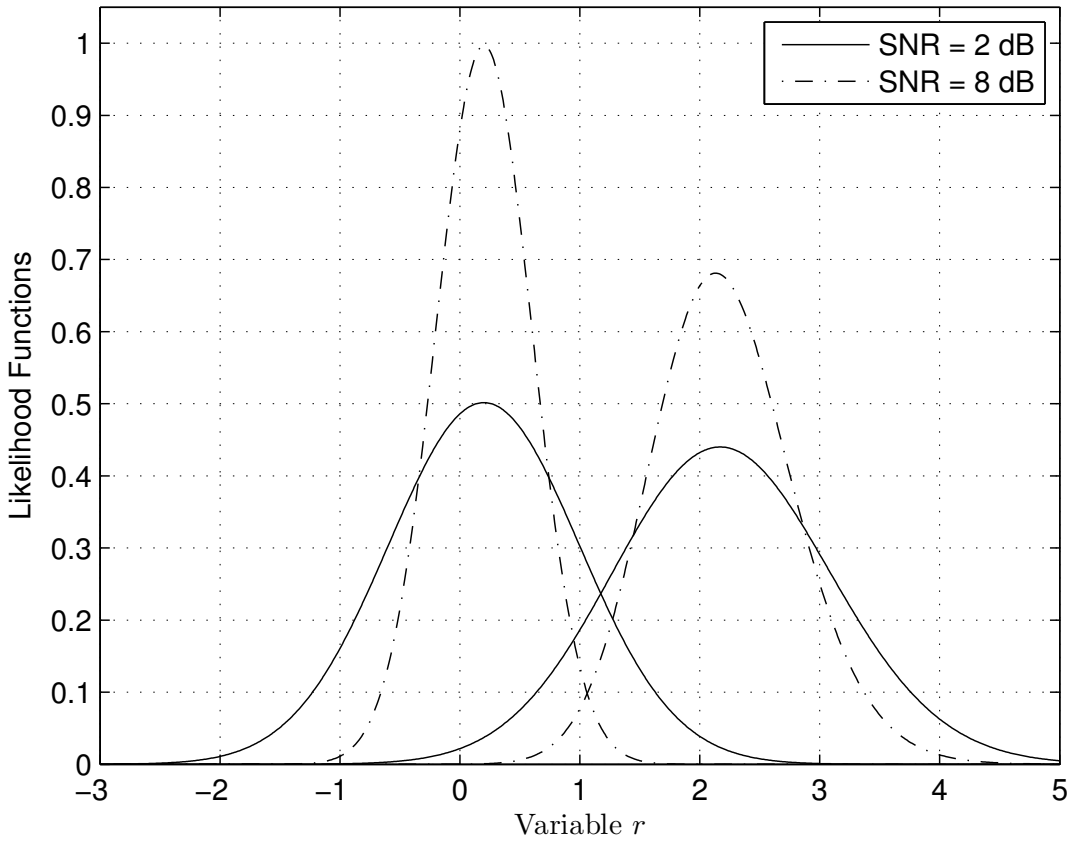

Figure 3.1: The likelihood functions $f(r|s_0)$ and $f(r|s_1)$ with $\sigma = 0.25$ and $\xi = 0.2$ when $\gamma = 2$ dB and $\gamma = 8$ dB. The likelihood functions are a result of the convolution of the lognormal pdf and the Gaussian pdf.

3.2.2 Electrical-SNR-Optimized Detection Based on an Unknown Turbulence pdf

To accommodate the fact that the FSO receiver may not always know the underlying characteristics of the turbulence model, the turbulence distribution can be approximated by sample moments. The approximated turbulence distribution can then be used to derive the electrical-SNR-optimized detection threshold.

The density functions of numerous statistical models on the positive half-line can be approximated by a sum of Laguerre polynomials [52], [53]. Using this approach, one can approximate the pdf of I as [54]

$$f_I(I) \approx \frac{I^v \exp(-I/c)}{c^{v+1}\Gamma(v+1)} \sum_{j=0}^{\infty} \delta_j L_j(v, I/c) \tag{3.15}$$

where $L_j(v, I/c)$ is a Laguerre polynomial of order j in I/c and is written as

$$L_j\left(v, \frac{I}{c}\right) = \sum_{k=0}^{j} \frac{(-1)^k \Gamma(v+j+1)}{k!(j-k)!\Gamma(v+j-k+1)} \left(\frac{I}{c}\right)^{j-k} \tag{3.16}$$

and

$$\delta_j = \sum_{k=0}^{j} (-1)^k \frac{j!\Gamma(v+1)}{k!(j-k)!\Gamma(v+j-k+1)} \mu_{\frac{I}{c}}[j-k] \tag{3.17}$$

where the jth moment of I is denoted by $\mu_I[j]$. In (3.15), the parameters $c = \frac{\mu_I[2]-\mu_I^2[1]}{\mu_I[1]}$ and $v = \frac{\mu_I[1]}{c} - 1$ are chosen to have the mean and variance of the Gamma RV I_0, whose pdf, $f_{I_0}(I) = \frac{I^v \exp(-I/c)}{c^{v+1}\Gamma(v+1)}$, matches that of the RV I. From (3.15), the corresponding characteristic function (CF) and moment generating function (MGF) for the RV I can also be obtained. The detailed derivations are given in Appendix A. These analytical expressions can be used to estimate the performance of an FSO system over lognormal fading. Substituting (3.15) into the last equalities of (3.1) and (3.2)

Table 3.3: Comparison of detection thresholds using an exact and approximated lognormal pdf with $\sigma = 0.25$.

SNR (dB)	Thresholds with exact pdf	Thresholds with approximated pdf	Sample variance
0	0.9497	0.9505	3.11×10^{-8}
4	0.8633	0.8637	2.27×10^{-8}
8	0.7528	0.7496	1.89×10^{-8}
12	0.6302	0.6214	2.56×10^{-8}
16	0.5087	0.4984	1.08×10^{-7}
20	0.3981	0.4697	8.62×10^{-6}
24	0.3036	0.5239	1.03×10^{-5}

yields the likelihood functions

$$\begin{aligned} f(r|s_0) = &\frac{1}{\xi\sqrt{2\pi}\sigma_g c^{v+1}} \sum_{j=0}^{\infty} \delta_j \int_0^{\infty} \left(\frac{x}{\xi}\right)^{v-1} \exp\left(-\frac{x}{\xi c}\right) \\ &\times \exp\left(-\gamma(r-x)^2\right) L_j\left(v, \frac{x}{\xi}\right) dx \end{aligned} \tag{3.18}$$

and

$$\begin{aligned} f(r|s_1) = &\frac{1}{(2+\xi)\sqrt{2\pi}\sigma_g c^{v+1}} \sum_{j=0}^{\infty} \delta_j \int_0^{\infty} \left(\frac{x}{2+\xi}\right)^{v-1} \exp\left(-\frac{x}{(2+\xi)c}\right) \\ &\times \exp\left(-\gamma(r-x)^2\right) L_j\left(v, \frac{x}{2+\xi}\right) dx. \end{aligned} \tag{3.19}$$

Substituting (3.18) and (3.19) into (3.13) yields

$$\begin{aligned} &-\frac{1-p_1}{\xi} \sum_{j=0}^{\infty} \delta_j \int_0^{\infty} \left(\frac{x}{\xi}\right)^{v-1} \exp\left(-\frac{x}{\xi c}\right) \exp\left(-\gamma(x^2 - 2xT_{th})\right) L_j\left(v, \frac{x}{\xi}\right) dx \\ &+\frac{p_1}{2+\xi} \sum_{j=0}^{\infty} \delta_j \int_0^{\infty} \left(\frac{x}{2+\xi}\right)^{v-1} \exp\left(-\frac{x}{(2+\xi)c}\right) \exp\left(-\gamma(x^2 - 2xT_{th})\right) \\ &\times L_j\left(v, \frac{x}{2+\xi}\right) dx = 0. \end{aligned} \tag{3.20}$$

The detection threshold can be obtained numerically with respect to a given offset ξ and electrical

SNR from (3.20). A comparison of the electrical-SNR-optimized detection thresholds, acquired by the approximated and exact lognormal pdfs, are presented in Table 3.3. The thresholds are obtained by averaging 10 calculated detection thresholds. As shown from Table 3.3, the approximated pdf can be used to calculate the detection threshold with high accuracy when the electrical SNR is less than 16 dB. For higher values of SNR, the calculated detection thresholds lose accuracy, and the corresponding BER curve deviates from the BER curve obtained with perfect knowledge of the lognormal pdf. This discrepancy occurs because the Laguerre-polynomial-based pdf approximation can not accurately describe the behaviours of the lognormal pdf near the origin. Fortunately, this inaccuracy does not concern most practical FSO systems, as they typically operate at relatively low SNR values [55].

3.3 Numerical Results

Figures 3.2 and 3.3 show the BER versus electrical SNR when the OOK modulated system uses fixed detection thresholds of $T_{th} = 1$ and $T_{th} = 1.2$. For expository purposes, the parameters are set as $\sigma = 0.25$ and $\xi = 0, 0.2$. It is observed that the BER curves obtained by using Monte Carlo simulation show excellent agreement with the derived error floors in large SNR regimes and the error floors decrease for lower fixed detection thresholds.

To eliminate the error floors and improve the performance, the system with electrical-SNR-optimized detection thresholds is used. The BERs for the system with the electrical-SNR-optimized detection thresholds are shown in Figs. 3.2 (with no state offset, $\xi = 0$) and 3.3 (with a finite state offset, $\xi = 0.2$), along with the BERs for the system with the adaptive detection thresholds. Both electrical-SNR-optimized detection thresholds are obtained by using the approximated lognormal pdf with $J = 3$ sample moments.

It is seen from Figs. 3.2 and 3.3 that the electrical-SNR-optimized and adaptive detection threshold results exhibit no error floors, for increasing electrical SNR values, and that there exists an SNR penalty factor between the system with electrical-SNR-optimized detection thresholds and the optimum OOK system using adaptive detection thresholds. For example, in Fig. 3.2, the OOK

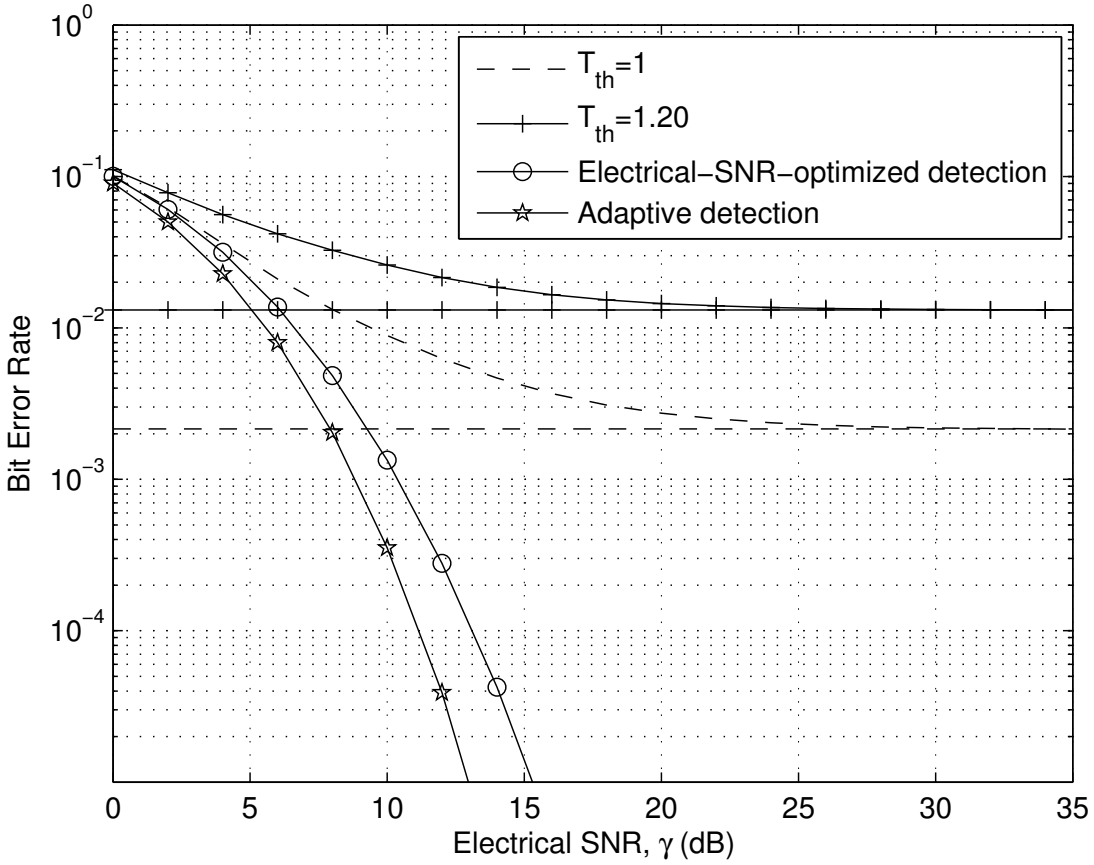

Figure 3.2: BERs of OOK modulated systems using fixed detection thresholds T_{th}, electrical-SNR-optimized detection thresholds and adaptive detection thresholds over a lognormal turbulence channel with $\sigma = 0.25$ and $\xi = 0$.

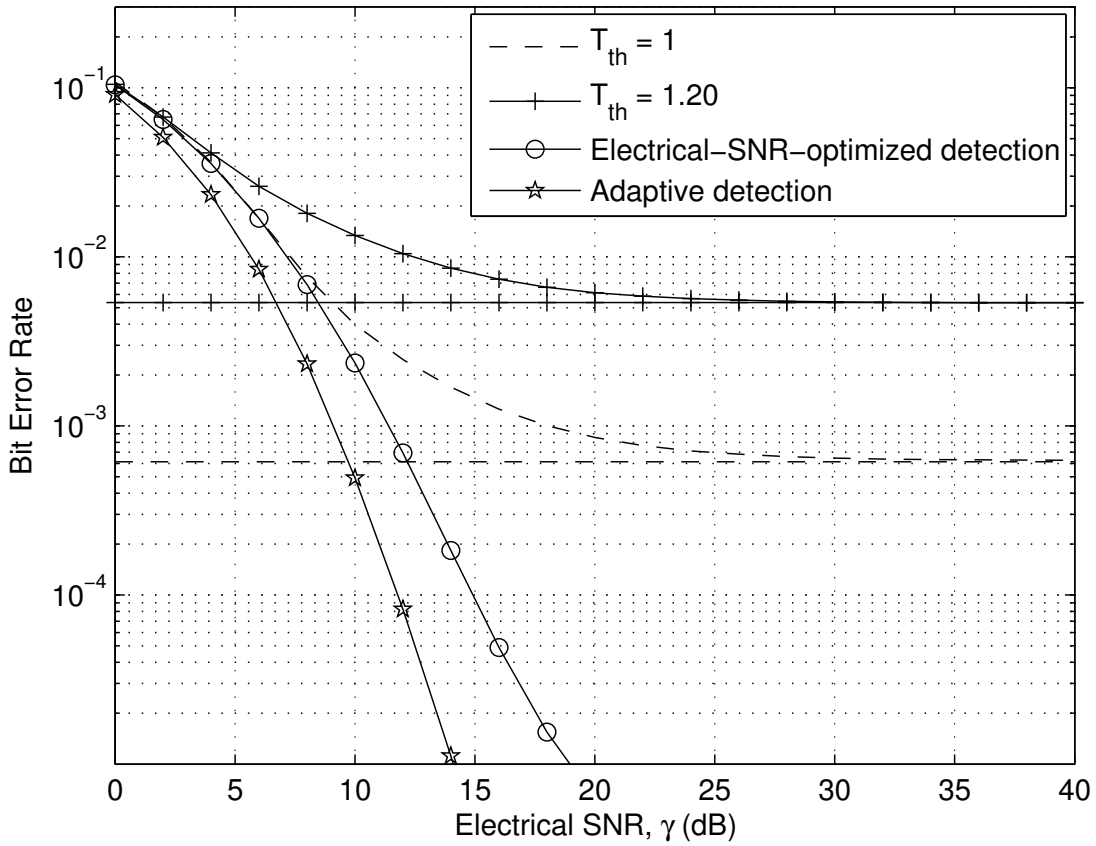

Figure 3.3: BERs of OOK modulated systems using fixed detection thresholds T_{th}, electrical-SNR-optimized detection thresholds and adaptive detection thresholds over a lognormal turbulence channel with $\sigma = 0.25$ and $\xi = 0.2$.

modulated system using adaptive detection thresholds requires an SNR of 13 dB to attain a BER of 10^{-5}, while the system using electrical-SNR-optimized detection thresholds requires an SNR of 15.3 dB to achieve the same BER performance. The corresponding SNR penalty factor in Fig. 3.2 for the system using an electrical-SNR-optimized detection threshold, is 2.3 dB at BER of 10^{-5}. The corresponding SNR penalty factor in Fig. 3.3 for the system using an electrical-SNR-optimized detection threshold, increases to 4.5 dB when $\xi = 0.2$. This performance difference can be factored into the ultimate FSO system design to offset the complexity of implementing systems with adaptive detection thresholds (and their need for knowledge of the instantaneous SNR).

It is also important to point out that the BER performance achieved by the electrical-SNR-optimized system does not require rapid adjustment of the detection threshold. Since practical FSO systems typically operate at constant transmit power, the detection threshold only needs to be calculated once over durations of seconds or even minutes. The electrical-SNR-optimized system can therefore reduce the implementation complexity, compared to that of the idealized system using adaptive threshold detection.

In Fig. 3.4, the approximated lognormal pdf using $J = 3$ sample moments is compared with the exact lognormal pdf, for $\sigma = 0.25$. The absolute errors between these pdfs are shown explicitly in Fig. 3.5. The approximated lognormal pdf shows good agreement with the exact lognormal pdf when $\sigma = 0.25$. However, for higher σ values ($\sigma > 0.75$), the approximation of the lognormal pdf becomes inaccurate as integer moments can not uniquely determine the lognormal pdf. Fortunately, such scintillation levels are not encounted in practice [56]. A comparison of absolute errors from the pdf approximations using different numbers of sample moments is also given in Fig. 3.5. Clearly, larger numbers of sample moments can reduce the absolute error, but this comes at the cost of higher computational complexity. In general, a higher scintillation level σ will require higher order sample moments and the resulting approximation can become increasingly inaccurate. The Laguerre-polynomial-based approximation is accurate for the 0.1 to 0.5 range of σ values that is of interest to FSO applications [21], [42].

In Fig. 3.6, we compare the BER performance between the approximated lognormal pdf, for

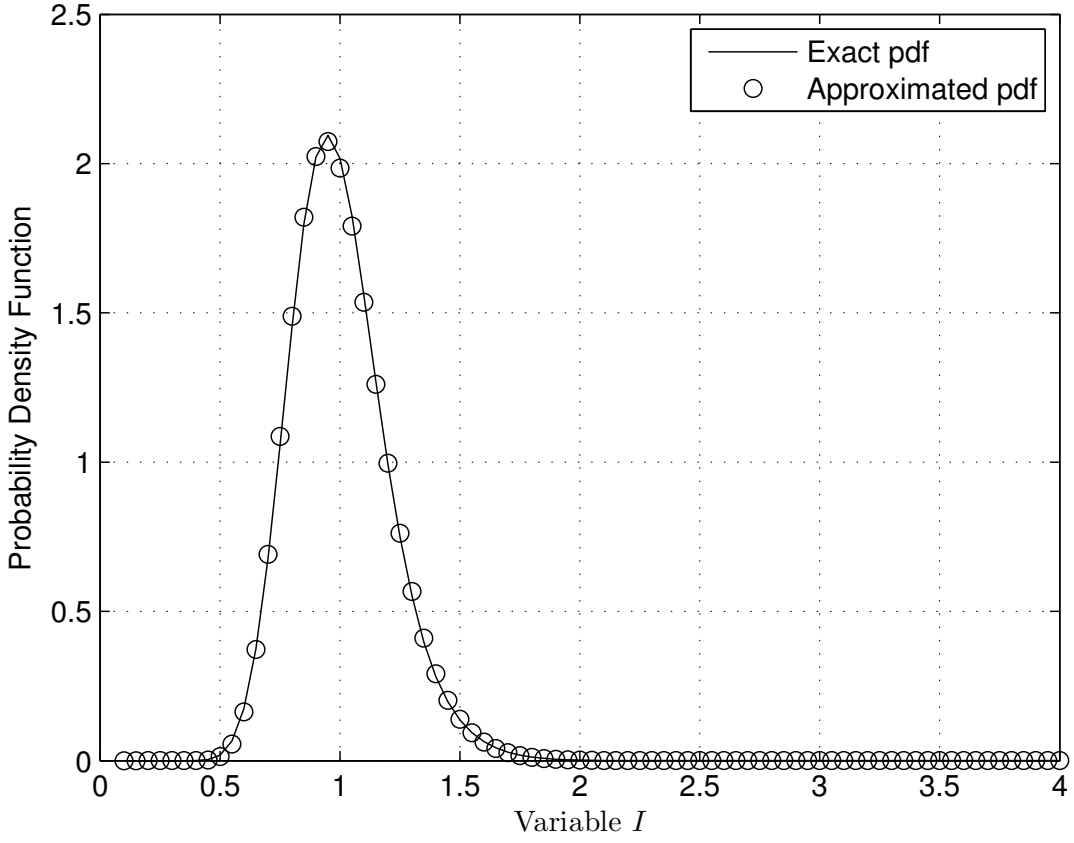

Figure 3.4: Comparison of an approximated pdf using $J = 3$ sample moments and an exact pdf for a lognormal fading channel with $\sigma = 0.25$.

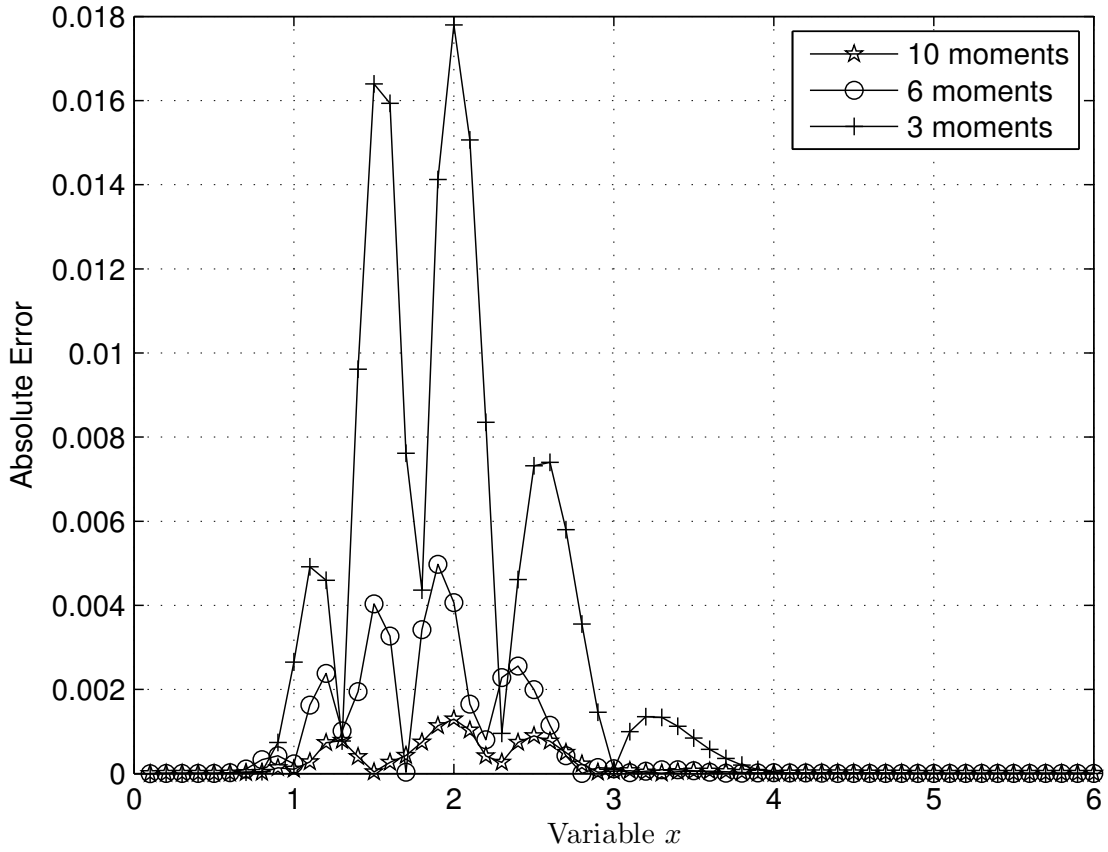

Figure 3.5: The absolute error between the approximated pdf and the exact lognormal pdf with $\sigma = 0.25$ and $J = 3, 6, 10$ sample moments.

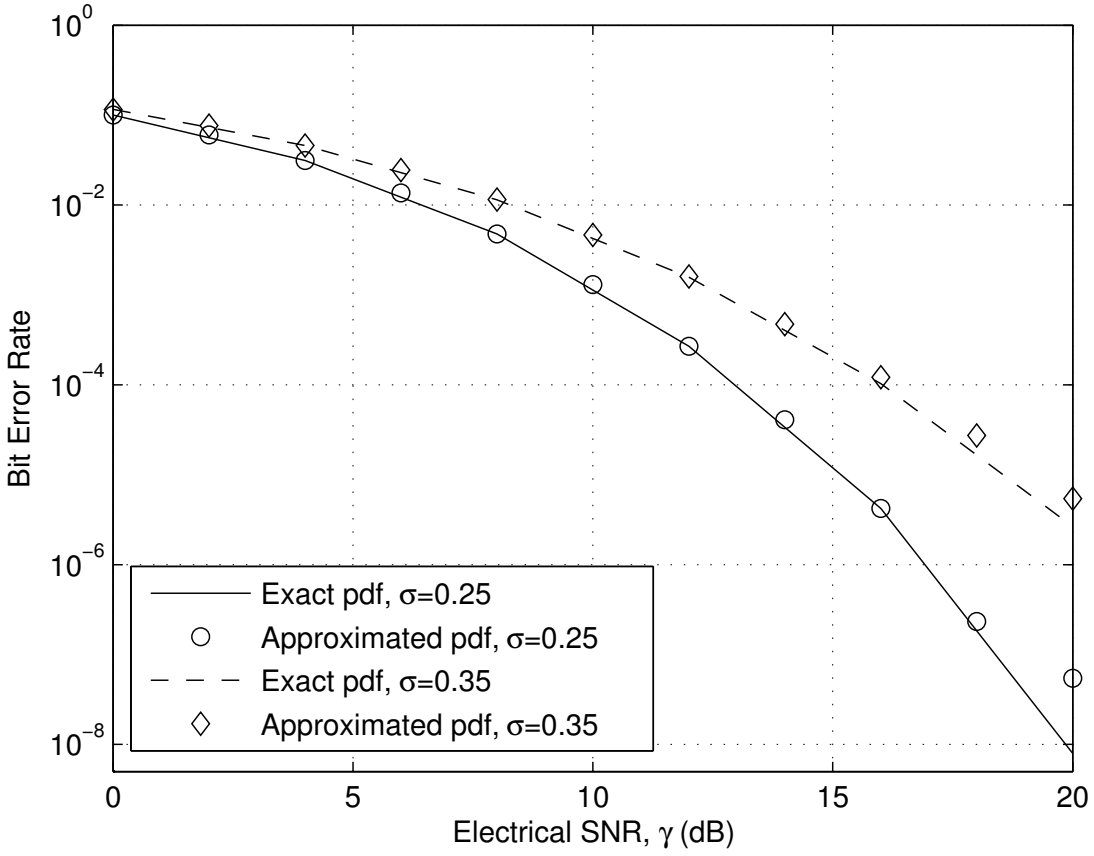

Figure 3.6: Comparison of BERs obtained by the approximated pdf and the exact lognormal pdf with $\xi = 0$ and $J = 3$ sample moments.

different values of σ with $J = 3$ sample moments, and the exact lognormal pdf. The two simulated error rate curves show good agreement over a wide range of SNR values. For the large SNR regime, the BER results from the approximate pdf have reduced accuracy, because the approximated pdf based on Laguerre polynomials is unable to characterize the behaviours of the lognormal pdf near the origin.

3.4 Summary

It is known that FSO systems operating with OOK and fixed detection thresholds can suffer from irreducible error floors and power inefficiency. With this in mind, the resulting error floors were analyzed here (and validated with simulations) for lognormal turbulence channels and quantified for the general case having low and high state offsets, i.e., for nonzero extinction ratios. It was shown that the error floors can be eliminated by using electrical-SNR-optimized detection thresholds that minimize the average BER. The electrical-SNR-optimized system with the Laguerre-polynomials-based approximate pdf for the turbulence was found to be effective for typical FSO systems, which operate at relatively low SNR values, as it yields near-optimal BER performance.

Chapter 4

Channel Parameters and Electrical SNR Estimation

In this chapter, the on-going challenges are addressed for the application of the lognormal-Rician turbulence model to FSO communication systems. MLE is applied to characterize the lognormal-Rician turbulence model parameters, and the EM algorithm is used to compute the MLE of the unknown parameters. As an FSO system that applies electrical-SNR-optimized detection must have knowledge of the electrical SNR, electrical SNR estimation is also investigated for FSO communication systems using IM/DD over the lognormal fading channels. Both MoME and MLE are studied for this electrical SNR estimation. The MSE is used to examine the performance of the estimators.

4.1 MLE for the Lognormal-Rician Shaping Parameter Estimation

The maximum likelihood principle is the most popular approach to obtain practical estimators. Its performance is optimal for large quantities of data, and it yields an approximation of the minimum-variance unbiased estimator.

Assuming that we have K independent and identically distributed (i.i.d.) observations of the lognormal-Rician distribution, $\boldsymbol{I} = [I[0] \quad ... \quad I[K-1]]^T$, with the unknown vectors $\boldsymbol{\theta} = [\sigma_z^2 \quad r]^T$,

the distribution of $\boldsymbol{I}$ can be written as

$$f_{\boldsymbol{I}}(\boldsymbol{I};\boldsymbol{\theta}) = \prod_{l=0}^{K-1} \frac{(1+r)e^{-r}}{\sqrt{2\pi}\sigma_z} \int_0^\infty \frac{dz}{z^2} I_0\left(2\left[\frac{(1+r)r}{z} I[l]\right]^{1/2}\right) \times \exp\left(-\frac{1+r}{z} I[l] - \frac{1}{2\sigma_z^2}\left(\ln z + \frac{1}{2}\sigma_z^2\right)^2\right). \tag{4.1}$$

The MLE of the unknown vector $\boldsymbol{\theta}$ is then obtained by maximizing the log-likelihood function

$$\begin{aligned} & L(\boldsymbol{I};\boldsymbol{\theta}) \\ & = \ln f(\boldsymbol{I};\boldsymbol{\theta}) \\ & = \sum_{l=0}^{K-1} \ln\left(\frac{(1+r)e^{-r}}{\sqrt{2\pi}\sigma_z} \int_0^\infty \frac{dz}{z^2} I_0\left(2\left[\frac{(1+r)r}{z} I[l]\right]^{1/2}\right)\right. \\ & \left. \times \exp\left(-\frac{1+r}{z} I[l] - \frac{1}{2\sigma_z^2}\left(\ln z + \frac{1}{2}\sigma_z^2\right)^2\right)\right). \end{aligned} \tag{4.2}$$

It is difficult to obtain closed-form estimates of the lognormal-Rician parameters, due to the integral form of the density function in (2.23), so the ensuring analysis uses the EM algorithm to find the MLE of $\boldsymbol{\theta}$ [57]. This method, although iterative in nature, is guaranteed under mild conditions to converge and produce a local maximum [58]. The vector $\boldsymbol{z} = [z[0] \quad \ldots \quad z[K-1]]^T$ is first defined, where each element of the vector follows the lognormal pdf

$$f(z[l];\sigma_z) = \frac{1}{\sqrt{2\pi}\sigma_z z[l]} \exp\left(-\frac{1}{2\sigma_z^2}\left(\ln z[l] + \frac{1}{2}\sigma_z^2\right)^2\right), \quad l = 0,1,\ldots,K-1. \tag{4.3}$$

By treating $\boldsymbol{z}$ as the unobserved data, we can write the complete-data log-likelihood function as

$$\begin{aligned} L(\boldsymbol{I},\boldsymbol{z};\boldsymbol{\theta}) &= \sum_{l=0}^{K-1} \ln f(z[l];\sigma_z) + \sum_{l=0}^{K-1} \ln f(I[l]|z[l];r) \\ &= K\Bigg\{ -\ln\sqrt{(2\pi\sigma_z^2)} + \ln(1+r) - \frac{5}{2K}\sum_{l=0}^{K-1}\ln z[l] \\ &\quad -\frac{\sigma_z^2}{8} - \frac{1}{2\sigma_z^2}\frac{1}{K}\sum_{l=0}^{K-1}(\ln z[l])^2 - \frac{1}{K}\sum_{l=0}^{K-1}\frac{1+r}{z[l]}I[l] \\ &\quad -r + \frac{1}{K}\sum_{l=0}^{K-1}\ln I_0\left(2\left[\frac{(1+r)r}{z[l]}I[l]\right]^{1/2}\right)\Bigg\} \end{aligned} \tag{4.4}$$

where

$$f(I[l]|z[l];r) = \frac{1+r}{z[l]} I_0\left(2\left[\frac{(1+r)r}{z[l]}I[l]\right]^{1/2}\right)\exp\left(-r-\frac{1+r}{z[l]}I[l]\right). \tag{4.5}$$

The resulting complete-data sufficient statistics are

$$T_1(\boldsymbol{z}) = \frac{1}{K}\sum_{l=0}^{K-1}\ln z[l] \tag{4.6a}$$

$$T_2(\boldsymbol{z}) = \frac{1}{K}\sum_{l=0}^{K-1}(\ln z[l])^2 \tag{4.6b}$$

$$T_3(\boldsymbol{z}) = -\frac{1}{K}\sum_{l=0}^{K-1}\frac{1+r}{z[l]}I[l] + \frac{1}{K}\sum_{l=0}^{K-1}\ln I_0\left(2\left[\frac{(1+r)r}{z[l]}I[l]\right]^{1/2}\right). \tag{4.6c}$$

The initial value of σ_z^2 is obtained by fitting the simple lognormal turbulence model, where $\hat{\sigma_z^2}^{(0)} = -\frac{2}{K}\sum_{l=0}^{K-1}\ln I[l]$. The initial value of the coherence parameter r can be obtained by solving the following polynomial equation [14, eq. (6)]

$$\begin{aligned} &\frac{[(\hat{r}^{(0)})^2 + 4\hat{r}^{(0)} + 2]^3}{[1+(\hat{r}^{(0)})^3][(\hat{r}^{(0)})^3 + 9(\hat{r}^{(0)})^2 + 18\hat{r}^{(0)} + 6]} \\ &= \frac{\left(\frac{1}{K}\sum_{l=0}^{K-1} I^2[l]\right)^3}{\frac{1}{K}\sum_{l=0}^{K-1} I^3[l]}. \end{aligned} \tag{4.7}$$

Iterations are then carried out with the expectation-step (E-step) and maximization-step (M-step) [58].

E-step: The E-step is carried out by computing

$$T_1\left(\boldsymbol{z};\hat{\boldsymbol{\theta}}^{(j)}\right) = \frac{1}{K}\sum_{l=0}^{K-1} E_{\boldsymbol{z}|\boldsymbol{I}}\left[\ln z[l]\,\middle|\,\boldsymbol{I};\hat{\boldsymbol{\theta}}^{(j)}\right] \tag{4.8}$$

$$T_2\left(\boldsymbol{z};\hat{\boldsymbol{\theta}}^{(j)}\right) = \frac{1}{K}\sum_{l=0}^{K-1} E_{\boldsymbol{z}|\boldsymbol{I}}\left[(\ln z[l])^2\,\middle|\,\boldsymbol{I};\hat{\boldsymbol{\theta}}^{(j)}\right] \tag{4.9}$$

$$\begin{aligned} T_3\left(\boldsymbol{z};\hat{\boldsymbol{\theta}}^{(j)}\right) &= -\frac{1}{K}\sum_{l=0}^{K-1}(1+r)E_{\boldsymbol{z}|\boldsymbol{I}}\left[z^{-1}[l]\,\middle|\,\boldsymbol{I};\hat{\boldsymbol{\theta}}^{(j)}\right] I[l] \\ &+ \frac{1}{K}\sum_{l=0}^{K-1} E_{\boldsymbol{z}|\boldsymbol{I}}\left[\ln I_0\left(2\left[\frac{(1+r)r}{z[l]}I[l]\right]^{1/2}\right)\middle|\,\boldsymbol{I};\hat{\boldsymbol{\theta}}^{(j)}\right] \end{aligned} \tag{4.10}$$

where $\hat{\boldsymbol{\theta}}^{(j)} = [\hat{\sigma}_z^{2(j)} \quad \hat{r}^{(j)}]^T$ is an estimate of $\boldsymbol{\theta}$ in the jth iteration. For the computations carried out as part of the E-step, it is noted that the expectation expressions in (8)-(10) are all functions of $z[l]$, so the conditional expectations in (8)-(10) can be expressed as

$$E_{\boldsymbol{z}|\boldsymbol{I}}\left[g(z[l])\,\middle|\,\boldsymbol{I};\hat{\boldsymbol{\theta}}^{(j)}\right] = \int g(z[l])f(z[l]\,\middle|\,\boldsymbol{I};\hat{\boldsymbol{\theta}}^{(j)})dz[l] \tag{4.11}$$

where $f(z[l]|\boldsymbol{I}[l];\hat{\boldsymbol{\theta}}^{(j)}) = \frac{f(I[l]|z[l];\hat{\boldsymbol{\theta}}^{(j)})f(z[l];\hat{\boldsymbol{\theta}}^{(j)})}{f(I[l];\hat{\boldsymbol{\theta}}^{(j)})}$ and where

$$\begin{aligned} f(I[l]|z[l];\hat{\boldsymbol{\theta}}^{(j)}) &= \exp\left(-\hat{r}^{(j)} - \frac{1+\hat{r}^{(j)}}{z[l]}I[l]\right) \\ &\times \frac{1+\hat{r}^{(j)}}{z[l]} I_0\left(2\left[\frac{(1+\hat{r}^{(j)})\hat{r}^{(j)}}{z[l]}I[l]\right]^{1/2}\right) \end{aligned} \tag{4.12}$$

$$\begin{aligned} f(z[l];\hat{\boldsymbol{\theta}}^{(j)}) &= \frac{1}{\sqrt{2\pi}\hat{\sigma}_z^{(j)}z[l]} \\ &\times \exp\left(-\frac{1}{2\left(\hat{\sigma}_z^{(j)}\right)^2}\left[\ln z[l] + \frac{1}{2}\left(\hat{\sigma}_z^{(j)}\right)^2\right]^2\right) \end{aligned} \tag{4.13}$$

and

$$f(I[l];\hat{\boldsymbol{\theta}}^{(j)}) = \frac{(1+\hat{r}^{(j)})e^{-\hat{r}^{(j)}}}{\sqrt{2\pi}\hat{\sigma}_z^{(j)}} \int_0^\infty I_0\left(2\left[\frac{(1+\hat{r}^{(j)})\hat{r}^{(j)}}{z[l]}I[l]\right]^{1/2}\right) \times \exp\left(-\frac{1+r}{z[l]}I[l] - \frac{1}{2\left(\hat{\sigma}_z^{(j)}\right)^2}\left[\ln z[l] + \frac{1}{2}\left(\hat{\sigma}_z^{(j)}\right)^2\right]^2\right)\frac{dz}{z[l]^2}. \tag{4.14}$$

M-step: The M-step is carried out by computing

$$\hat{\sigma_z^2}^{(j+1)} = T_2\left(\boldsymbol{z};\hat{\boldsymbol{\theta}}^{(j)}\right) - \left(T_1\left(\boldsymbol{z};\hat{\boldsymbol{\theta}}^{(j)}\right)\right)^2 \tag{4.15}$$

and finding $\hat{r}^{(j+1)}$ such that it maximizes

$$\hat{r}^{(j+1)} = \arg\max_r \left\{T_3\left(\boldsymbol{z};\hat{\boldsymbol{\theta}}^{(j)}\right)\right\} \tag{4.16}$$

where $\hat{\boldsymbol{\theta}}^{(j+1)} = [\hat{\sigma_z^2}^{(j+1)} \quad \hat{r}^{(j+1)}]^T$ is the new estimate of $\boldsymbol{\theta}$. For the EM algorithm, the conditional expectation of the complete data is nondecreasing until it reaches a fixed point. This fixed point is the MLE of $\boldsymbol{\theta}$, i.e., $\hat{\boldsymbol{\theta}}_{ML} = [\hat{\sigma}^2_{z,ML} \quad \hat{r}_{ML}]^T$.

4.2 Electrical SNR Estimation

As the electrical-SNR-optimized detection threshold introduced in Chapter 3 requires knowledge of the state offset ξ and electrical SNR γ, it is necessary to estimate ξ and γ. MoME and MLE are used for such estimation in this section.

It is assumed that there are $2L$ sampled signals during the observation interval. The vectors $\mathbf{R} = [r[0] \quad ... \quad r[2L-1]]^T$, $\mathbf{I}_f = [I[0] \quad ... \quad I[2L-1]]^T$, and $\mathbf{N} = [n[0] \quad ... \quad n[2L-1]]^T$ represent the received signal vector, fading coefficient vector, and noise vector, respectively. Assuming that a training sequence of length $2L$ is transmitted with L consecutive 1's followed by L consecutive

0's, one can write the received signal at the lth bit interval when bit 1 is transmitted as

$$r[l]|s_1 = (2+\xi)I[l]+n[l],\ \ l=0,1,...,L-1 \tag{4.17}$$

where $I[l]$ and $n[l]$ represent the fading coefficient and noise during the lth bit interval, respectively. Similarly, if L 0's are transmitted, the received signal at the kth bit interval can be written as

$$r[k]|s_0 = \xi I[k]+n[k],\ \ k=L,L+1,...,2L-1. \tag{4.18}$$

4.2.1 Method of Moments Estimation

Using (4.17) and (4.18), one can obtain the estimation of ξ as

$$\hat{\xi} = \frac{\frac{1}{L}\sum_{k=L}^{2L-1} r[k]|s_0}{\frac{1}{2L}\sum_{l=0}^{L-1} r[l]|s_1 - \frac{1}{2L}\sum_{k=L}^{2L-1} r[k]|s_0}. \tag{4.19}$$

To assess the performance of the moment estimator $\hat{\xi}$, approximate expressions can be derived for the mean and variance of $\hat{\xi}$ when the sample size is asymptotically large. Assuming the statistics $\mathbf{T} = [T_1 \quad T_2]^T$, where $T_1 = \frac{1}{L}\sum_{l=0}^{L-1} r[l]|s_1$ and $T_2 = \frac{1}{L}\sum_{k=L}^{2L-1} r[k]|s_0$, one can obtain the covariance matrix as

$$\begin{aligned}\mathbf{C}_T &= \begin{pmatrix} \mathrm{Var}[T_1] & \mathrm{Cov}[T_1,T_2] \\ \mathrm{Cov}[T_2,T_1] & \mathrm{Var}[T_2] \end{pmatrix} \\ &= \begin{pmatrix} \frac{1}{L}[\sigma_g^2 + (2+\xi)^2\mathrm{Var}[I]] & 0 \\ 0 & \frac{1}{L}(\sigma_g^2 + \xi^2\mathrm{Var}[I]) \end{pmatrix}.\end{aligned} \tag{4.20}$$

Here, $\mathrm{Var}[\cdot]$ denotes the variance, and $\mathrm{Cov}[\cdot,\cdot]$ denotes covariance of two RVs. The estimator $\hat{\xi}$ can be rewritten as

$$\hat{\xi} \stackrel{\Delta}{=} \varphi(\mathbf{T}) = \frac{2T_2}{T_1 - T_2}. \tag{4.21}$$

The estimator in (4.19) is consistent, i.e., $\hat{\xi} \xrightarrow{Pr} \xi$ as $L \longrightarrow \infty$, and is asymptotically Gaussian

distributed, i.e., $\sqrt{L}(\hat{\xi}-\xi) \xrightarrow{L} \mathcal{N}(0,\sigma_{\hat{\xi}}^2)$. Performing a first-order Taylor expansion of $\varphi(\cdot)$ about the point $\mathbf{T}=E[\mathbf{T}]$ gives [59]

$$\hat{\xi} \approx \varphi(\mathbf{T})\Big|_{\mathbf{T}=E[\mathbf{T}]} + \sum_{i=1}^{2} \frac{\partial \varphi}{\partial T_i}\Big|_{\mathbf{T}=E[\mathbf{T}]} (T_i - E[T_i]) \tag{4.22}$$

where $E[\mathbf{T}] = \begin{bmatrix}(2+\xi)E[I] & \xi E[I]\end{bmatrix}^T$. Taking the expectation of (4.22) gives

$$E[\hat{\xi}] \approx \varphi(\mathbf{T})\Big|_{\mathbf{T}=E[\mathbf{T}]} = \xi \tag{4.23}$$

and the asymptotic variance of $\hat{\xi}$ can be expressed as [58]

$$\begin{aligned}\sigma_{\hat{\xi}}^2 =& \mathrm{Var}[\hat{\xi}] = \frac{\partial \varphi}{\partial T_i}\Big|^{T}_{\mathbf{T}=E[\mathbf{T}]} \mathbf{C}_{\mathbf{T}} \frac{\partial \varphi}{\partial T_i}\Big|_{\mathbf{T}=E[\mathbf{T}]} \\ =& \frac{\sigma_g^2[\xi^2+(2+\xi)^2]+2\xi^2(2+\xi)^2\mathrm{Var}[I]}{4L(E[I])^2}.\end{aligned} \tag{4.24}$$

Using (4.17) and (4.18), one can obtain the estimation of the turbulence mean $m=\exp(\mu+\sigma^2/2)$ and N_0, respectively, as

$$\hat{m} = \frac{1}{2L}\sum_{l=0}^{L-1} r[l]|s_1 - \frac{1}{2L}\sum_{k=L}^{2L-1} r[k]|s_0 \tag{4.25}$$

and

$$\hat{N}_0 = 2\frac{(\hat{m}|s_1)^2\,\hat{\mu}_r[2]|s_0 - (\hat{m}|s_0)^2\,\hat{\mu}_r[2]|s_1}{(\hat{m}|s_1)^2 - (\hat{m}|s_0)^2} \tag{4.26}$$

where

$$\hat{m}|s_1 = \frac{1}{L}\sum_{l=0}^{L-1} r[l]|s_1 \tag{4.27}$$

$$\hat{\mu}_r[2]|s_0 = \frac{1}{L}\sum_{k=L}^{2L-1} r^2[k]|s_0 \tag{4.28}$$

$$\hat{m}|s_0 = \frac{1}{L}\sum_{k=L}^{2L-1} r[k]|s_0 \tag{4.29}$$

and

$$\hat{\mu}_r[2]|s_1 = \frac{1}{L}\sum_{l=0}^{L-1} r^2[l]|s_1. \tag{4.30}$$

Using (4.25) and (4.26), one can obtain the estimation of γ as

$$\hat{\gamma} = \frac{\hat{m}^2}{\hat{N}_0} = \frac{(\hat{m}|s_1 - \hat{m}|s_0)^2 \left[(\hat{m}|s_1)^2 - (\hat{m}|s_0)^2\right]}{8\left[(\hat{m}|s_1)^2 \hat{\mu}_r[2]|s_0 - (\hat{m}|s_0)^2 \hat{\mu}_r[2]|s_1\right]}. \tag{4.31}$$

4.2.2 Maximum Likelihood Estimation

For the MLE, we transmit a training sequence consisting of $2L$ consecutive 1's. Assuming the received signal model is the same as (4.17), one can write the pdf of the received signal as [23]

$$\begin{aligned} f(r[k]|s_1;\boldsymbol{\theta}_\gamma) =& f_I(r[k]) * f_N(r[k]) \\ =& \int_0^\infty \frac{1}{\sqrt{2\pi}\sigma x}\exp\left(-\frac{(\ln x - \ln(2+\xi) - \mu)^2}{2\sigma^2}\right) \\ & \times \frac{1}{\sqrt{\pi N_0}}\exp\left(-\frac{(r[k]-x)^2}{N_0}\right) dx \end{aligned} \tag{4.32}$$

where $\boldsymbol{\theta}_\gamma = [\mu \quad \sigma^2 \quad N_0 \quad \xi]^T$ denotes the unknown vector, and $f_N(r[k]) = \frac{1}{\sqrt{\pi N_0}}\exp\left(-\frac{r^2[k]}{N_0}\right)$ is the noise pdf. Assuming that the components of the received signal vector $\mathbf{R}$ are independent, we can write the pdf of the received signal when s_1 is true as

$$\begin{aligned} f(\mathbf{R};\boldsymbol{\theta}_\gamma) =& \prod_{k=0}^{2L-1} f(r[k]|s_1;\boldsymbol{\theta}_\gamma) \\ =& \prod_{k=0}^{2L-1} \int_0^\infty \frac{1}{\sqrt{2\pi}\sigma x}\exp\left(-\frac{(\ln x - \ln(2+\xi) - \mu)^2}{2\sigma^2}\right) \\ & \times \frac{1}{\sqrt{\pi N_0}}\exp\left(-\frac{(r[k]-x)^2}{N_0}\right) dx. \end{aligned} \tag{4.33}$$

The MLE of the unknown vector $\boldsymbol{\theta}_\gamma$ is obtained by maximizing the log-likelihood function

$$\begin{aligned} L(\mathbf{R};\boldsymbol{\theta}_\gamma) &= \ln f(\mathbf{R};\boldsymbol{\theta}_\gamma) \\ &= \ln \prod_{k=0}^{2L-1} f_I(r[k]) * f_N(r[k]) \\ &= \sum_{k=0}^{2L-1} \ln \int_0^\infty \frac{1}{\sqrt{2\pi}\sigma x} \exp\left(-\frac{(\ln x - \ln(2+\xi)-\mu)^2}{2\sigma^2}\right) \\ &\quad \times \frac{1}{\sqrt{\pi N_0}} \exp\left(-\frac{(r[k]-x)^2}{N_0}\right) dx. \end{aligned} \tag{4.34}$$

Taking the derivative of (4.34) with respect to the unknown parameter and setting it equal to zero, we can obtain the MLE of the unknown vector $\boldsymbol{\theta}_\gamma$. As it is difficult to obtain a closed-form expression for each unknown parameter, the EM algorithm can be implemented numerically to determine the MLE.

In order to simplify the problem, we decompose the original data sets into the independent data sets $y_1[k] = I[k]$ and $y_2[k] = n[k]$, where $y_1[k]$ and $y_2[k]$ are the complete data, and they are related to the original data as $r[k] = y_1[k] + y_2[k]$. Instead of maximizing $\ln f(\mathbf{R};\boldsymbol{\theta}_\gamma)$, we can maximize $\ln f(\mathbf{Y};\boldsymbol{\theta}_\gamma)$, where $\mathbf{Y} = [\boldsymbol{y}_1 \quad \boldsymbol{y}_2]^T$, $\boldsymbol{y}_1 = [y_1[0] \quad \ldots \quad y_1[2L-1]]^T$ and $\boldsymbol{y}_2 = [y_2[0] \quad \ldots \quad y_2[2L-1]]^T$. Since $y_1[k] = I[k]$, we have

$$\begin{aligned} \ln f(y_1[k];\boldsymbol{\theta}_\gamma) &= \ln\left(\frac{1}{\sqrt{2\pi\sigma^2}y_1[k]} \exp\left(-\frac{(\ln y_1[k] - \ln(2+\xi)-\mu)^2}{2\sigma^2}\right)\right) \\ &= -\ln\sqrt{2\pi\sigma^2} - \ln y_1[k] - \frac{(\ln y_1[k] - \ln(2+\xi)-\mu)^2}{2\sigma^2}. \end{aligned} \tag{4.35}$$

Similarly, we have

$$\begin{aligned} \ln f(y_2[k];\boldsymbol{\theta}_\gamma) &= \ln\left(\frac{1}{\sqrt{\pi N_0}} \exp\left(-\frac{y_2^2[k]}{N_0}\right)\right) \\ &= -\ln\sqrt{\pi N_0} - \frac{y_2^2[k]}{N_0}. \end{aligned} \tag{4.36}$$

Assuming $\hat{\boldsymbol{\theta}}_\gamma^{(j)} = [\hat{\mu}^{(j)} \quad (\hat{\sigma}^2)^{(j)} \quad (\hat{N}_0)^{(j)} \quad (\xi)^{(j)}]^T$ is an estimate of $\boldsymbol{\theta}_\gamma$ in the jth iteration, each

iteration of the EM algorithm can be carried out with the following E- and M-steps.

E-step: This step determines the conditional expectation of the complete data

$$\begin{aligned} U(\boldsymbol{\theta}_\gamma, \hat{\boldsymbol{\theta}}_\gamma^{(j)}) &= E_{\mathbf{Y}|\mathbf{R};\hat{\boldsymbol{\theta}}_\gamma^{(j)}}[\ln f(\mathbf{Y};\boldsymbol{\theta}_\gamma)] \\ &= E_{\boldsymbol{y}_1|\mathbf{R};\hat{\boldsymbol{\theta}}_\gamma^{(j)}}[\ln f(\boldsymbol{y}_1;\boldsymbol{\theta}_\gamma)] + E_{\boldsymbol{y}_2|\mathbf{R};\hat{\boldsymbol{\theta}}_\gamma^{(j)}}[\ln f(\boldsymbol{y}_2;\boldsymbol{\theta}_\gamma)] \\ &= \int \ln f(\boldsymbol{y}_1;\boldsymbol{\theta}_\gamma) f(\boldsymbol{y}_1|\mathbf{R};\hat{\boldsymbol{\theta}}_\gamma^{(j)}) d\boldsymbol{y}_1 + \int \ln f(\boldsymbol{y}_2;\boldsymbol{\theta}_\gamma) f(\boldsymbol{y}_2|\mathbf{R};\hat{\boldsymbol{\theta}}_\gamma^{(j)}) d\boldsymbol{y}_2. \end{aligned} \tag{4.37}$$

where we have

$$f(\boldsymbol{y}_1|\mathbf{R};\hat{\boldsymbol{\theta}}_\gamma^{(j)}) = \frac{f(\mathbf{R}|\boldsymbol{y}_1;\hat{\boldsymbol{\theta}}_\gamma^{(j)}) f(\boldsymbol{y}_1;\hat{\boldsymbol{\theta}}_\gamma^{(j)})}{f(\mathbf{R};\hat{\boldsymbol{\theta}}_\gamma^{(j)})} \tag{4.38}$$

and

$$f(\boldsymbol{y}_2|\mathbf{R};\hat{\boldsymbol{\theta}}_\gamma^{(j)}) = \frac{f(\mathbf{R}|\boldsymbol{y}_2;\hat{\boldsymbol{\theta}}_\gamma^{(j)}) f(\boldsymbol{y}_2;\hat{\boldsymbol{\theta}}_\gamma^{(j)})}{f(\mathbf{R};\hat{\boldsymbol{\theta}}_\gamma^{(j)})} \tag{4.39}$$

and where

$$\begin{aligned} f(\mathbf{R}|\boldsymbol{y}_1;\hat{\boldsymbol{\theta}}_\gamma^{(j)}) = \prod_{k=0}^{2L-1} & \frac{1}{\sqrt{2\pi(\hat{\sigma}^2)^{(j)}}(r[k]-y_1[k])} \\ & \times \exp\left(-\frac{(\ln(r[k]-y_1[k]) - \ln(2+(\xi)^{(j)}) - \hat{\mu}^{(j)})^2}{2(\hat{\sigma}^2)^{(j)}}\right) \end{aligned} \tag{4.40}$$

and

$$f(\mathbf{R}|\boldsymbol{y}_2;\hat{\boldsymbol{\theta}}_\gamma^{(j)}) = \prod_{k=0}^{2L-1} \frac{1}{\sqrt{\pi(N_0)^{(j)}}} \exp\left(-\frac{(r[k]-y_2[k])^2}{(N_0)^{(j)}}\right). \tag{4.41}$$

M-step: This step maximizes (4.37) with respect to $\boldsymbol{\theta}_\gamma$, by way of

$$\boldsymbol{\theta}_\gamma^{(j+1)} = \arg\max_{\boldsymbol{\theta}_\gamma} U(\boldsymbol{\theta}_\gamma, \hat{\boldsymbol{\theta}}_\gamma^{(j)}) \tag{4.42}$$

where $\hat{\boldsymbol{\theta}}_\gamma^{(j+1)}$ is the new estimate of $\boldsymbol{\theta}_\gamma$. For the EM algorithm, the conditional expectation of the

complete data is nondecreasing until it reaches a fixed point. This fixed point is the MLE of $\boldsymbol{\theta}_\gamma$

$$\hat{\boldsymbol{\theta}}_{\gamma,ML} = [\hat{\mu}_{ML} \quad \hat{\sigma}^2_{ML} \quad \hat{N}_{0,ML} \quad \hat{\xi}_{ML}]^T. \tag{4.43}$$

Based on the invariance property of the MLE, we obtain the MLE of μ_I as $\hat{\mu}_{I,ML} = \exp\left(\hat{\mu}_{ML} + \frac{\hat{\sigma}^2_{ML}}{2}\right)$. The MLE of γ can be obtained as

$$\hat{\gamma}_{ML} = \frac{(\hat{\mu}_{I,ML})^2}{\hat{N}_{0,ML}} = \frac{\left(\exp\left(\hat{\mu}_{ML} + \frac{\hat{\sigma}^2_{ML}}{2}\right)\right)^2}{\hat{N}_{0,ML}}. \tag{4.44}$$

The Cramér-Rao lower bound (CRLB) of $\hat{\gamma}$ can be calculated using [58]

$$\text{Var}[\hat{\gamma}] \geq \begin{bmatrix} \frac{\partial\gamma}{\partial\mu} & \frac{\partial\gamma}{\partial\sigma^2} & \frac{\partial\gamma}{\partial N_0} & \frac{\partial\gamma}{\partial\xi} \end{bmatrix} \mathbf{I}^{-1}(\boldsymbol{\theta}_\gamma) \begin{bmatrix} \frac{\partial\gamma}{\partial\mu} & \frac{\partial\gamma}{\partial\sigma^2} & \frac{\partial\gamma}{\partial N_0} & \frac{\partial\gamma}{\partial\xi} \end{bmatrix}^T \tag{4.45}$$

where $\mathbf{I}(\boldsymbol{\theta}_\gamma)$ is the Fisher information matrix that can be found as

$$\mathbf{I}(\boldsymbol{\theta}_\gamma) = \begin{bmatrix} -E\left[\frac{\partial^2 \ln f(\mathbf{R};\boldsymbol{\theta}_\gamma)}{\partial m^2}\right] & -E\left[\frac{\partial^2 \ln f(\mathbf{R};\boldsymbol{\theta}_\gamma)}{\partial m \partial\sigma^2}\right] & -E\left[\frac{\partial^2 \ln f(\mathbf{R};\boldsymbol{\theta}_\gamma)}{\partial m \partial N_0}\right] & -E\left[\frac{\partial^2 \ln f(\mathbf{R};\boldsymbol{\theta}_\gamma)}{\partial m \partial\xi}\right] \\ -E\left[\frac{\partial^2 \ln f(\mathbf{R};\boldsymbol{\theta}_\gamma)}{\partial\sigma^2 \partial m}\right] & -E\left[\frac{\partial^2 \ln f(\mathbf{R};\boldsymbol{\theta}_\gamma)}{(\partial\sigma^2)^2}\right] & -E\left[\frac{\partial^2 \ln f(\mathbf{R};\boldsymbol{\theta}_\gamma)}{\partial\sigma^2 \partial N_0}\right] & -E\left[\frac{\partial^2 \ln f(\mathbf{R};\boldsymbol{\theta}_\gamma)}{\partial\sigma^2 \partial\xi}\right] \\ -E\left[\frac{\partial^2 \ln f(\mathbf{R};\boldsymbol{\theta}_\gamma)}{\partial N_0 \partial m}\right] & -E\left[\frac{\partial^2 \ln f(\mathbf{R};\boldsymbol{\theta}_\gamma)}{\partial N_0 \partial\sigma^2}\right] & -E\left[\frac{\partial^2 \ln f(\mathbf{R};\boldsymbol{\theta}_\gamma)}{\partial N_0^2}\right] & -E\left[\frac{\partial^2 \ln f(\mathbf{R};\boldsymbol{\theta}_\gamma)}{\partial N_0 \partial\xi}\right] \\ -E\left[\frac{\partial^2 \ln f(\mathbf{R};\boldsymbol{\theta}_\gamma)}{\partial\xi \partial m}\right] & -E\left[\frac{\partial^2 \ln f(\mathbf{R};\boldsymbol{\theta}_\gamma)}{\partial\xi \partial\sigma^2}\right] & -E\left[\frac{\partial^2 \ln f(\mathbf{R};\boldsymbol{\theta}_\gamma)}{\partial\xi \partial N_0}\right] & -E\left[\frac{\partial^2 \ln f(\mathbf{R};\boldsymbol{\theta}_\gamma)}{\partial\xi^2}\right] \end{bmatrix}. \tag{4.46}$$

4.3 Numerical Results

To evaluate the estimator performance, the MSE of the estimator $\hat{\boldsymbol{\theta}}$ is studied. The MSE is $\text{MSE}[\hat{\boldsymbol{\theta}}] = \text{Var}[\hat{\boldsymbol{\theta}}] + (E[\hat{\boldsymbol{\theta}}] - \boldsymbol{\theta})^2$, where $\text{Var}[\hat{\boldsymbol{\theta}}]$ is the variance of the estimator, i.e., $\text{Var}[\hat{\boldsymbol{\theta}}] = \frac{1}{M-1}\sum_{i=0}^{M-1}(\hat{\boldsymbol{\theta}}_i - \bar{\hat{\boldsymbol{\theta}}})^2$, $\bar{\hat{\boldsymbol{\theta}}}$ is the sample mean of the estimator, and $E[\hat{\boldsymbol{\theta}}] = \frac{1}{M}\sum_{i=0}^{M-1}\hat{\boldsymbol{\theta}}_i$ is the mean of the estimator [60]. The simulation uses $K = 1,000$ data samples to estimate the lognormal-Rician parameters and $M = 100$ trials to calculate the MSE of the estimator.

In Fig. 4.1, we present the simulated MSE and NMSE performance of $\hat{r}$ and $\hat{\sigma}_z^2$ when $\sigma_z^2 = 0.25$ and r ranges from 1 to 9. The NMSE is defined as the MSE scaled by the true value of the

estimator. The performance trends at or above $r = 2$ are especially noteworthy. Increasing the value of r decreases the NMSE of $\hat{r}$ but it does not change the NMSE of $\hat{\sigma}_z^2$ to any great extent. Thus, changes to the value of r have minimal effects on the estimation performance of σ_z^2, and the MLE is insensitive to the value of r. The same conclusion can be seen for the MSE of $\hat{r}$ and $\hat{\sigma}_z^2$, which remain relatively flat as r increases.

In Fig. 4.2, we present the simulated MSE and NMSE performance of $\hat{r}$ and $\hat{\sigma}_z^2$ when $r = 4$ and σ_z^2 ranges from 0.1 to 0.8. From the figure, we note that the MSE of $\hat{\sigma}_z^2$ increases with the value of σ_z^2 while the MSE performance curve of $\hat{r}$ stays flat with changing values of σ_z^2. It can be seen that the MLE performance of the lognormal-Rician parameter σ_z^2 is insensitive to the value of r but sensitive to the value of σ_z^2, while the MLE performance of the lognormal-Rician parameter r is insensitive to both the values of r and σ_z^2.

Overall, the results for the MSE and NMSE in Figs. 4.1 and 4.2 are indicative of accurate estimation. The MSE and NMSE performance is comparable with that of the prior study [14], albeit with three orders of magnitude fewer data samples being required for the method proposed here.

In order to evaluate the estimator performance, the sample variance of the electrical SNR estimator is compared with the CRLB. The variance of the electrical SNR estimator is given by

$$\hat{\sigma}_{\hat{\gamma}}^2 = \frac{1}{M-1} \sum_{i=0}^{M-1} (\hat{\gamma}_i - \bar{\hat{\gamma}})^2 \tag{4.47}$$

where $\hat{\gamma}_i$ is the estimation by using MoME or MSE at the ith trials, M represents the total number of trails, and $\bar{\hat{\gamma}}$ is the sample mean of the electrical SNR estimator. In order to assess the estimator, Monte Carlo simulations are used to obtain $\hat{\sigma}_{\hat{\gamma}}^2$. In the simulation, different training sequence lengths are used to estimate the mean and noise variance, $M = 1 \times 10^4$ trials are used to calculate the variance of the electrical SNR estimator, and ξ is set at 0.2. Figure 4.3 plots the normalized sample variance of the electrical SNR estimator, which is defined as the sample variance scaled by γ, versus the average electrical SNR. It is shown that the normalized sample variance for MLE attains the normalized CRLB, which is obtained by scaling the CRLB by γ. However, there is a discrepency

between the normalized sample variance for MoME and the normalized CRLB for SNR values greater than 12 dB due to the inaccurate estimation of the noise variance. It can be shown that the discrepency between the normalized sample variance for MoME and the normalized CRLB will disappear when $\xi = 0$. In this case, the received signal is characterized completely by the noise when 0 is transmitted. Thus, the noise variance can be accurately estimated by transmitting a training sequence with consecutive 0's. (When $\xi \neq 0$ and 0 is transmitted, the received signal is the noise as well as the fading coefficient term, and this leads to inaccurate estimation of the noise variance if a training sequence is transmitted with consecutive 0's.)

In Fig. 4.4, we compare the BER performance between the estimated electrical SNR, for different values of σ, and the exact electrical SNR. The pdf of the lognormal turbulence model is approximated by using Laguerre-polynomials with $J = 3$ sample moments. The two simulated error rate curves show good agreement over a wide range of SNR values.

4.4 Summary

The challenges were addressed in this chapter for the application of the lognormal-Rician turbulence model to FSO communications. The proposed technique used MLE, to estimate the parameters of the lognormal-Rician fading channels and the EM algorithm, to compute the MLE of the unknown parameters. The performance was simulated in terms of MSE. Numerical results showed that MLE with the EM algorithm can effectively characterize FSO communications over lognormal-Rician fading channels, given a wide range of turbulence conditions. Accurate estimation was shown with reduced demands on the quantity of data samples.

For FSO communication systems, the reduced demand on the number of data samples for the proposed method leads to a shortened latency, being on the order of $10^3 \times 10^{-3}$ seconds = 1 second, for turbulence-induced fading on a millisecond timescale. (In contrast, the method introduced in [14] demands a large number of data samples, on the order of 10^6, and it becomes necessary to operate with a latency on the order of $10^6 \times 10^{-3}$ seconds = 10^3 seconds.) The second-long latency enabled by the work in this chapter is sufficiently short to support electrical-SNR-optimized

adaptive detection in FSO channels exhibiting stationary statistics, i.e., constant channel model parameters, over several seconds or minutes. To the authors' best knowledge, this is the first practical implementation capable of electrical-SNR-optimized adaptive detection using the highly-accurate lognormal-Rician turbulence model.

Electrical SNR estimation was studied for FSO systems using IM/DD over lognormal fading channels. Training sequences based on MoME and MLE were proposed. It was found that MoME could produce a closed-form expression for the estimator, while MLE requires numerical computation to produce the estimator. The estimator performance was examined in terms of MSE. Monte Carlo simulations were used to assess the performance of the proposed estimators. The proposed estimators can be effective tools for future FSO systems implementing electrical-SNR-optimized detection.

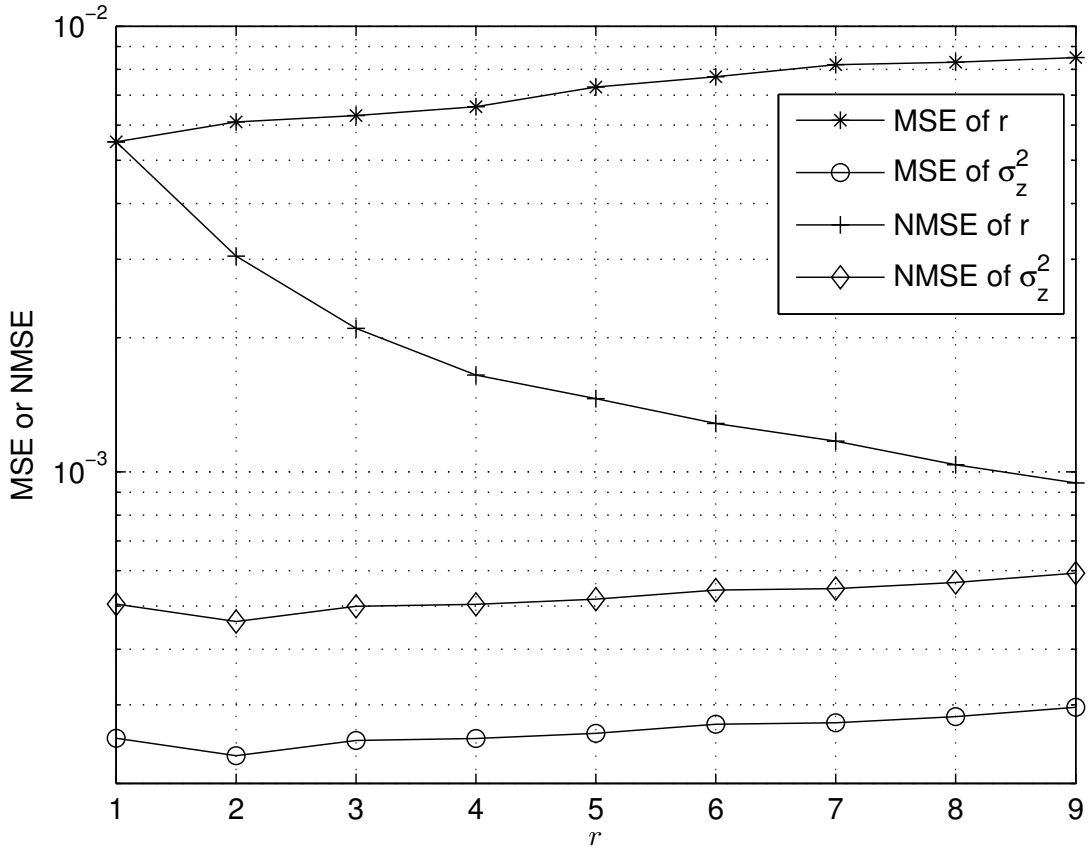

Figure 4.1: MSE and NMSE performance of the maximum likelihood estimators for the lognormal-Rician parameters r and σ_z^2 with $\sigma_z^2 = 0.25$.

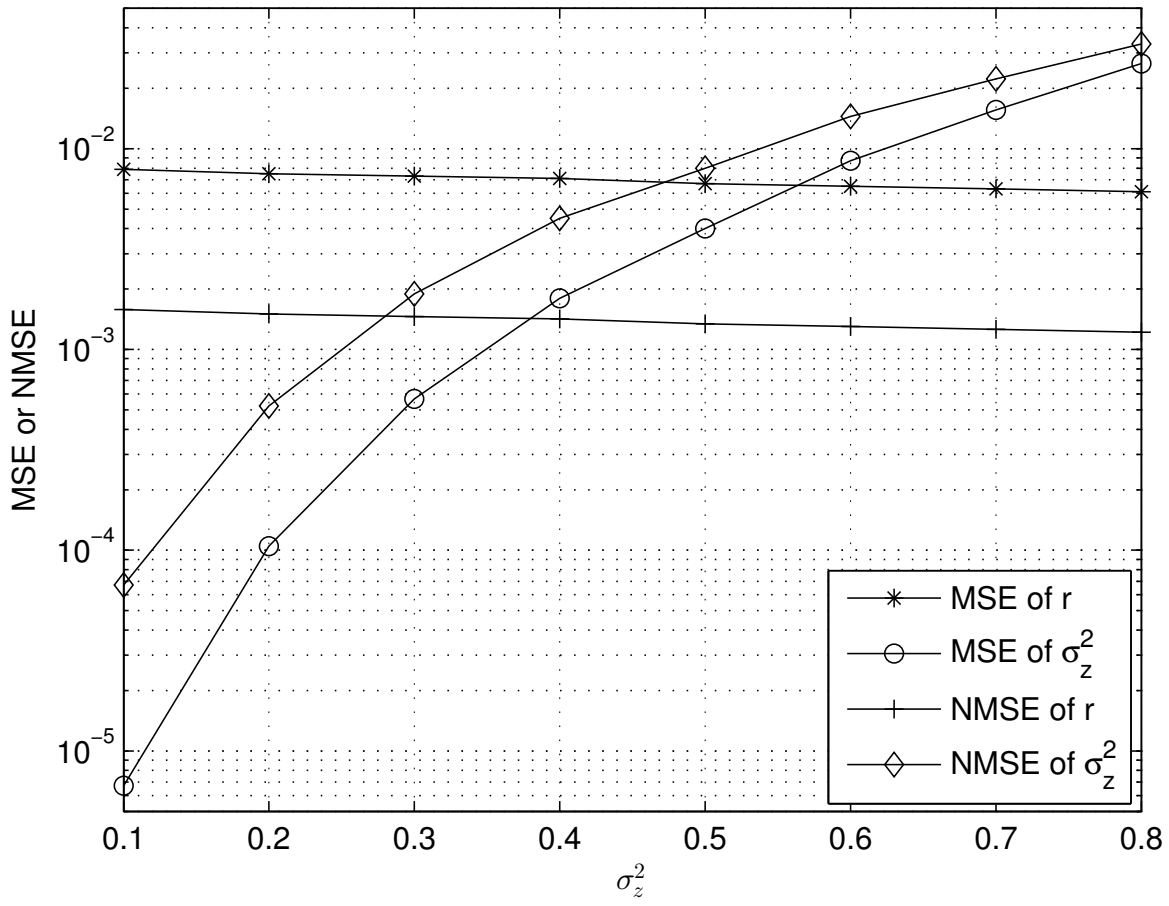

Figure 4.2: MSE and NMSE performance of the maximum likelihood estimators for the lognormal-Rician parameters r and σ_z^2 with $r = 4$.

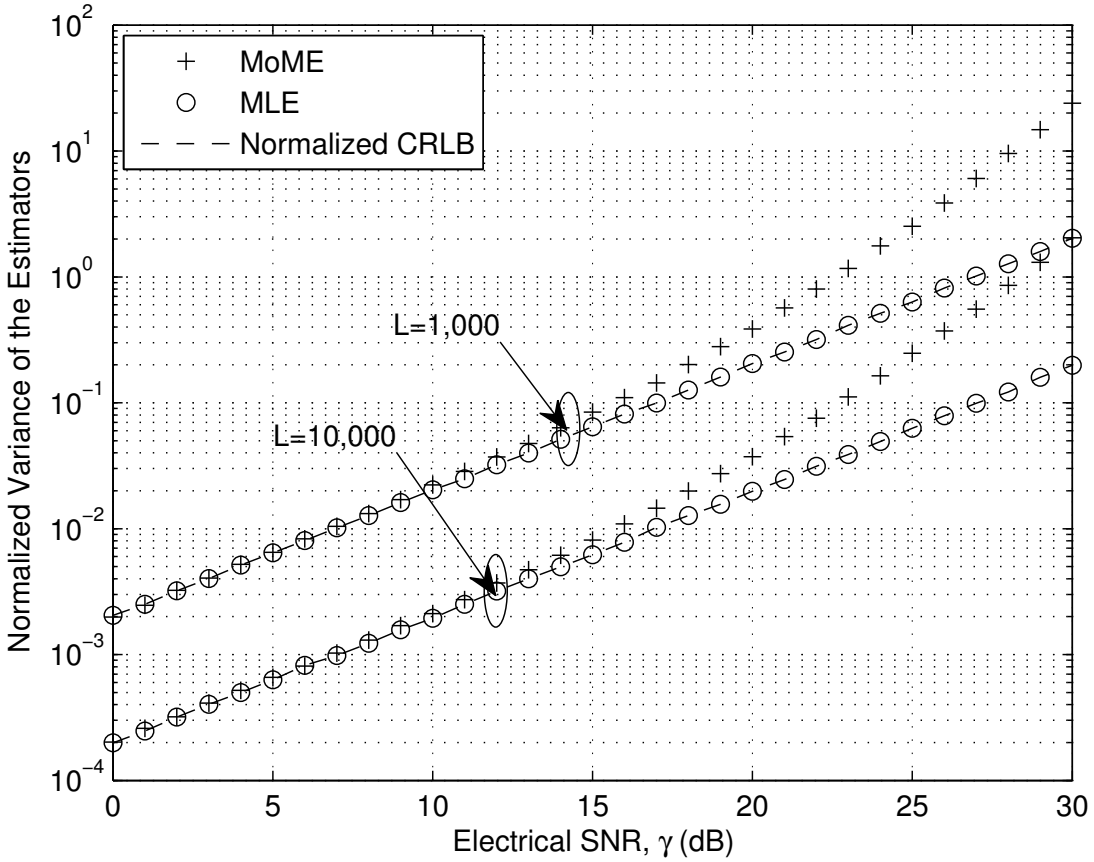

Figure 4.3: Comparison of MoME and MLE normalized sample variance for different training sequence lengths over a lognormal turbulence channel with $\sigma = 0.25$. The normalized MSE is computed over $M = 1 \times 10^4$ trials.

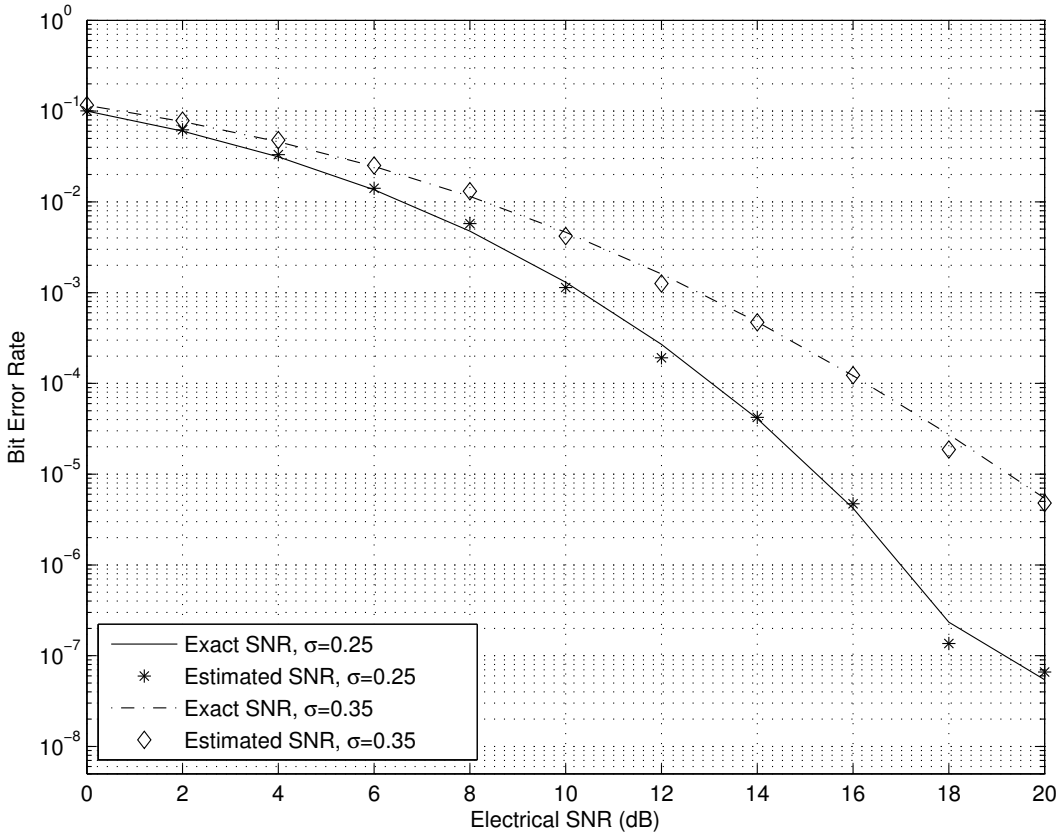

Figure 4.4: Comparison of BERs obtained by the estimated electrical SNR and the exact electrical SNR with $\xi = 0$ and $J = 3$ sample moments.

Chapter 5

OOK IM/DD System with Source Information Transformation

In this chapter, an FSO communication system using OOK and source information transformation is proposed. This system can detect the OOK signal without knowledge of the instantaneous CSI and pdf of the turbulence model. The pdf of the detection threshold and an upper bound on the average BER are derived. Numerical studies show that the proposed system can achieve comparable performance to the idealized adaptive detection system, with a greatly reduced level of implementation complexity and an SNR performance loss of only 1.85 dB at a BER of 2.17×10^{-7} for a lognormal turbulence channel with $\sigma = 0.25$.

5.1 System and Channel Models

We consider an IM/DD system with M laser source transmitters and M photodetectors operating through atmospheric turbulence channels.

The operation of the proposed scheme is described as follows. At the transmitter, which is shown in Fig. 5.1, there are M distinct optical wavelengths, $\lambda_1, \lambda_2, \ldots, \lambda_M$, assigned to the M laser transmitters. Each wavelength is used to transmit an independent information sequence, with source information transformation used to ensure that one or more lasers transmit bit "1" during each symbol duration. When $M = 2$, the proposed system can almost double the multiplexing gain achieved in the system of [25] using double-laser differential signaling. For source information transformation, we first convert a binary information sequence of length L to a $(2^M - 1)$-nary

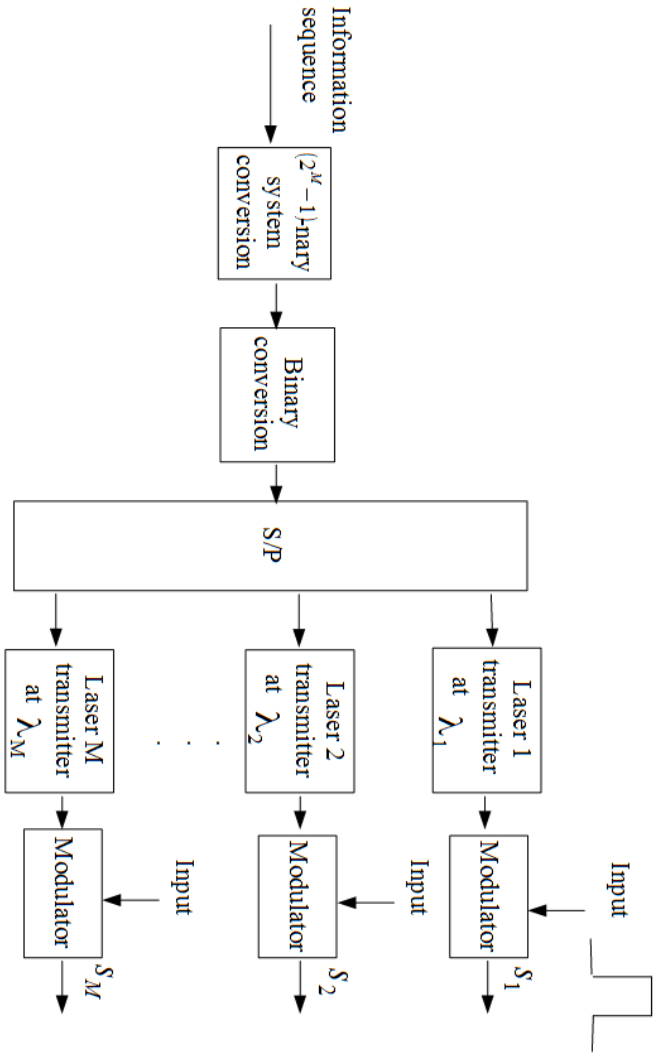

Figure 5.1: Block diagram of the transmitter for the system using source information transformation.

information sequence of length J as shown in Fig. 5.2. This mapping can be written as

$$T_1 : \{0,1\}^L \rightarrow \{0,\ldots,2^M-1\}^J. \tag{5.1}$$

Then we map each element of the (2^M-1)-nary sequence into an M-bit binary sequence that does not contain the all-zero binary sequence. The resulting M-bit binary sequence after the serial-to-parallel conversion determines, among M transmitted lasers, which link transmits bit "0" and which link transmits bit "1". For example, when $M=3$, we map the seven elements of the 7-nary sequence $(0,1,2,3,4,5,6)$ to the binary sequence $\{001,010,011,100,101,110,\ 111\}$. This mapping can be written as

$$T_2 : \{0,\ldots,2^M-1\}^J \rightarrow \{0,1\}^{JM}. \tag{5.2}$$

The mapping described in (5.1) and (5.2), which we call source information transformation, will ensure that the M received signals have an explicit turbulence fading reference for detection in each symbol duration, meaning that at least one laser is on (bit "1" is transmitted). When bit "1" is transmitted, the signal will suffer turbulence distortion. It is desirable to select values of L and J that make the mapping of T_1 be a one-to-one mapping, i.e.,

$$2^L = (2^M-1)^J. \tag{5.3}$$

However, the above equality is difficult to achieve in practice for arbitrary values of L and J. To approximate the ideal case of (5.3), we consider

$$\begin{aligned} &\min_{(L,J)} \left[(2^M-1)^J - 2^L\right] \\ &\text{Subject to } \ 2^L \leq (2^M-1)^J. \end{aligned} \tag{5.4}$$

Since there might be more than one pair (L,J) that satisfies (5.4), we will choose the smallest pair

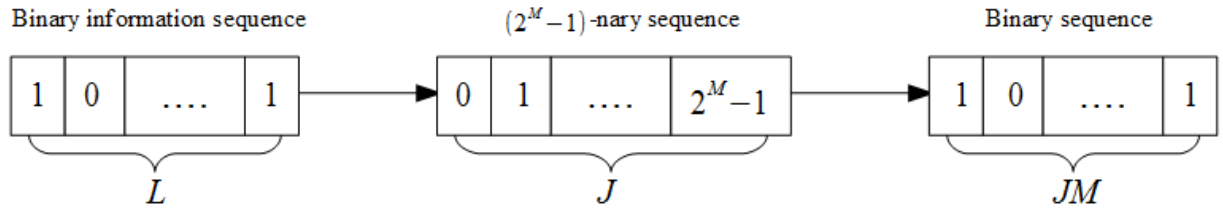

Figure 5.2: Block diagram of the source information transformation.

(L,J) for our system, i.e., the value of $L+J$ is the smallest among the pairs which satisfy (5.4), as it is desirable to minimize the system delay. For example, when $M=3$, we select $L=14$ and $J=5$ by using a computer search.

At the receiver, as shown in Fig. 5.3, diffractive optical elements and/or narrowband optical filters are used to separate the prescribed wavelengths for the detection of the M transmitted signals. In Fig. 5.3, we use the acronym PD to represent the photodetector. After the M parallel photodetectors and the parallel-to-serial conversion, in each symbol duration, a value of one-half of the largest received signal is used to define the detection threshold for the M received signals. If all of the M-bit binary sequence are demodulated as bit "0", which may happen due to the noise, this is an incorrect decision (since an all-zero binary sequence is not transmitted for our system), and we will assume the source transmits $00\ldots01$. The demodulated JM-bit binary sequence will be mapped to a (2^M-1)-nary sequence of length J, and then this (2^M-1)-nary sequence of length J will ultimately be converted back to a binary information sequence of length L.

At the mth transmitter, the transmitted intensity can be expressed as

$$s_m(t) = 1 + \sum_i a_{i,m} g_m(t - iT_p), \quad m = 1,2,\ldots,M \tag{5.5}$$

where $a_{i,m} \in \{-1,1\}$ is the ith data in the mth transmitter, and T_p is the symbol duration. In (5.5), pulse shaping in the mth transmitter is defined as $g_m(t) = 1$ for $0 < t < T_p$, and $g_m(t) = 0$ otherwise. These M signals are transmitted through atmospheric turbulence channels and are distorted by a multiplicative process $I(u,t)$. We have assumed that the channel fading is the same for all the wavelengths in each symbol duration. This assumption can be achieved by ensuring that

the transmitter wavelengths are sufficiently close to each other (being separated only by tens of nanometers), which will ensure that the transmitter beams are spatially overlapped and experience the same atmospheric turbulence distortion [25].

At the mth receiver, the received signal after the photodetection can be written as

$$r_m(t) = R[(1+\xi)I(u,t) + I(u,t)\sum_i a_{i,m} g_m(t - iT_p)] + n_m(t), \quad m = 1,2,\ldots,M. \tag{5.6}$$

Without loss of generality, the photodetector responsivity R is assumed to be unity. In (5.6), the positive parameter ξ is the low and high state offset that quantifies a nonzero extinction ratio, $I(u,t)$ is assumed to be a stationary random process for signal scintillation caused by atmospheric turbulence, and $n_m(t)$ is AWGN due to thermal noise and/or ambient shot noise in mth receiver. Using a p-i-n photodiode and following [21], the shot noise is assumed to be dominated by ambient shot noise. (Both ambient shot noise and thermal noise are statistically independent of the desired signal.) The total noise power is $\sigma_g^2 = \sigma_s^2 + \sigma_T^2$, where σ_s^2 and σ_T^2 denote the respective ambient shot noise power and the thermal noise power.

The mth received signal is sampled at time T_p. The sample $I(u,t = T_p)$ is a RV I, and the sample $n_m(t = T_p)$ is a RV n_m having zero mean and variance σ_g^2. When bit "0" is transmitted, s_0 becomes true and the laser is off. The demodulation sample is $r_m|_{s_0} = n_m$. When bit "1" is transmitted, s_1 becomes true and the laser is on. The demodulation sample is $r_m|_{s_1} = I + n_m$.

5.2 The Probability Density Function of the Detection Threshold

With perfect knowledge of the instantaneous CSI, the minimum error probability is provided by the ML based decision threshold expressed by [22]

$$T_{th} = \frac{\sigma_0(I_0 + I_1) + \sigma_1 I_0}{\sigma_0 + \sigma_1} \tag{5.7}$$

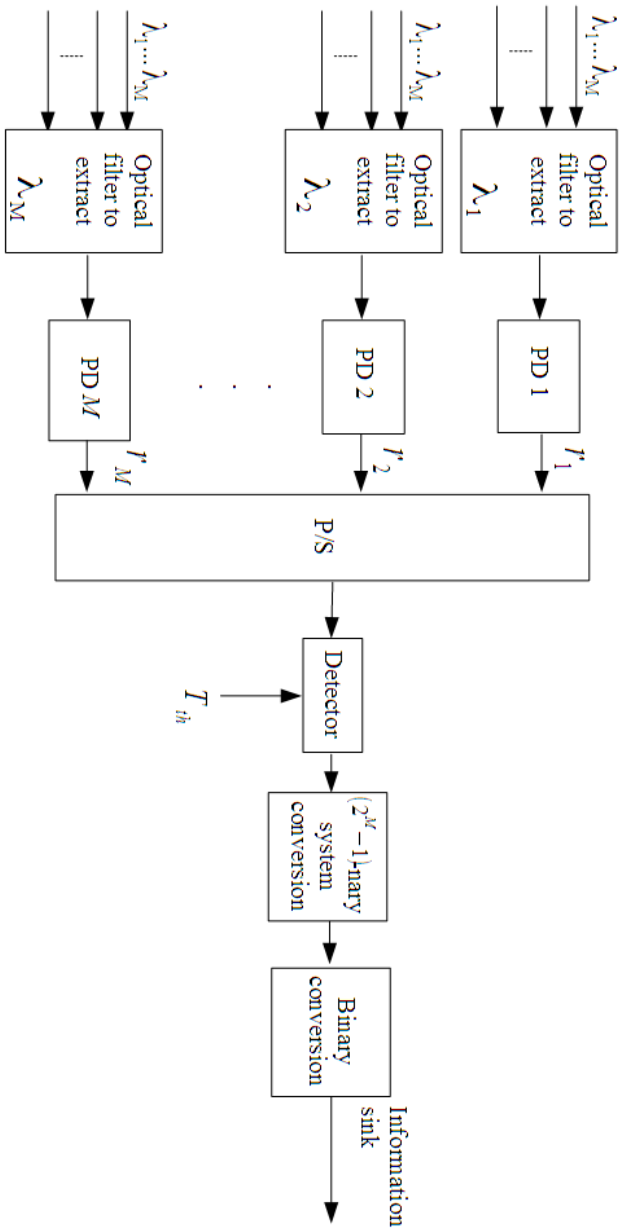

Figure 5.3: Block diagram of the receiver for the system using source information transformation.

where σ_1 and σ_0 are the standard deviations of the noise currents for bits "1" and "0", respectively; I_1 and I_0 are averages of the generated currents at the receiver for bits "1" and "0". For simplicity, we assume $\sigma_0 = \sigma_1 = \sigma_g$, $I_0 = 0$ and $I_1 = I$. The ML-based detection threshold is $T_{th} = I/2$, which is an adaptive detection threshold and varies with the fading coefficient. Note that this is complex to realize in practice, as it requires perfect knowledge of the instantaneous CSI for each symbol detection. However, when the average SNR (denoted by γ) approaches infinity, or for a noiseless system, we have

$$\lim_{\gamma \to \infty} \max\{r_1, r_2, \ldots, r_M\} = I. \tag{5.8}$$

Thus, we can intuitively set the detection threshold for the system to be

$$T_{th} = \frac{\max\{r_1, r_2, \ldots, r_M\}}{2}. \tag{5.9}$$

The most important feature of the detection threshold proposed in (5.9) is that it only depends on the received signal, and unlike a coherent OOK detection scheme, an estimate of the CSI is not required.

We now derive the pdf of the detection threshold T_{th} in (5.9). In a symbol duration, we first consider the case for which k branches transmit bit "1", where $k = 1, 2, \ldots, M$, and the rest of the $M-k$ branches transmit bit "0". Without loss of generality, we assume the first k branches transmit bit "1", and the rest of the $M-k$ branches transmit bit "0". The conditional CDF of T_{th} can be written as

$$\begin{aligned} F_{T_{th}}(t_{th}|I,k) &= P\left(\frac{\max\{I+n_1, \ldots, I+n_k, n_{k+1}, \ldots, n_M\}}{2} < t_{th}\right) \\ &= P\left(\frac{I+n_1}{2} < t_{th}, \ldots, \frac{I+n_k}{2} < t_{th}, \frac{n_{k+1}}{2} < t_{th}, \ldots, \frac{n_M}{2} < t_{th}\right) \\ &= P(n_1 < 2t_{th} - I, \ldots, n_k < 2t_{th} - I, n_{k+1} < 2t_{th}, \ldots, n_M < 2t_{th}). \end{aligned} \tag{5.10}$$

Since all the noise components $n_1, n_2, \ldots, n_M$ are assumed to i.i.d., we have

$$\begin{aligned} &P(n_1 < 2t_{th} - I, \ldots, n_k < 2t_{th} - I, n_{k+1} < 2t_{th}, \ldots, n_M < 2t_{th}) \\ &= P(n_1 < 2t_{th} - I) \ldots P(n_k < 2t_{th} - I) P(n_{k+1} < 2t_{th}) \ldots P(n_M < 2t_{th}) \\ &= [P(n_1 < 2t_{th} - I)]^k [P(n_M < 2t_{th})]^{M-k}. \end{aligned} \tag{5.11}$$

It follows that

$$\begin{aligned} F_{T_{th}}(t_{th}|I,k) &= [P(n_1 < 2t_{th} - I)]^k [P(n_M < 2t_{th})]^{M-k} \\ &= [\Phi(2t_{th} - I)]^k [\Phi(2t_{th})]^{M-k} \end{aligned} \tag{5.12}$$

where $\Phi(x) = \int_{-\infty}^{x} \frac{1}{\sqrt{2\pi}} \exp\left(-\frac{r^2}{2}\right) dr$ is the CDF of a standard Gaussian RV. The pdf of T_{th} conditioned on k branches transmitting bits "1"s and I can be written as

$$\begin{aligned} f_{T_{th}}(t_{th}|I,k) = \frac{d}{dt_{th}} F_{T_{th}}(t_{th}|I,k) =& 2k \left(\Phi\left(\frac{2t_{th} - I}{\sigma_g}\right)\right)^{k-1} \left(\Phi\left(\frac{2t_{th}}{\sigma_g}\right)\right)^{M-k} f_N(2t_{th} - I) \\ &+ 2(M-k) \left(\Phi\left(\frac{2t_{th} - I}{\sigma_g}\right)\right)^{k} \left(\Phi\left(\frac{2t_{th}}{\sigma_g}\right)\right)^{M-k-1} f_N(2t_{th}) \end{aligned} \tag{5.13}$$

where $f_N(x) = \frac{1}{\sqrt{2\pi}\sigma_g} \exp\left(-\frac{x^2}{2\sigma_g^2}\right)$ denotes the pdf of the noise term. The pdf of T_{th} conditioned on I can be obtained as

$$\begin{aligned} f_{T_{th}}(t_{th}|I) &= \sum_{k=1}^{M} f_{T_{th}}(t_{th}|I,k) p(k) \\ &= \frac{f_N(2T_{th} - I)}{2^{M-1}} \left\{ M \left[\Phi\left(\frac{2T_{th}}{\sigma_g}\right) + \Phi\left(\frac{2T_{th} - I}{\sigma_g}\right)\right]^{M-1} \right. \\ &+ \left. \left(\Phi\left(\frac{2T_{th}}{\sigma_g}\right)\right)^{M-1} \right\} + \frac{f_N(2T_{th})}{2^{M-1}} \left\{ M \left(\Phi\left(\frac{2T_{th}}{\sigma_g}\right) + \Phi\left(\frac{2T_{th}}{\sigma_g}\right)\right)^{M-1} \right. \\ &+ \left. \left(\Phi\left(\frac{2T_{th}}{\sigma_g}\right)\right)^{M-2} \left[(M-1)\Phi\left(\frac{2T_{th}}{\sigma_g}\right) - M\Phi\left(\frac{2T_{th}}{\sigma_g}\right)\right] \right\} \end{aligned} \tag{5.14}$$

where $p(k) = \frac{\binom{M}{k}}{2^M}$ is the probability that there are k branches transmitting bit "1". Averaging (5.14) with respect to the fading coefficient I, one can obtain the pdf of T_{th} as

$$f_{T_{th}}(t_{th}) = E_I\left[f_{T_{th}}(t_{th}|I)\right] \tag{5.15}$$

where $E_I[\cdot]$ represents the statistical expectation with respect to I.

5.3 The Upper Bound on the Average BER

As it is challenging to find the exact BER expression for our proposed system, we will find an upper bound on the average BER. For expository purposes, we first analyze the error caused in the detection process. The error caused in the detection process, before the $(2^M - 1)$-nary sequence conversion at the receiver, is the turbulence induced error when the binary sequence is transmitted through the turbulence channel. We then analyze the average BER of the output binary sequence.

5.3.1 The Error Caused In The Detection At The Receiver

If k branches transmit bit "1", and the rest of the $M-k$ branches transmit bit "0". Without loss of generality, we assume the first k branches transmit bit "1" values and the detection threshold becomes

$$\tilde{T}_{th} = \frac{\max\{I+n_1,\ldots,I+n_k,n_{k+1},\ldots,n_M\}}{2}. \tag{5.16}$$

We define $\mathbf{N} = \begin{bmatrix} n[1] & \ldots & n[M] \end{bmatrix}^T$ as the noise vector, and $\mathbf{N}_{k^\odot} = \begin{bmatrix} n[1] & \ldots & n[k-1] & n[k+1] & \ldots & n[M] \end{bmatrix}^T$ as the noise vector without the kth noise component n_k. The probability of having incorrect

detection in one or more links can be written as

$$\begin{aligned} P(e|k) = &\frac{1}{M}\left\{E_{\mathbf{N}_{1^{\odot}}}\left[E_I\left[P\left(I+n_1<\tilde{T}_{th}\middle|\mathbf{N}_{1^{\odot}},I\right)\right]\right]\right. \\ &+\cdots+E_{\mathbf{N}_{k^{\odot}}}\left[E_I\left[P\left(I+n_k<\tilde{T}_{th}\middle|\mathbf{N}_{k^{\odot}},I\right)\right]\right] \\ &+E_{\mathbf{N}_{k+1^{\odot}}}\left[E_I\left[P\left(n_{k+1}>\tilde{T}_{th}\middle|\mathbf{N}_{k+1^{\odot}},I\right)\right]\right] \\ &\left.+\cdots+E_{\mathbf{N}_{M^{\odot}}}\left[E_I\left[P\left(n_M>\tilde{T}_{th}\middle|\mathbf{N}_{M^{\odot}},I\right)\right]\right]\right\}. \end{aligned} \tag{5.17}$$

Since all components of the noise vector $\mathbf{N}$ are i.i.d., for $k_1 \neq k_2$, where $k_1, k_2 \in \{1,2,\ldots,M\}$, we have

$$E_{\mathbf{N}_{k_1^{\odot}}}\left[E_I\left[P\left(I+n_{k_1}<\tilde{T}_{th}\middle|\mathbf{N}_{k_1^{\odot}},I\right)\right]\right] = E_{\mathbf{N}_{k_2^{\odot}}}\left[E_I\left[P\left(I+n_{k_2}<\tilde{T}_{th}\middle|\mathbf{N}_{k_2^{\odot}},I\right)\right]\right] \tag{5.18}$$

and

$$E_{\mathbf{N}_{k_1^{\odot}}}\left[E_I\left[P\left(n_{k_1}>\tilde{T}_{th}\middle|\mathbf{N}_{k_1^{\odot}},I\right)\right]\right] = E_{\mathbf{N}_{k_2^{\odot}}}\left[E_I\left[P\left(n_{k_2}>\tilde{T}_{th}\middle|\mathbf{N}_{k_2^{\odot}},I\right)\right]\right]. \tag{5.19}$$

Thus, the probability of having incorrect detection in one or more links can be written as

$$\begin{aligned} P(e|k) = &\frac{k}{M}E_{\mathbf{N}_{1^{\odot}}}\left[E_I\left[P\left(I+n_1<\tilde{T}_{th}\middle|\mathbf{N}_{1^{\odot}},I\right)\right]\right] \\ &+\frac{M-k}{M}E_{\mathbf{N}_{M^{\odot}}}\left[E_I\left[P\left(n_M>\tilde{T}_{th}\middle|\mathbf{N}_{M^{\odot}},I\right)\right]\right]. \end{aligned} \tag{5.20}$$

The first term in (5.20) can be upper-bounded as

$$\begin{aligned}
&P\left(I+n_1<\tilde{T}_{th}\middle|\mathbf{N}_{1^{\odot}},I\right)=P\left(I+n_1<\frac{\max\{I+n_1,\ldots,I+n_k,n_{k+1},\cdots,n_M\}}{2}\middle|\mathbf{N}_{1^{\odot}},I\right)\\
&=P\left(\left\{I+n_1<\frac{I+n_1}{2}\right\}\cup\cdots\cup\left\{I+n_1<\frac{I+n_k}{2}\right\}\right.\\
&\left.\cup\left\{I+n_1<\frac{n_{k+1}}{2}\right\}\cup\cdots\cup\left\{I+n_1<\frac{n_M}{2}\right\}\middle|\mathbf{N}_{1^{\odot}},I\right)\\
&\le P\left(I+n_1<\frac{I+n_1}{2}\middle|I\right)+P\left(I+n_1<\frac{I+n_2}{2}\middle|n_2,I\right)+\cdots\\
&+P\left(I+n_1<\frac{I+n_k}{2}\middle|n_k,I\right)+P\left(I+n_1<\frac{n_{k+1}}{2}\middle|n_{k+1},I\right)\\
&+\cdots+P\left(I+n_1<\frac{n_M}{2}\middle|n_M,I\right)\\
&=P\left(n_1<-I|I\right)+P\left(n_1<\frac{n_2-I}{2}\middle|n_2,I\right)+\cdots+P\left(n_1<\frac{n_k-I}{2}\middle|n_k,I\right)\\
&+P\left(n_1<\frac{n_{k+1}}{2}-I\middle|n_{k+1},I\right)+\cdots+P\left(n_1<\frac{n_M}{2}-I\middle|n_M,I\right)\\
&=P(n_1<-I)+(k-1)P\left(n_1<\frac{n_2-I}{2}\middle|n_2,I\right)+(M-k)P\left(n_1<\frac{n_M}{2}-I\middle|n_M,I\right).
\end{aligned}\tag{5.21}$$

The second term in (5.20) can be upper-bounded as

$$\begin{aligned}
&P\left(n_M>\tilde{T}_{th}\middle|\mathbf{N}_{M^{\odot}},I\right)=P\left(n_M>\frac{\max\{I+n_1,\ldots,I+n_k,n_{k+1},\ldots,n_M\}}{2}\middle|\mathbf{N}_{M^{\odot}},I\right)\\
&=P\left(\left\{n_M>\frac{I+n_1}{2}\right\}\cap\cdots\cap\left\{n_M>\frac{I+n_k}{2}\right\}\right.\\
&\left.\cap\left\{n_M>\frac{n_{k+1}}{2}\right\}\cap\cdots\cap\left\{n_M>\frac{n_M}{2}\right\}\middle|\mathbf{N}_{M^{\odot}},I\right)\\
&\le P\left(n_M>\frac{I+n_1}{2}\middle|n_M,I\right).
\end{aligned}\tag{5.22}$$

Subtituting (5.21) and (5.22) into (5.20), we have

$$\begin{aligned}
P(e|k)<\frac{k}{M}\Bigg\{&E_I\left[P\left(n_1<-I\right)\right]+(k-1)E_{n_2}\left[E_I\left[P\left(n_1<\frac{n_2-I}{2}\middle|n_2,I\right)\right]\right]\\
&+(M-k)E_{n_M}\left[E_I\left[P\left(n_1<\frac{n_M}{2}-I\middle|n_M,I\right)\right]\right]\Bigg\}\\
&+\frac{M-k}{M}E_{n_1}\left[E_I\left[P\left(n_M>\frac{I+n_1}{2}\middle|n_1,I\right)\right]\right].
\end{aligned}\tag{5.23}$$

The upper bound on the average BER for the binary sequence transmitted through the turbulence channel with M transmit lasers is obtained as

$$\begin{aligned}
P_{e_2} &= \sum_{k=1}^{M} P(e|k)p(k) \\
&< \sum_{k=1}^{M} \frac{\binom{M}{k}}{2^M-1} \left\{ \frac{k}{M} \left[E_I\left[P\left(n_1 < -I\right)\right] + (k-1)E_{n_2}\left[E_I\left[P\left(n_1 < \frac{n_2-I}{2}\middle| n_2, I\right)\right]\right] \right.\right. \\
&\quad + (M-k)E_{n_M}\left[E_I\left[P\left(n_1 < \frac{n_M}{2} - I\middle| n_M, I\right)\right]\right] \\
&\quad \left.\left. + \frac{M-k}{M}E_{n_1}\left[E_I\left[P\left(n_M > \frac{I+n_1}{2}\middle| n_1, I\right)\right]\right]\right\} \\
&= \sum_{k=1}^{M} \frac{\binom{M}{k}}{2^M-1} \left\{ \frac{k}{M}\left(E_I\left[Q\left(\frac{I}{\sigma_g}\right)\right] + (k-1)E_{n_2}\left[E_I\left[Q\left(\frac{I-n_2}{2\sigma_g}\right)\right]\right]\right.\right. \\
&\quad \left.\left. + (M-k)E_{n_M}\left[E_I\left[Q\left(\frac{2I-n_M}{2\sigma_g}\right)\right]\right]\right) + \frac{M-k}{M}E_{n_1}\left[E_I\left[Q\left(\frac{I+n_1}{2\sigma_g}\right)\right]\right]\right\}.
\end{aligned} \tag{5.24}$$

It is difficult to find a closed-form expression of (5.24) that contains a double integral; however, this integral can be evaluated numerically with high accuracy.

5.3.2 Average BER of the Output Binary Sequence

At the transmitter, a binary sequence $a_L \ldots a_2 a_1$ is converted into a (2^M-1)-nary sequence $h_J h_{J-1} \ldots h_2 h_1$. This (2^M-1)-nary sequence of length J is mapped to a binary sequence of length JM. At the receiver, after the demodulation, we will map a binary sequence of length JM to a (2^M-1)-nary sequence $\hat{h}_J \hat{h}_{J-1} \ldots \hat{h}_2 \hat{h}_1$. The decimal value of a (2^M-1)-nary sequence $\hat{h}_J \hat{h}_{J-1} \ldots \hat{h}_2 \hat{h}_1$ of length J can be calculated as

$$X = (2^M-1)^{J-1}\hat{h}_J + \cdots + (2^M-1)\hat{h}_2 + \hat{h}_1 = \sum_{j=1}^{J} (2^M-1)^{j-1}\hat{h}_j. \tag{5.25}$$

To convert the (2^M-1)-nary sequence $\hat{h}_J \hat{h}_{J-1} \ldots \hat{h}_2 \hat{h}_1$ to a binary sequence, denoted as $\hat{a}_{L+1}\hat{a}_L \ldots \hat{a}_2 \hat{a}_1$, the lowest element of the binary sequence is

$$\hat{a}_1 = \mathrm{mod}(X, 2) \tag{5.26}$$

where mod$(\cdot)$ yields the remainder after division of X by 2. Similarly, the second element of the binary sequence is

$$\hat{a}_2 = \text{mod}\left(\frac{X-\hat{a}_1}{2}, 2\right). \tag{5.27}$$

The third element of the binary sequence is

$$\hat{a}_3 = \text{mod}\left(\frac{X-2\hat{a}_2-\hat{a}_1}{2^2}, 2\right). \tag{5.28}$$

Thus, the lth element of the binary sequence is

$$\begin{aligned}\hat{a}_l &= \text{mod}\left(\frac{X-2^{l-2}\hat{a}_{l-1}-\cdots-2\hat{a}_2-\hat{a}_1}{2^{l-1}}, 2\right) \\ &= \text{mod}\left(\frac{X-\sum_{i=1}^{l-1}2^{i-1}\hat{a}_i}{2^{l-1}}, 2\right) \\ &= \text{mod}\left(\frac{\sum_{j=1}^{J}(2^M-1)^{j-1}\hat{h}_j-\sum_{i=1}^{l-1}2^{i-1}\hat{a}_i}{2^{l-1}}, 2\right)\end{aligned} \tag{5.29}$$

or

$$\hat{a}_l = \left\lfloor \frac{\sum_{j=1}^{J}(2^M-1)^{j-1}\hat{h}_j-\sum_{i=1}^{l-1}2^{i-1}\hat{a}_i}{2^{l-1}} \right\rfloor \tag{5.30}$$

where $\lfloor\cdot\rfloor$ is the floor function that returns the largest integer, and this integer is less than or equal to the argument. We comment that when a (2^M-1)-nary sequence of length J is converted to a binary sequence of length $L+1$; however, at the transmitter, we convert a binary information sequence of length L to a (2^M-1)-nary information sequence of length J. Thus, at the receiver, we will ignore $\hat{a}_{L+1}$ and use $\hat{a}_L \ldots \hat{a}_2\hat{a}_1$ as our binary information sequence.

To calculate the probability of having an incorrect decision in the binary sequence $\hat{a}_L \ldots \hat{a}_2\hat{a}_1$, for expository purposes, we consider $M = 3$. When $M = 3$, we will convert $L = 14$ binary information bits $a_{14} \ldots a_2a_1$ to a 7-nary sequence with a length of $J = 5$ ($h_5h_{J-1} \ldots h_2h_1$). Then we map the 7-nary sequence of length of $J = 5$ into a binary sequence of length $JM = 15$. At the receiver, after the demodulation, we will map each $M = 3$ binary bits to an element of the 7-nary sequence.

Table 5.1: The conditional probability of the received (2^M-1)-nary number is $\hat{h}_l$ given the transmitted (2^M-1)-nary number is h_l.

$\hat{h}_l$	0	1	2	3	4	5	6
$P(\hat{h}_l\|h_l=0)$	$P(0\|0)$	$P(1\|0)$	$P(2\|0)$	$P(3\|0)$	$P(4\|0)$	$P(5\|0)$	$P(6\|0)$
$P(\hat{h}_l\|h_l=1)$	$P(0\|1)$	$P(1\|1)$	$P(2\|1)$	$P(3\|1)$	$P(4\|1)$	$P(5\|1)$	$P(6\|1)$
$P(\hat{h}_l\|h_l=2)$	$P(0\|2)$	$P(1\|2)$	$P(2\|2)$	$P(3\|2)$	$P(4\|2)$	$P(5\|2)$	$P(6\|2)$
$P(\hat{h}_l\|h_l=3)$	$P(0\|3)$	$P(1\|3)$	$P(2\|3)$	$P(3\|3)$	$P(4\|3)$	$P(5\|3)$	$P(6\|3)$
$P(\hat{h}_l\|h_l=4)$	$P(0\|4)$	$P(1\|4)$	$P(2\|4)$	$P(3\|4)$	$P(4\|4)$	$P(5\|4)$	$P(6\|4)$
$P(\hat{h}_l\|h_l=5)$	$P(0\|5)$	$P(1\|5)$	$P(2\|5)$	$P(3\|5)$	$P(4\|5)$	$P(5\|5)$	$P(6\|5)$
$P(\hat{h}_l\|h_l=6)$	$P(0\|6)$	$P(1\|6)$	$P(2\|6)$	$P(3\|6)$	$P(4\|6)$	$P(5\|6)$	$P(6\|6)$

The mapping can be seen as follows:

$$\begin{aligned} 000 &\rightarrow 0 \\ 001 &\rightarrow 0 \\ 010 &\rightarrow 1 \\ 011 &\rightarrow 2 \\ 100 &\rightarrow 3 \\ 101 &\rightarrow 4 \\ 110 &\rightarrow 5 \\ 111 &\rightarrow 6. \end{aligned} \tag{5.31}$$

Table 5.1 shows the conditional probability of the received (2^M-1)-nary number is $\hat{h}_l$ given the transmitted (2^M-1)-nary number is h_l. The conditional probability in Table 5.1 can be calculated by using the bit error probability for the binary bit transmitted through the turbulence channel, i.e., $P(0|0) = P(000|001) + P(001|001) = (1-P_{e_2})^2 P_{e_2} + (1-P_{e_2})^3$. This is shown in Table 5.2. In Tabel 5.2, P_{e_2} is the error probability for the binary bit transmitted through the turbulence channel, and its upper-bound has been derived in accordance with (5.24).

Since each element of $\hat{h}_5 \ldots \hat{h}_2 \hat{h}_1$ and $h_5 \ldots h_2 h_1$ is independent, the conditional probability for

Table 5.2: The conditional probability of the received (2^M-1)-nary number is $\hat{h}_l$ given the transmitted (2^M-1)-nary number is h_l.

$\hat{h}_l$	0	1	2	3	4	5	6
$P(\hat{h}_l \mid h_l=0)$	$(1-P_{e_2})^2P_{e_2}+(1-P_{e_2})^3$	$(1-P_{e_2})P_{e_2}^2$	$(1-P_{e_2})P_{e_2}^2$	$(1-P_{e_2})P_{e_2}^2$	$(1-P_{e_2})P_{e_2}^2$	$(1-P_{e_2})P_{e_2}^2$	$(1-P_{e_2})P_{e_2}^2$
$P(\hat{h}_l \mid h_l=1)$	$(1-P_{e_2})^2P_{e_2}+(1-P_{e_2})P_{e_2}^2$	$(1-P_{e_2})^3$	$(1-P_{e_2})P_{e_2}^2$	$(1-P_{e_2})P_{e_2}^2$	$P_{e_2}^3$	$(1-P_{e_2})^2P_{e_2}$	$(1-P_{e_2})P_{e_2}^2$
$P(\hat{h}_l \mid h_l=2)$	$(1-P_{e_2})^2P_{e_2}+(1-P_{e_2})P_{e_2}^2$	$(1-P_{e_2})^2P_{e_2}$	$(1-P_{e_2})^3$	$P_{e_2}^3$	$(1-P_{e_2})P_{e_2}^2$	$(1-P_{e_2})P_{e_2}^2$	$(1-P_{e_2})^2P_{e_2}$
$P(\hat{h}_l \mid h_l=3)$	$(1-P_{e_2})^2P_{e_2}+(1-P_{e_2})P_{e_2}^2$	$(1-P_{e_2})P_{e_2}^2$	$P_{e_2}^3$	$(1-P_{e_2})^3$	$(1-P_{e_2})^2P_{e_2}$	$(1-P_{e_2})^2P_{e_2}$	$(1-P_{e_2})P_{e_2}^2$
$P(\hat{h}_l \mid h_l=4)$	$(1-P_{e_2})^2P_{e_2}+(1-P_{e_2})P_{e_2}^2$	$P_{e_2}^3$	$(1-P_{e_2})P_{e_2}^2$	$(1-P_{e_2})^2P_{e_2}$	$(1-P_{e_2})^3$	$(1-P_{e_2})P_{e_2}^2$	$(1-P_{e_2})P_{e_2}^2$
$P(\hat{h}_l \mid h_l=5)$	$P_{e_2}^3+(1-P_{e_2})P_{e_2}^2$	$(1-P_{e_2})^2P_{e_2}$	$(1-P_{e_2})P_{e_2}^2$	$(1-P_{e_2})^2P_{e_2}$	$(1-P_{e_2})P_{e_2}^2$	$(1-P_{e_2})^3$	$(1-P_{e_2})P_{e_2}^2$
$P(\hat{h}_l \mid h_l=6)$	$P_{e_2}^3+(1-P_{e_2})P_{e_2}^2$	$(1-P_{e_2})P_{e_2}^2$	$(1-P_{e_2})^2P_{e_2}$	$(1-P_{e_2})P_{e_2}^2$	$(1-P_{e_2})P_{e_2}^2$	$(1-P_{e_2})P_{e_2}^2$	$(1-P_{e_2})^3$

the received (2^M-1)-nary sequence is $\hat{h}_5\ldots\hat{h}_2\hat{h}_1$ given the transmitted (2^M-1)-nary sequence is $h_5\ldots h_2h_1$ is

$$P(\hat{h}_5\ldots\hat{h}_2\hat{h}_1|h_5\ldots h_2h_1)=\Pi_{j=1}^{5}P(\hat{h}_j|h_5\ldots h_2h_1)=\Pi_{j=1}^{5}P(\hat{h}_j|h_j). \tag{5.32}$$

The conditional probability of the received binary sequence is $\hat{a}_L\ldots\hat{a}_2\hat{a}_1$ given the transmitted binary sequence $a_L\ldots a_2a_1$ can be written as

$$P(\hat{a}_{14}\ldots\hat{a}_2\hat{a}_1|a_L\ldots a_2a_1)=P(\hat{h}_5\ldots\hat{h}_2\hat{h}_1|h_5\ldots h_2h_1)=\Pi_{j=1}^{5}P(\hat{h}_j|h_j). \tag{5.33}$$

If the transmitted binary sequence is $a_{14}\ldots a_2a_1$, and the received binary sequence is $\hat{a}_{14}\ldots\hat{a}_2\hat{a}_1$, the conditional error probability of this system given $a_{14}\ldots a_2a_1$ and $\hat{a}_{14}\ldots\hat{a}_2\hat{a}_1$ is

$$P(e|a_{14}\ldots a_2a_1,\hat{a}_{14}\ldots\hat{a}_2\hat{a}_1)=\frac{\sum_{l=1}^{14}a_l\oplus\hat{a}_l}{14} \tag{5.34}$$

where $\oplus$ implements an exclusive OR. Thus, the BER of this system with $M=3$ can be written as

$$\begin{aligned}P(e)&=\sum_{a_{14}\ldots a_2a_1,\hat{a}_{14}\ldots\hat{a}_2\hat{a}_1}P(e|a_{14}\ldots a_2a_1,\hat{a}_{14}\ldots\hat{a}_2\hat{a}_1)P(a_{14}\ldots a_2a_1,\hat{a}_{14}\ldots\hat{a}_2\hat{a}_1)\\&=\sum_{a_{14}\ldots a_2a_1,\hat{a}_{14}\ldots\hat{a}_2\hat{a}_1}\frac{\sum_{l=1}^{14}a_l\oplus\hat{a}_l}{14}P(a_{14}\ldots a_2a_1,\hat{a}_{14}\ldots\hat{a}_2\hat{a}_1)\\&=\sum_{a_{14}\ldots a_2a_1,\hat{a}_{14}\ldots\hat{a}_2\hat{a}_1}\frac{\sum_{l=1}^{14}a_l\oplus\hat{a}_l}{14}P(\hat{a}_{14}\ldots\hat{a}_2\hat{a}_1|a_{14}\ldots a_2a_1)P(a_{14}\ldots a_2a_1).\end{aligned} \tag{5.35}$$

In (5.35), the elements of $a_{14}\ldots a_2a_1$ are independent, so we have $P(a_{14}\ldots a_2a_1)=\frac{1}{2^{14}}$. Substituting (5.33) into (5.35), we have

$$\begin{aligned}P(e)&=\sum_{a_{14}\ldots a_2a_1,\hat{a}_{14}\ldots\hat{a}_2\hat{a}_1}\frac{\sum_{l=1}^{14}a_l\oplus\hat{a}_l}{14}\Pi_{j=1}^{5}P(\hat{h}_j|h_j)P(a_{14}\ldots a_2a_1)\\&=\frac{1}{2^{14}}\sum_{a_{14}\ldots a_2a_1,\hat{a}_{14}\ldots\hat{a}_2\hat{a}_1}\frac{\sum_{l=1}^{14}a_l\oplus\hat{a}_l}{14}\Pi_{j=1}^{5}P(\hat{h}_j|h_j).\end{aligned} \tag{5.36}$$

In general, the BER for the proposed system with M transmitted lasers can be written as

$$P(e) = \frac{1}{2^L} \sum_{a_L \ldots a_2 a_1, \hat{a}_L \ldots \hat{a}_2 \hat{a}_1} \frac{\sum_{l=1}^{L} a_l \oplus \hat{a}_l}{14} \Pi_{j=1}^{J} P(\hat{h}_j | h_j). \tag{5.37}$$

5.4 Numerical Results

In this section, the pdf of the detection threshold is first verified, and the BER performance of the proposed system is numerically studied.

In Fig. 5.4, the derived pdf of the detection threshold T_{th} is compared with the simulated pdf. For expository purposes, we let $M = 3$ and $\xi = 0$. The simulated pdf is obtained by using Monte Carlo computer simulations with 10^4 trials. The derived pdf shows excellent agreement with the simulated pdf.

In Fig. 5.5, we plot the BER versus electrical SNR when the OOK IM/DD system uses a fixed detection threshold of $T_{th} = 0.5$. Note that an error floor appears in the large SNR regime. The system using source information transformantion can eliminate the error floor, although its BER performace is worse than that of the OOK IM/DD system using fixed detection threshold in low SNR regimes. This is due to the fact that a value of one-half of the largest received signal is used to define the detection threshold for the M received signals in each symbol duration. This detection threshold is only optimum when the electrical SNR approaches infinity and/or there is no noise. In the low SNR regimes, the detection threshold is not an optimum detection threshold for our proposed system, due to the noise influence, and the BER of our proposed system becomes worse than that of the OOK IM/DD system using a fixed detection threshold.

In Fig. 5.5, we also plot the upper bounds on the average BER for the proposed system over lognormal fading channels with different turbulence conditions. Simulated BER curves are also used to verify the analytical BER upper bound solutions. The upper bound is tight when $M = 3$. However, as we have used the union upper bound technique, it can be shown that the upper bound becomes loose with increased M. It is seen from Fig. 5.5 that the OOK modulated system using idealized adaptive detection thresholds with a lognormal turbulence model having $\sigma = 0.25$

requires an SNR of 22 dB to attain a BER of 2.17×10^{-7}, while the proposed system requires an SNR of 23.85 dB to achieve the same BER performance. Thus, the corresponding SNR penalty factor for the system using OOK and source information transformation in a lognormal turbulence channel with $\sigma = 0.25$ is only 1.85 dB at BER of 2.17×10^{-7}. This performance difference can be factored into the ultimate FSO system design to offset the complexity of implementing systems with adaptive detection thresholds (and their need for knowledge of the instantaneous CSI).

5.5 Summary

An FSO communication system using OOK and source information transformation has been proposed. It was shown that such a system can achieve good BER performance, without the need for knowledge of the instantaneous CSI and pdf of the turbulence model. We derived an analytical expression for the pdf of the detection threshold and developed an upper bound on the average BER. Numerical studies ultimately showed that the proposed system achieves comparable performance to the idealized adaptive detection system, with a greatly reduced level of implementation complexity and a SNR penalty factor of only 1.85 dB at a BER of 2.17×10^{-7} for a lognormal turbulence channel with $\sigma = 0.25$.

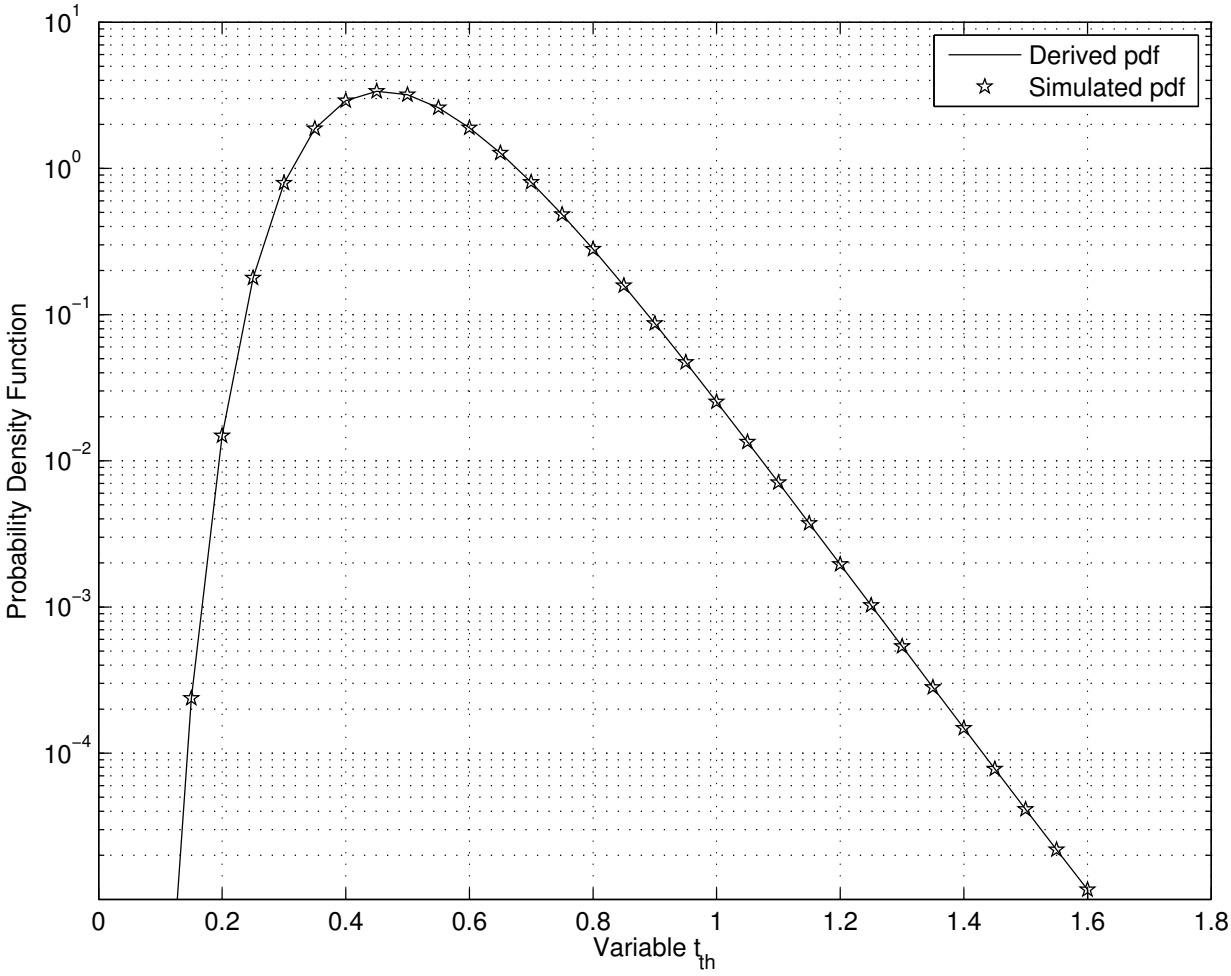

Figure 5.4: Comparison of the derived and simulated pdfs for the detection threshold T_{th} over a lognormal fading channel with $\sigma = 0.25$ and $M = 3$.

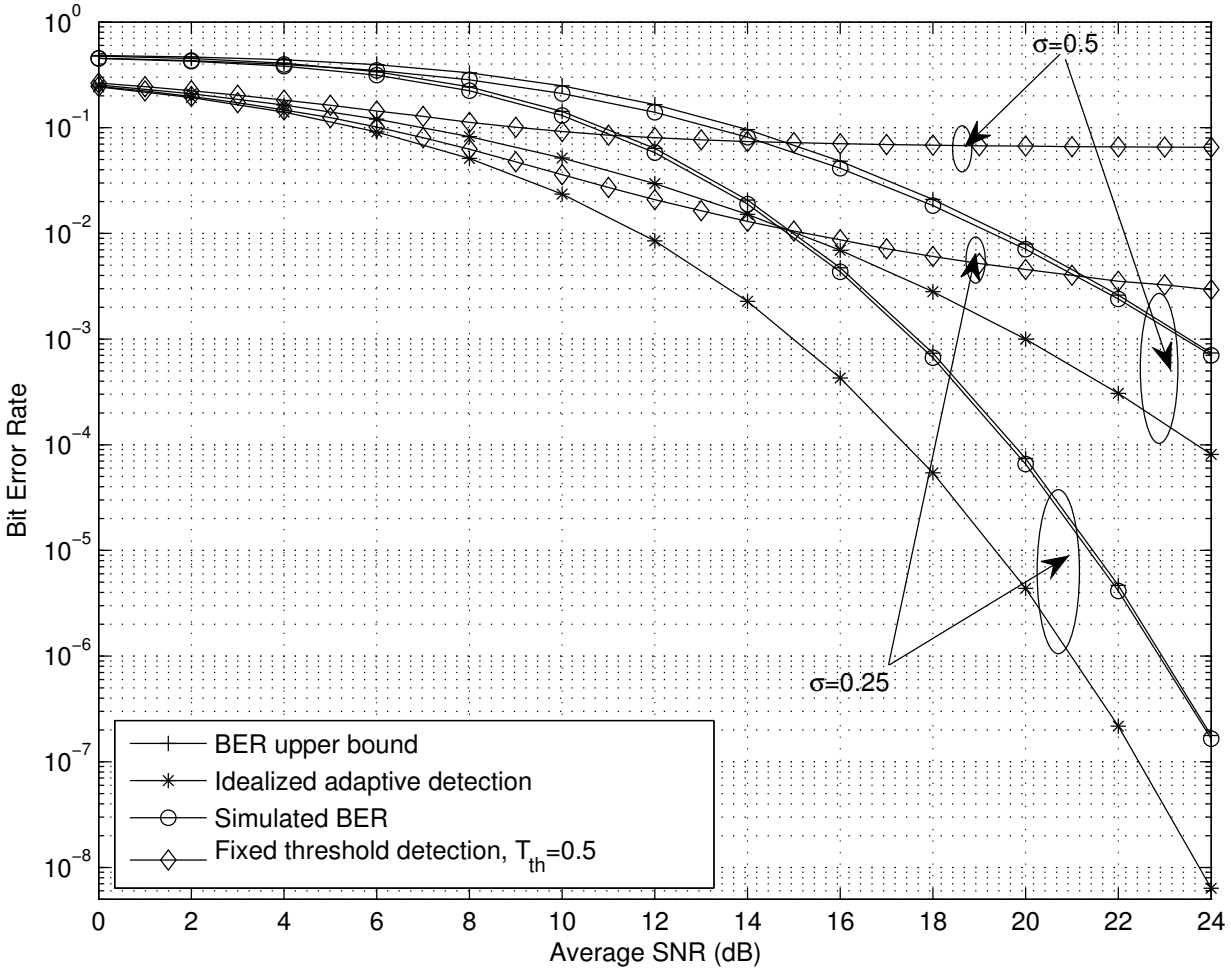

Figure 5.5: The simulated BER and BER upper bounds of the system using source information transformation over lognormal turbulence channels (with $\sigma = 0.25$, $\sigma = 0.5$, $\xi = 0$ and $M = 3$).

Chapter 6

OOK IM/DD Systems with Convolutional Code

In this chapter, we investigate IM/DD systems employing OOK and SIM-BPSK with convolutional code. We analyze the error rate performance of OOK IM/DD systems operating over weak and strong turbulence conditions and compare the BER performance of OOK to that of SIM-BPSK systems. A highly accurate convergent series solution is derived for the PEP of the OOK IM/DD system. The solution establishes a simplified upper bound on the average BER. For quasi-static fading channels, we also study the BER performance of a convolutional coded system using block interleaving where each block experiences independent fading.

6.1 Bit-By-Bit Interleaved Channels

6.1.1 Pairwise Codeword Error Probability Calculation

The PEP for a coded OOK IM/DD system conditioning on a sequence of M fading coefficients $\mathbf{I} = [I_1, I_2, ..., I_M]$ is [29]

$$P(\mathbf{C}, \hat{\mathbf{C}}|\mathbf{I}) = Q\left(\sqrt{\frac{\varepsilon(\mathbf{C}, \hat{\mathbf{C}})}{2N_0}}\right) \tag{6.1}$$

where $\hat{\mathbf{C}} = [\hat{c}_1, \hat{c}_2, ..., \hat{c}_M]$ is the chosen incorrect sequence when the coded sequence $\mathbf{C} = [c_1, c_2, ..., c_M]$ is transmitted. In (6.1), $\varepsilon(\mathbf{C}, \hat{\mathbf{C}}) = E_b \sum_{k \in \Omega} I_k^2$ is the energy difference of these two coded sequences, where the set Ω contains the indices of bit locations in which the sequences $\mathbf{C}$ and $\hat{\mathbf{C}}$ differ, and E_b is the transmitted bit energy.

Using an alternative expression of the Gaussian Q-function, i.e., $Q(x) = \frac{1}{\pi}\int_0^{\frac{\pi}{2}} \exp\left(-\frac{x^2}{2\sin^2\theta}\right) d\theta$, one can write the conditional PEP as [29, eq. (7)]

$$\begin{aligned} P(\mathbf{C},\hat{\mathbf{C}}|\mathbf{I}) &= \frac{1}{\pi}\int_0^{\frac{\pi}{2}} \exp\left(-\frac{E_b}{4N_0\sin^2\theta}\sum_{k\in\Omega} I_k^2\right) d\theta \\ &= \frac{1}{\pi}\int_0^{\frac{\pi}{2}} \prod_{k\in\Omega} \exp\left(-\frac{\gamma}{4\sin^2\theta} I_k^2\right) d\theta \end{aligned} \tag{6.2}$$

where $\gamma = E_b/N_0$ denotes the SNR per bit. Following [29], we assume perfect bit-by-bit interleaving and average (6.2) with respect to the independent fading coefficients. The PEP is

$$\begin{aligned} P(\mathbf{C},\hat{\mathbf{C}}) &= \frac{1}{\pi}\int_0^{\frac{\pi}{2}} E\left[\prod_{k\in\Omega} \exp\left(-\frac{\gamma I_k^2}{4\sin^2\theta}\right)\right] d\theta \\ &= \frac{1}{\pi}\int_0^{\frac{\pi}{2}} \prod_{k\in\Omega} E\left[\exp\left(-\frac{\gamma I_k^2}{4\sin^2\theta}\right)\right] d\theta \\ &= \frac{1}{\pi}\int_0^{\frac{\pi}{2}} \prod_{k\in\Omega} \int_0^{\infty} \exp\left(-\frac{\gamma I_k^2}{4\sin^2\theta}\right) f_I(I_k)\, dI_k\, d\theta \\ &= \frac{1}{\pi}\int_0^{\frac{\pi}{2}} \left[\int_0^{\infty} \exp\left(-\frac{\gamma I^2}{4\sin^2\theta}\right) f_I(I)\, dI\right]^{|\Omega|} d\theta \end{aligned} \tag{6.3}$$

where $|\Omega|$ denotes the cardinality of set Ω and represents the number of error events. Applying an accurate series representation of the Gamma-Gamma pdf [61]

$$\begin{aligned} f_I(I) = &\frac{\Gamma(\alpha-\beta)\Gamma(\beta-\alpha+1)}{\Gamma(\alpha)\Gamma(\beta)} \\ &\times \sum_{p=0}^{\infty}\left[\frac{(\alpha\beta)^{p+\beta} I^{p+\beta-1}}{\Gamma(p-\alpha+\beta+1)p!} - \frac{(\alpha\beta)^{p+\alpha} I^{p+\alpha-1}}{\Gamma(p+\alpha-\beta+1)p!}\right] \end{aligned}$$

to (6.3) yields

$$\begin{aligned} P(\mathbf{C},\hat{\mathbf{C}}) = &\frac{(2\lambda(\alpha,\beta))^{|\Omega|}}{\pi} \\ &\times \int_0^{\frac{\pi}{2}} \left\{\sum_{p=0}^{\infty} \left[a_p(\alpha,\beta) g_p(\beta) + a_p(\beta,\alpha) g_p(\alpha)\right]\right\}^{|\Omega|} d\theta \end{aligned} \tag{6.4}$$

where $a_p(x,y) = \frac{\Gamma(x-y)\Gamma(y-x+1)(xy)^{p+y}}{\Gamma(p-x+y+1)p!}$, $\lambda(\alpha,\beta) = \frac{1}{2\Gamma(\alpha)\Gamma(\beta)}$, and $g_p(x) = \int_0^\infty I^{p+x-1}\exp\left(-\frac{\gamma I^2}{\sin^2\theta}\right) dI = \frac{\Gamma(\frac{p+x}{2})}{2(\frac{\bar{\gamma}}{\sin^2\theta})^{\frac{p+x}{2}}}$ [51, eq. 3.326(2)]. Substituting $a_p(x,y)$ and $g_p(x)$ into (6.4) gives

$$\begin{aligned} P(\mathbf{C},\hat{\mathbf{C}}) = \frac{(\lambda(\alpha,\beta))^{|\Omega|}}{\pi}\int_0^{\frac{\pi}{2}} \Bigg\{ \sum_{p=0}^{\infty} \frac{\gamma^{-\frac{p+\beta}{2}}}{(2\alpha\beta\sin\theta)^{-(p+\beta)}} \\ \times b_p(\alpha,\beta) + \frac{\gamma^{-\frac{p+\alpha}{2}}}{(2\alpha\beta\sin\theta)^{-(p+\alpha)}} b_p(\beta,\alpha) \Bigg\}^{|\Omega|} d\theta \end{aligned} \tag{6.5}$$

where $b_p(x,y) = \frac{\Gamma(\frac{p+y}{2})\Gamma(x-y)\Gamma(y-x+1)}{\Gamma(p-x+y+1)p!}$. Applying two power series identities [51, eqs. (0.314), (0.316)] gives

$$\left(\sum_{k=0}^{\infty} a_k x^k\right)^n = \sum_{k=0}^{\infty} c_k x^k \tag{6.6}$$

where $c_0 = a_0^n$ and $c_m = \frac{1}{ma_0}\sum_{k=1}^{m}(kn-m+k)a_k c_{m-k}$, and

$$\sum_{k=0}^{\infty} a_k x^k \sum_{k=0}^{\infty} b_k x^k = \sum_{k=0}^{\infty} c_k x^k \tag{6.7}$$

where $c_k = \sum_{n=0}^{k} a_n b_{k-n}$, we then obtain

$$\begin{aligned} P(\mathbf{C},\hat{\mathbf{C}}) &= \frac{(\lambda(\alpha,\beta))^{|\Omega|}}{\pi}\sum_{m=0}^{|\Omega|}\binom{|\Omega|}{m}\sum_{p=0}^{\infty} C_p(|\Omega|-m,m) \\ &\times \left(\frac{\sqrt{\gamma}}{2\alpha\beta}\right)^{-p-|\Omega|-(\alpha-1)m}\int_0^{\frac{\pi}{2}}(\sin\theta)^{p+(|\Omega|-m)\beta+\alpha m+1}\,d\theta \\ &= \frac{(\lambda(\alpha,\beta))^{|\Omega|}}{2\sqrt{\pi}}\sum_{m=0}^{|\Omega|}\binom{|\Omega|}{m}\sum_{p=0}^{\infty} C_p(|\Omega|-m,m) \\ &\times \left(\frac{\sqrt{\gamma}}{2\alpha\beta}\right)^{-p-(|\Omega|-m)\beta-\alpha m}\frac{\Gamma\left(\frac{p+(|\Omega|-m)\beta+\alpha m+1}{2}\right)}{\Gamma\left(1+\frac{p+(|\Omega|-m)\beta+\alpha m}{2}\right)} \end{aligned} \tag{6.8}$$

where $C_p(i,j) \triangleq b_p^{(i)}(\alpha,\beta) * b_p^{(j)}(\beta,\alpha)$, and $b_p^{(i)}(\alpha,\beta)$ is calculated by convolving $b_p(\alpha,\beta)$ with itself $i-1$ times, i.e., $b_p^{(2)}(\alpha,\beta) = b_p(\alpha,\beta) * b_p(\alpha,\beta)$. The last equality of (6.8) is obtained by

using the integral identity [61, eq. (20)]

$$\int_0^{\frac{\pi}{2}} (\sin\theta)^{p+(|\Omega|-m)\beta+\alpha m+1}\, d\theta = \frac{\sqrt{\pi}\Gamma\left(\frac{p+(|\Omega|-m)\beta+\alpha m+1}{2}\right)}{2\Gamma\left(1+\frac{p+(|\Omega|-m)\beta+\alpha m}{2}\right)}. \tag{6.9}$$

6.1.2 Truncation Error Analysis

Truncation error is introduced when we approximate the infinite series in (6.8) with the first P terms. We define the truncation error as

$$\varepsilon(P) \triangleq \frac{(\lambda(\alpha,\beta))^{|\Omega|}}{2\sqrt{\pi}} \sum_{m=0}^{|\Omega|} \binom{|\Omega|}{m} \sum_{p=P+1}^{\infty} u_p(m) \left(\frac{2\alpha\beta}{\sqrt{\gamma}}\right)^p \tag{6.10}$$

where

$$\begin{aligned} u_p(m) \triangleq C_p(|\Omega|-m,m) &\frac{\Gamma\left(\frac{p+(|\Omega|-m)\beta+\alpha m+1}{2}\right)}{\Gamma\left(1+\frac{p+(|\Omega|-m)\beta+\alpha m}{2}\right)} \\ &\times \left(\frac{2\alpha\beta}{\sqrt{\gamma}}\right)^{(|\Omega|-m)\beta+\alpha m}. \end{aligned} \tag{6.11}$$

It can be shown that the infinite series solution in (6.8) is a converging series by verifying that the truncation error $\varepsilon(P)$ decreases as P increases. Following [62], we use the Taylor series expansion of $x^n/(1-x) = \sum_{j=n}^{\infty} x^j$ and obtain an upper bound of the truncation error as

$$\begin{aligned} \varepsilon(P) \leq &\frac{(\lambda(\alpha,\beta))^{|\Omega|}}{2\sqrt{\pi}(\sqrt{\gamma}/2\alpha\beta-1)(\sqrt{\gamma}/2\alpha\beta)^P} \\ &\times \sum_{m=0}^{|\Omega|} \binom{|\Omega|}{m} \max_{p>P}\{u_p(m)\}. \end{aligned} \tag{6.12}$$

If $a > b$ and p approaches ∞, $\frac{\Gamma(p+b)}{\Gamma(p+a)}$ approaches zero. After examining the first two terms in (6.11), we note that $u_p(m)$ approaches 0 when p approaches ∞. Therefore, the truncation error $\varepsilon(P)$ will diminish when P increases. We also note from (6.12) that the truncation error diminishes rapidly with increasing γ. This suggests that the PEP solution in (6.8) is a convergent series and our series

solution is accurate with high SNR values.

6.1.3 Asymptotic Analysis of PEP

Without loss of generality, we assume $\alpha > \beta > 0$ so that the term in (6.5) with $\gamma^{-\frac{p+\alpha}{2}}$ decreases faster than the term with $\gamma^{-\frac{p+\beta}{2}}$ for increasing γ [61]. When p approaches ∞, $\frac{\Gamma(\frac{p+y}{2})}{\Gamma(p+y-x+1)}$ in (6.5) approaches 0. The PEP expression in (6.5) can therefore be approximated at asymptotically high SNR by

$$\begin{aligned}
&P^{\infty}(\mathbf{C},\hat{\mathbf{C}}) \\
&= \frac{1}{\pi}\int_0^{\frac{\pi}{2}} \left[\lambda(\alpha,\beta)b_0(\alpha,\beta)\left(\frac{\sqrt{\gamma}}{2\alpha\beta}\right)^{-\beta}(\sin\theta)^{\beta}\right]^{|\Omega|} d\theta \\
&= \frac{1}{\pi}\left[\lambda(\alpha,\beta)b_0(\alpha,\beta)\left(\frac{\sqrt{\gamma}}{2\alpha\beta}\right)^{-\beta}\right]^{|\Omega|}\int_0^{\frac{\pi}{2}}(\sin\theta)^{\beta|\Omega|}d\theta \\
&= \frac{\Gamma\left(\frac{\beta|\Omega|+1}{2}\right)}{2\sqrt{\pi}\Gamma\left(1+\frac{\beta|\Omega|}{2}\right)}\left[\lambda(\alpha,\beta)b_0(\alpha,\beta)\left(\frac{\sqrt{\gamma}}{2\alpha\beta}\right)^{-\beta}\right]^{|\Omega|}.
\end{aligned}$$

6.1.4 Upper Bound on Average BER

Since the convolutional code is linear, the set of distances of the code sequences with respect to the all-zero sequence is the same as the set of distances with respect to any other code sequences. Thus, without loss of generality, we assume an all-zero sequence is transmitted. For a (K_c, k_c, n_c) convolutional code where K_c is the constraint length and k_c/n_c is the code rate, the transfer function can be written as [63, 64]

$$T(D,N) = \sum_{d=d_{free}}^{\infty} a_d D^d N^{f(d)} \tag{6.13}$$

where d represents the number of different bits between the selected path and the all-zero path, d_{free} is the free distance of the convolutional code, a_d denotes the number of nonzero paths with distance d from the all-zero path that merge with the all-zero path for the first time, D denotes the distance of the particular path from the all-zero path, N indicates the transition caused by the input

bit "1", and $f(d)$ determines the number of bit errors for the path corresponding to the term N.

By taking the derivative of $T(D,N)$ with respect to N and setting $N=1$, we obtain

$$\left.\frac{\partial T(D,N)}{\partial N}\right|_{N=1} = \sum_{d=d_{free}}^{\infty} B_d D^d \tag{6.14}$$

where $B_d = a_d f(d)$ is the total number of errors on all paths of distance d.

Accordingly, an upper bound on the average BER based on PEP can be obtained as [65]

$$P_{ub} \leq \frac{1}{k_c} \sum_{\mathbf{C}} p(\mathbf{C}) \sum_{d=d_{free}}^{\infty} B_d P(\mathbf{C}, \hat{\mathbf{C}}) \tag{6.15}$$

where $P(\mathbf{C})$ is the probability that the codeword $\mathbf{C}$ is transmitted. Using the transfer function technique for (6.15) and the alternative form for the Q-function, i.e., $Q(x) = \frac{1}{\pi}\int_0^{\frac{\pi}{2}} \exp\left(-\frac{x^2}{2\sin^2\theta}\right) d\theta$, one can obtain an upper bound on the average BER as [65]

$$P_b \leq \frac{1}{\pi}\int_0^{\pi/2} \frac{1}{k_c} \left.\frac{\partial T(D(\theta),N)}{\partial N}\right|_{N=1} d\theta \tag{6.16}$$

where $T(D(\theta),N)$ is the transfer function of the convolutional code, and $D(\theta)$ is given by [29]

$$D(\theta) = \int_0^{\infty} \exp\left(-\frac{\gamma}{4\sin^2\theta} I^2\right) f_I(I)\, dI. \tag{6.17}$$

From (6.3) and (6.17), we note that the PEP equals a single integral of $D(\theta)$ to the power of $|\Omega|$. Substituting (6.4) into (6.17), we obtain $D(\theta)$ as

$$\begin{aligned} D(\theta) = \lambda(\alpha,\beta) \sum_{p=0}^{\infty} \Bigg[& b_p(\alpha,\beta) \left(\frac{\sqrt{\gamma}}{2\alpha\beta\sin\theta}\right)^{-(p+\beta)} \\ & + b_p(\beta,\alpha) \left(\frac{\sqrt{\gamma}}{2\alpha\beta\sin\theta}\right)^{-(p+\alpha)} \Bigg]. \end{aligned} \tag{6.18}$$

For expository purposes, we set the parameters of the convolutional code to $K_c = 3$, $k_c = 1$ and $n_c = 2$, with the two function generators being $\mathbf{g}_0 = [1 \quad 1 \quad 1]$ and $\mathbf{g}_1 = [1 \quad 0 \quad 1]$. Such a

nonsystematic convolutional code will not produce catastrophic errors. The corresponding transfer function becomes

$$T(D(\theta),N) = \frac{D^5(\theta)N}{1-2ND(\theta)}. \tag{6.19}$$

Substituting (6.19) into (6.16) gives

$$P_b \leq \frac{1}{\pi}\int_0^{\frac{\pi}{2}} \frac{D^5(\theta)}{(1-2D(\theta))^2}\,d\theta. \tag{6.20}$$

Finally, applying (6.18) to (6.20), we obtain a simplified expression of the upper bound on the average BER for a $(3,1,2)$ convolutional coded OOK IM/DD system.

6.2 Quasi-static Fading Channels

Since the coherence time of an atmospheric turbulence channel is on the order of milliseconds [26] and the data rate of a typical FSO system is on the order of Gb/s, the ideal bit-by-bit interleaving assumed in Section 6.1 is difficult to achieve. Therefore, it is of practical importance to consider a coded FSO system in a realistic quasi-static fading channel where the same fading coefficient affects a block of data symbols. Following [66], we consider a convolutional code with rate $R_c = k_c/n_c$ for a quasi-static fading channel[3] using a block interleaver of depth n. For this system, which is shown in Fig. 6.1, $(B+K_c-1)k_c$ information bits are convolutionally encoded into $(B+K_c-1)n_c$ coded bits. The $(B+K_c-1)n_c$ coded bits are denoted by x_{lj}, where $l = 1,2,\ldots,n_c$ and $j = 1,2,\ldots,B+k_c-1$. Each coded bit is placed on one of n blocks where each block experiences independent fading, i.e., I_l is the fading coefficient for lth block. Using interleaving will result in latency on a millisecond timescale or longer, but this latency can be reduced. A recent example by researchers at the MIT Lincoln Lab showed this with interleavers and forward error correction for

[3]When the codeword is affected by the same fading coefficient, the channel is called quasi-static. However, we can transform a quasi-static channel into a block fading channel by way of block interleaving [67]. In such a system, we place each coded bit in different blocks, such that each block experiences independent fading from that of neighbouring blocks and bits within a block suffer the same fading coefficient.

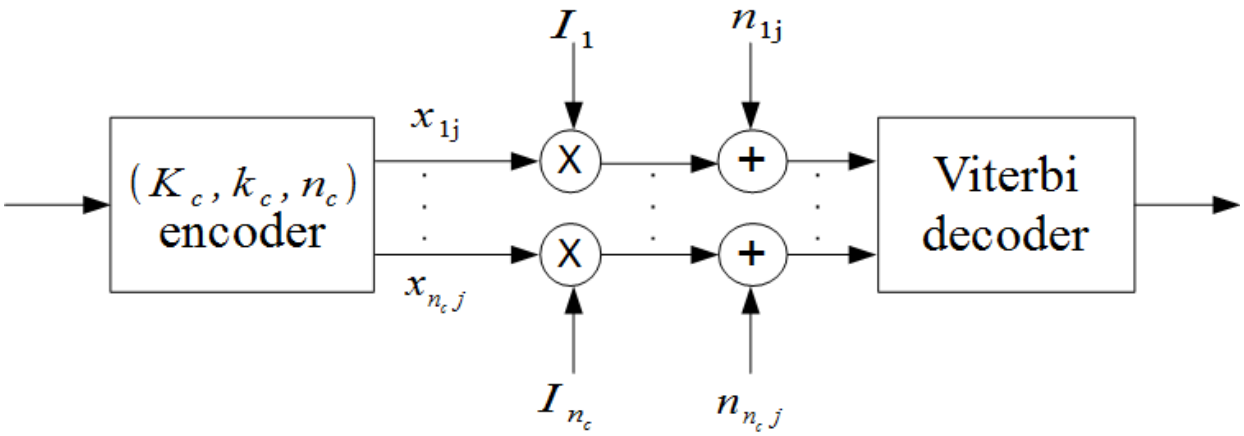

Figure 6.1: Block diagram of a coded FSO system through quasi-static atmospheric turbulence channels.

OTU-1 (2.66 Gb/s) and OTU-2 (10.70 Gb/s) over a 5.4 km optical wireless communication link [68].

Assuming first that the fading coefficients $\tilde{\mathbf{I}} = [\tilde{I}_1, \tilde{I}_2, ..., \tilde{I}_n]$ for n_c blocks are fixed, and using the same technique as discussed in Section 6.1, the conditional union upper bound on the BER can be obtained as

$$P_e(\tilde{\mathbf{I}}) \leq \frac{1}{k_c} \sum_{\mathbf{d}=\mathbf{d}_f}^{\infty} c(\mathbf{d}) P_2(\mathbf{d}|\tilde{\mathbf{I}}) \tag{6.21}$$

where $\mathbf{d} = [d_1, d_2, ..., d_n]$ are the Hamming distances of the n blocks, $\mathbf{d}_f = [d_{1f}, d_{2f}, ..., d_{nf}]$ are the free component distances of the n blocks, $P_2(\mathbf{d}|\tilde{\mathbf{I}})$ is the conditional PEP given by $P_2(\mathbf{d}|\tilde{\mathbf{I}}) = Q\left(\sqrt{2\gamma \sum_{l=1}^{n_c} d_l \tilde{I}_l^2}\right)$, $c(\mathbf{d}) = \sum_{i=1}^{\infty} ia(\mathbf{d}, i)$ are the coefficients obtained from the generalized transfer function of the code, and $a(\mathbf{d}, i)$ is the number of error events with distance vector $\mathbf{d}$ [66]. The average BER over the quasi-static Gamma-Gamma turbulence channel can be upper-bounded by [66]

$$P_e \leq \int_{\tilde{\mathbf{I}}} \min\left[\frac{1}{2}, \frac{1}{k_c} \sum_{\mathbf{d}=\mathbf{d}_f}^{\infty} c(\mathbf{d}) P_2(\mathbf{d}|\tilde{\mathbf{I}})\right] f_{\tilde{\mathbf{I}}}(\tilde{\mathbf{I}}) d\tilde{\mathbf{I}} \tag{6.22}$$

where the fading coefficients $\tilde{\mathbf{I}}$ for n blocks are assumed to be independent, i.e., $f_{\tilde{\mathbf{I}}}(\tilde{\mathbf{I}}) = \prod_{l=1}^{n_c} f_{\tilde{I}_l}(\tilde{I}_l)$, and where $f_{\tilde{I}_l}(\tilde{I}_l)$ is the Gamma-Gamma pdf given by (2.20).

6.3 Numerical Results

In this section, the PEP and BER performances are numerically studied for IM/DD systems employing OOK with convolutional code. The PEP performance of OOK is compared with that of SIM-BPSK. The BER performance is then compared for uncoded and coded OOK systems.

In Fig. 6.2, the PEP results of coded IM/DD systems are shown for OOK and SIM-BPSK systems operating over Gamma-Gamma turbulence channels with weak $(\alpha = 4.62, \beta = 4.24)$ and strong $(\alpha = 2.14, \beta = 1.21)$ turbulence conditions. For the coded SIM-BPSK system with $\varepsilon(\mathbf{C}, \hat{\mathbf{C}}) = 4E_b \sum_{k\in\Omega} I_k^2$ [26], we evaluate the PEP performance numerically for comparison purposes. The length of the error event is chosen to be $|\Omega| = 3$. Our series approximation of PEP (with $P = 60$) shows excellent agreement with the exact PEP for weak and strong turbulence conditions. The PEP of the coded SIM-BPSK has better BER performance compared to that of a coded OOK system. As expected, the PEP is better in weak turbulence conditions. For example, at $\gamma = 20$ dB, the PEP for strong turbulence $(\alpha = 2.14, \beta = 1.21)$ is 2.18×10^{-4}, and the PEP for weak turbulence $(\alpha = 4.62, \beta = 4.24)$ is 3.57×10^{-8}. For comparison, we also plot in Fig. 6.2 the approximate PEP for coded OOK (diamonds) and SIM-BPSK (stars) systems by using [29, eq. (17)]. The approximate PEP results of [29] show reasonable agreement with the exact PEP results for large SNRs, but the approximations are less accurate at the lower SNRs. The series representation of the Gamma-Gamma pdf relies on a series expansion of $K_\nu(x)$ where ν is non-integer. As a result, our series PEP expression requires $(\alpha - \beta) \notin \mathbb{Z}$. When $(\alpha - \beta) \in \mathbb{Z}$, one can use the small constant adjustment method to circumvent this minor restriction [69]. In Fig. 6.2, as expected, asymptotic PEPs approach exact PEPs faster for strong turbulence conditions compared to those of weak turbulence conditions. A similar asymptotic behaviour for series solutions is seen in [61] for uncoded SIM-BPSK systems.

In Fig. 6.3, we compare the simulated BER performance of uncoded and coded IM/DD systems (with perfect interleaving) employing OOK versus average SNR operating over Gamma-Gamma turbulence channels for weak $(\alpha = 4.62, \beta = 4.24)$ and strong $(\alpha = 2.14, \beta = 1.21)$ turbulence conditions. The simulated BER results of the uncoded system have been numerically verified with

BER results of the exact analytical expression. It is seen that strong turbulence can significantly degrade the error rate performance of an uncoded system. However, the convolutional code can be used to introduce coding gain and improve the BER performance in these strong turbulence conditions. For example, when $\gamma = 20$ dB $(\alpha = 2.14, \beta = 1.21)$, the BER for an uncoded system can be reduced from 8.48×10^{-2} to 1.02×10^{-5} with a convolutional coded $(R_c = 1/2, K_c = 3)$ system. In Fig. 6.3, we also plot the exact upper bounds of BER and the upper bounds obtained by a series solution. The simplified series solution shows excellent agreement with the exact solution obtained by using (6.17) and (6.20). Simulated BER curves are also used to verify the analytical BER upper bound solutions.

In Fig. 6.4, we plot the upper bounds on the average BER for a convolutional coded $(R_c = 1/2, K_c = 3, B = 999998)$ IM/DD system employing OOK over quasi-static Gamma-Gamma fading channels with weak $(\alpha = 4.62, \beta = 4.24)$ and strong $(\alpha = 2.14, \beta = 1.21)$ turbulence conditions. The block length B is chosen to represent Gb/s transmission with a one millisecond coherence time. The upper bounds obtained from (6.22) are truncated at $d_{\max} = 40$, where only the error events having the total distance $d_1 + d_2 \leq d_{\max}$ are considered. The simulated BERs in Fig. 6.4, for quasi-static channels, clearly demonstrate the benefits of block-interleaved convolutional code over a convolutional coded system without interleaving.

6.4 Summary

In this chapter, we derived an accurate series PEP expression for convolutional coded OOK IM/DD FSO systems using a series representation of the Gamma-Gamma pdf for ideal bit-by-bit interleaved channels. This novel PEP expression can facilitate rapid calculation of upper bounds on the average SNR in weak-to-strong Gamma-Gamma distributed turbulence conditions. We also studied BER performance of a convolutional coded system using a block interleaver over realistic quasi-static Gamma-Gamma turbulence channels. While our analysis has been presented by way of an OOK based IM/DD FSO system, the same analysis can be easily extended to an SIM-BPSK based FSO system. For an SIM-BPSK based FSO system, we only need to change the energy

difference of these two coded sequence to $\varepsilon(\mathbf{C},\hat{\mathbf{C}}) = 4E_b \sum_{k\in\Omega} I_k^2$.

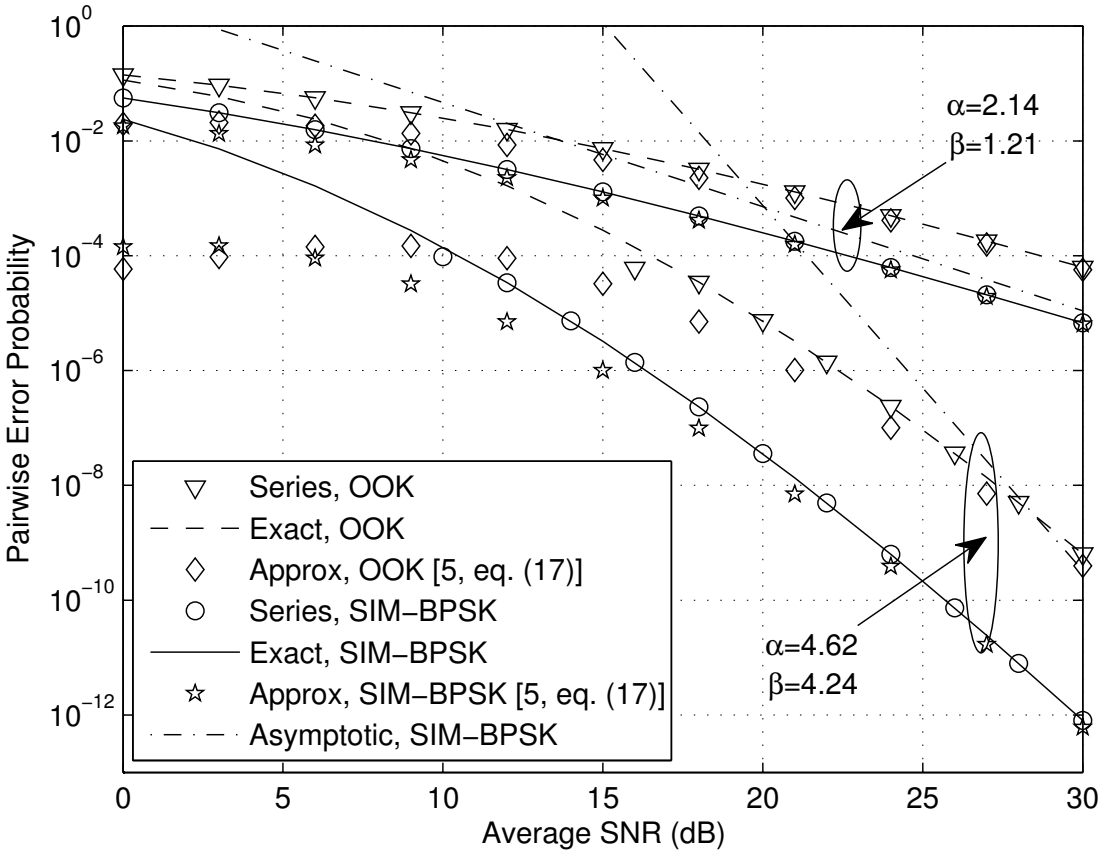

Figure 6.2: The PEP of coded IM/DD systems using OOK and SIM-BPSK versus average SNR operating over Gamma-Gamma turbulence channels. Results are shown for weak ($\alpha = 4.62, \beta = 4.24$) and strong ($\alpha = 2.14, \beta = 1.21$) turbulence conditions using series, exact, and approximate solutions.

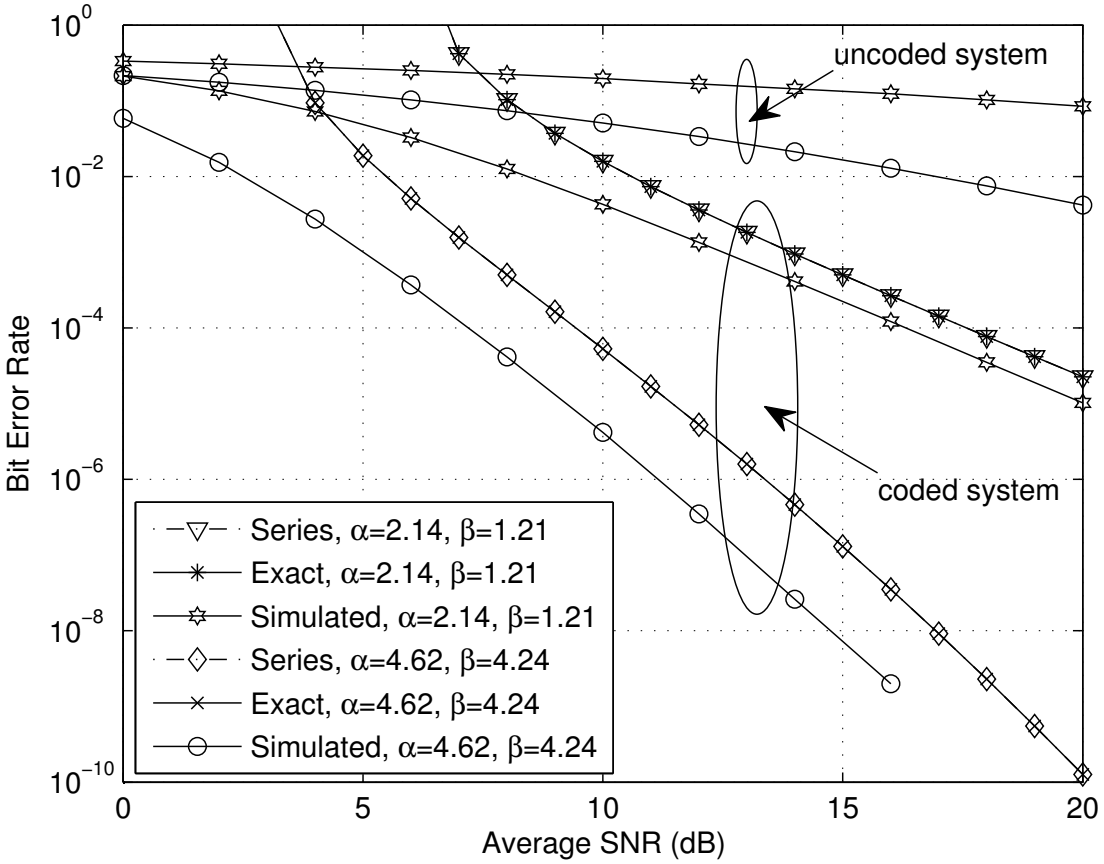

Figure 6.3: The BER of uncoded and coded IM/DD systems (with perfect interleaving) and upper bounds on average BER of convolutional coded ($R_c = 1/2, K_c = 3$) OOK IM/DD systems versus average SNR over Gamma-Gamma turbulence channels. Results are for weak ($\alpha = 4.62, \beta = 4.24$) and strong ($\alpha = 2.14, \beta = 1.21$) turbulence conditions.

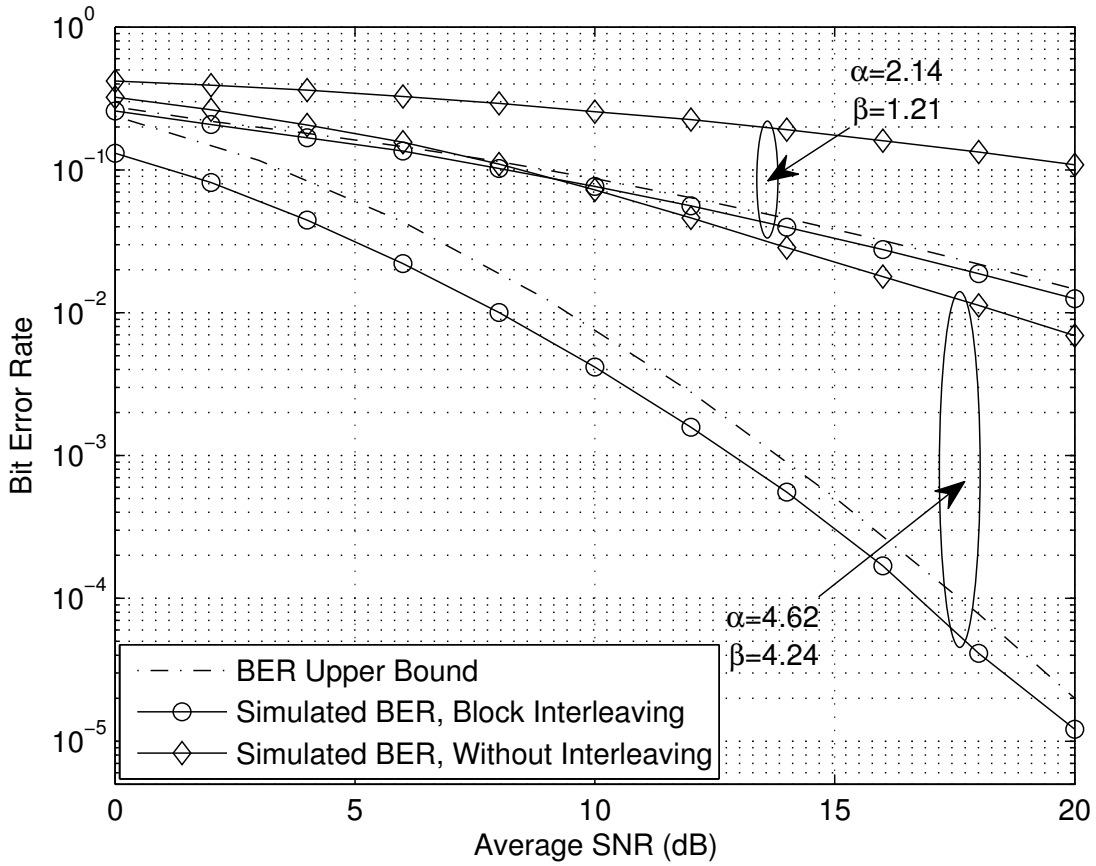

Figure 6.4: The simulated BER and upper bounds ($d_{\max} = 40$) on average BER of terminated convolutional coded ($R_c = 1/2, K_c = 3, B = 999998$) OOK IM/DD systems versus average SNR over quasi-static Gamma-Gamma turbulence channels with and without block interleaving. Results are for weak ($\alpha = 4.62, \beta = 4.24$) and strong ($\alpha = 2.14, \beta = 1.21$) turbulence conditions.

Chapter 7

Conclusions

In this chapter, we conclude the thesis by summarizing the accomplished work and suggesting some potential further research topics.

7.1 Summary of Accomplished Work

In this thesis, we investigated the BER performance of OOK IM/DD systems using different detection thresholds over atmospheric turbulence channels. Such investigations can be used as guidelines for practical FSO system design. Besides the BER performance investigation, turbulence channel parameter and electrical SNR estimation were investigated. The proposed estimators can be effective tools for future FSO systems implementing electrical-SNR-optimized detection. We also introduced coding techniques to mitigate the effects of turbulence induced fading and showed analytically that the convolutional coded OOK IM/DD systems have greatly improved BER performance.

We will summarize the accomplished work as follows:

- In Chapter 3, we studied the error rate performance of OOK IM/DD systems using fixed, electrical-SNR-optimized and idealized adaptive detection thresholds. We obtained error floor expressions for various turbulence channel models for OOK IM/DD systems using fixed detection thresholds. We approximated the turbulence pdf by a sum of Laguerre polynomials. The electrical-SNR-optimized system with the Laguerre-polynomials-based approximate pdf for the turbulence was found to be effective for typical FSO systems, which operate at relatively low SNR values, as it yields comparable BER performance to that of the electrical-SNR-optimized system with perfect knowledge of turbulence pdf.

- In Chapter 4, we studied the MoME and MLE method. We used MLE to estimate the parameters of the lognormal-Rician fading channels, and used the EM algorithm to compute the MLE of the unknown parameters. Electrical SNR estimation was also studied for FSO systems using IM/DD over the lognormal fading channels. Training sequence based MoME and MLE were investigated. It was found that MoME could produce a closed-form expression for the estimator, while MLE requires numerical computation to produce the estimator.

- Chapter 5 investigated FSO communication systems using OOK and source information transformation. It was shown that such a system can achieve good BER performance without the need for knowledge of the instantaneous CSI and pdf of the turbulence model. We also derived an analytical expression for the pdf of the detection threshold and developed a tight upper bound on the average BER.

- In Chapter 6, we derived an accurate series PEP expression for convolutional coded OOK IM/DD FSO systems for ideal bit-by-bit interleaved channels using a series representation of the Gamma-Gamma pdf. This novel PEP expression can facilitate rapid calculation of upper bounds on the average SNR in weak-to-strong Gamma-Gamma distributed turbulence conditions. We also studied BER performance of a convolutional coded system using a block interleaver over realistic quasi-static Gamma-Gamma turbulence channels.

7.2 Suggested Future Work

In Chapter 5, we presented FSO communication systems using OOK and source information transformation. However, we assumed that the largest of the M signals contain the CSI, i.e., $\lim_{\gamma\to\infty} \max\{r_1, r_2, \ldots, r_M\} \approx I$, and defined the detection threshold as a value of one-half of the largest received signal. The BER performance for the system with this detection threshold was acceptable only when the SNR is sufficiently large. Thus, it would be of future interest to further optimize the detection threshold for operation in low SNR regimes.

In Chapter 6, we investigated the BER performance of FSO communication systems using

OOK and convolutional code, but there are other effective coding techniques. Turbo codes are a family of powerful error-correcting codes. Turbo codes have an impressive near-Shannon-limit for error correcting performance. Thus, it would be of future interest to investigate the BER performance of FSO communication systems using OOK and turbo code.

Overall, in this thesis, we introduced new implementations and thorough performance analyses for OOK IM/DD systems using various detection schemes operating over atmospheric turbulence channels. These findings can support future developments and innovations in FSO systems.

Bibliography

[1] V. W. S. Chan, "Free-space optical communications," *IEEE/OSA Journal of Lightwave Technology*, vol. 24, pp. 4750–4762, Dec. 2006.

[2] J. H. Shapiro and R. C. Harney, "Burst-mode atmospheric optical communication," in *Proc.1980 National Telecommunications Conference*, 1980, pp. 27.5.1–27.5.7.

[3] M. Niu, *Coherent Optical Wireless Communications over Atmospheric Turbulence Channels*. The University of British Columbia: Ph.D. Thesis, 2012.

[4] L. C. Andrews and R. L. Phillips, *Laser Beam Propagation through Random Media*. Upper Saddle River: Prentice Hall, 1998.

[5] S. Karp, R. Gagliardi, S. E. Moran, and L. B. Stotts, *Optical Channels*. New York: Plenum, 1988.

[6] D. A. DeWolf, "Are strong irradiance fluctuations log normal or rayleigh distributed," *Journal of the Optical Society of America A*, vol. 57, pp. 787–797, June 1967.

[7] A. Prokeš, "Modeling of atmospheric turbulence effect on terrestrial fso link," *Radioengineering*, vol. 18, pp. 42–47, Apr. 2009.

[8] M. Niu, J. Cheng, and J. F. Holzman, "Exact error rate analysis of equal gain and selection diversity for coherent free-space optical systems on strong turbulence channels," *Optics Express*, vol. 18, pp. 13915–13926, June 2010.

[9] K. P. Peppas, F. Lazarakis, A. Alexandridis, and K. Dangakis, "Simple, accurate formula for the average bit error probability of multiple-input multiple-output free-space optical links

over negative exponential turbulence channels," *Optics Letter*, vol. 37, pp. 3243–3245, Aug. 2012.

[10] L. C. Andrews, R. L. Phillips, and C. Y. Hopen, *Laser Beam Scintillation With Applications*. Bellingham, WA: SPIE Press, 2001.

[11] R. J. Hill and R. G. Frehlich, "Probability distribution of irradiance for the onset of strong scintillation," *Journal of the Optical Society of America A*, vol. 14, pp. 1530–1540, July 1997.

[12] J. F. Paris, "Advances in the statistical characterization of fading: from 2005 to present," *International Journal of Antennas and Propagation*, vol. 2014, pp. 1–5, Jun. 2014.

[13] J. H. Churnside and S. F. Clifford, "Log-normal rician probability-density function of optical scintillations in the turbulent atmosphere," *Journal of the Optical Society of America A*, vol. 4, pp. 727–733, Oct. 1987.

[14] X. Song and J. Cheng, "Joint estimation of the lognormal-rician atmospheric turbulence model by the generalized method of moments," *Optical Communication*, vol. 285, pp. 4727–4732, Nov. 2012.

[15] J. Li, J. Q. Liu, and D. P. Tayler, "Optical communication using subcarrier psk intensity modulation through atmospheric turbulence channels," *IEEE Transactions on Communications*, vol. 55, pp. 1598–1606, Aug. 2007.

[16] H. Moradi, M. Falahpour, H. H. Refai, P. G. LoPresti, and M. Atiquzzaman, "BER analysis of optical wireless signals through lognormal fading channels with perfect CSI," in *Proc.17th International Conference on Telecommunications*, Doha, Qatar, Apr. 2010, pp. 493–497.

[17] M. L. B. Riediger, R. Schober, and L. Lampe, "Blind detection of on-off keying for free-space optical communications," in *Proc. Canadian Conference on Electrical and Computer Engineering*, Niagara Falls, Canada, May 2008, pp. 1361–1364.

[18] X. Zhu and J. M. Kahn, "Markov chain model in maximum-likelihood sequence detection for free-space optical communication through atmospheric turbulence channels," *IEEE Transactions on Communications*, vol. 51, pp. 509–516, Mar. 2003.

[19] M. L. B. Riediger, R. Schober, and L. Lampe, "Fast multiple-symbol detection for free-space optical communications," *IEEE Transactions on Communications*, vol. 57, pp. 1119–1128, Apr. 2009.

[20] H. R. Burris, "Laboratory implementation of an adaptive thresholding system for free-space optical communication receivers with signal dependent noise," *Proceedings of SPIE*, vol. 5892, pp. 1–20, Aug. 2005.

[21] X. Zhu and J. M. Kahn, "Free-space optical communication through atmospheric turbulence channels," *IEEE Transactions on Communications*, vol. 50, pp. 1293–1300, Oct. 2002.

[22] H. Moradi, H. H. Refai, and P. G. LoPresti, "Thresholding-based optimal detection of wireless optical signals," *IEEE/OSA Journal of Optical Communications and Networking*, vol. 2, pp. 689–700, Sept. 2010.

[23] L.Yang, J. Cheng, and J. F. Holzman, "Electrical-snr-optimized detection threshold for ook im/dd optical wireless communications," in *Proc. Canadian Workshop Information Theory*, Toronto, ON, Canada, June 2013, pp. 186–189.

[24] X. Zhu and J. M. Kahn, "Pilot-symbol assisted modulation for correlated turbulent free-space optical channels," *Proceedings of SPIE*, vol. 4489, pp. 138–145, Jan. 2002.

[25] M. Khalighi, F. Xu, Y. Jaafar, and S. Bourennane, "Double-laser differential signaling for reducing the effect of background radiation in free-space optical systems," *IEEE/OSA Journal of Optical Communications and Networking*, vol. 3, pp. 145–154, Feb. 2011.

[26] X. Zhu and J. M. Kahn, "Performance bounds for coded free-space optical communications through atmospheric turbulence channels," *IEEE Transactions on Communications*, vol. 51, pp. 1233–1239, Aug. 2003.

[27] X. Zhu and J. M. Kahn, "Pairwise codeword error probability for coded free-space optical communication through atmospheric turbulence channels," in *Proc. International Conference of Commununications*, Helsinki, Finland, June 2001, pp. 161–164.

[28] M. Uysal, M. Navidpour, and J. Li, "Error rate performance of coded free-space optical links over strong turbulence channels," *IEEE Communications Letters*, vol. 8, pp. 635–637, Oct. 2004.

[29] M. Uysal, J. Li, and M. Yu, "Error rate performance analysis of coded free-space optical links over gamma-gamma atmospheric turbulence channels," *IEEE Transactions on Wireless Communications*, vol. 5, pp. 1229–1233, June 2006.

[30] M. Uysal and J. Li, "Error performance analysis of coded wireless optical links over atmospheric turbulence channels," in *Proc. IEEE Wireless Communication Networking Conference*, Atlanta, GA, Mar. 2004, pp. 2405–2410.

[31] W. Gappmair and M. Flohberger, "Error performance of coded fso links in turbulent atmosphere modeled by gamma-gamma distributions," *IEEE Transactions on Wireless Communications*, vol. 8, pp. 2209–2213, May 2009.

[32] G. P. Agrawal, *Fiber-Optic Communication Systems*, fourth ed. New York: Wiley, 2010.

[33] Agilent Technologies. (2001). Measuring extinction ratio of optical transmitters. [online]. Available: http://literature.cdn.keysight.com/litweb/pdf/5966-4316E.pdf

[34] J. B. Johnson, "Thermal agitation of electricity in conductors," *Physical Review*, vol. 32, pp. 97–109, July 1928.

[35] H. Nyquist, "Thermal agitation of electric charge in conductors," *Physical Review*, vol. 32, pp. 110–113, July 1928.

[36] W. Schottky, "über spontane stromschwankungen in verschiedenen elektrizitätsleitern," *Annalen der Physik*, vol. 362, pp. 541–567, 1918.

[37] D. K. C. MacDonald, *Noise and Fluctuations: An Introduction*. New York: Dover Publications, 2006.

[38] F. N. H. Robinson, *Noise and Fluctuations in Electronic Devices and Circuits*. Oxford: Clarendon Press, 1974.

[39] E. J. Lee and V. W. S. Chan, "Part 1: Optical communication over the clear turbulent atmospheric channel using diversity," *IEEE Journal on Selected Areas in Communications*, vol. 22, pp. 1896–1906, Nov. 2004.

[40] W. O. Popoola and Z. Ghassemlooy, "Bpsk subcarrier intensity modulated free-space optical communications in atmospheric turbulence," *IEEE/OSA Journal of Lightwave Technology*, vol. 27, pp. 967–973, Apr. 2009.

[41] A. Al-Habash, L. C. Andrews, and R. L. Phillips, "Mathematical model for the irradiance probability density function of a laser beam propagating through turbulent media," *Optics Engineering*, vol. 40, pp. 1554–1562, Aug. 2001.

[42] M. Uysal, J. Li, and M. Yu, "Signal detection in optical communications through the atmospheric turbulence channel," *IEEE Transactions on Wireless Communications*, vol. 5, pp. 1229–1233, June 2006.

[43] E. Jakeman and P. N. Pusey, "A model for non-Reyleigh sea echo," *IEEE Transactions on Antennas and Propagation*, vol. AP-24, pp. 806–814, Nov. 1976.

[44] K. Kiasaleh, "Performance of coherent dpsk free-space optical communication systems in k-distributed turbulence," *IEEE Transactions on Communications*, vol. 54, pp. 604–607, Apr. 2006.

[45] E. Jakeman, "On the statistics of K-distributed noise," *Journal of Physics A: Mathematical and General*, vol. 13, pp. 31–48, Jan. 1980.

[46] Z. Sodnik, B. Furch, and H. Lutz, "Free-space laser communication activities in europe: Silex and beyond," in *Proc. IEEE Lasers and Electro-Optics Society*, pp. 78–79, Oct. 2006.

[47] H. Hemmati, "Interplanetary laser communications," *Optics and Photonics News*, vol. 18, pp. 22–27, Nov. 2007.

[48] G. R. Osche, *Optical Detection Theory for Laser Applications*. New Jersey: Wiley, 2002.

[49] A. Garcia-Zambrana, "Error rate performance for stbc in free-space optical communications through strong atmospheric turbulence," *IEEE Communications Letters*, vol. 11, pp. 390–392, May 2007.

[50] J. H. Churnside and R. G. Frehlich, "Experimental evaluation of lognormally modulated rician and ik models of optical scintillation in the atmosphere," *Optics Express*, vol. 6, pp. 1760–1766, Nov. 1989.

[51] I. S. Gradshteyn and I. M. Ryzhik, *Table of Integrals, Series, and Products*, sixth ed. San Diego: Academic Press, 2000.

[52] S. B. Provost, "Moment-based density approximants," *The Mathematica Journal*, vol. 9, pp. 727–756, May 2005.

[53] R. Price, "An orthonormal laguerre expansion yielding rices envelope density function for two sine waves in noise," *IEEE Transactions on Information Theory*, vol. 34, pp. 1375–1382, Nov. 1988.

[54] L. Devroye, "On random variate generation when only moments or fourier coefficients are known," *Mathematics and Computers in Simulation*, vol. 31, pp. 71–89, Feb. 1989.

[55] A. A. Farid and S. Hranilovic, "Capacity bounds for wireless optical intensity channels with gaussian noise," *IEEE Transactions on Information Theory*, vol. 36, pp. 6066–6077, Dec. 2010.

[56] I. I. Kim, E. Woodbridge, V. Chan, and B. R. Strickland, "Scintillation measurements performed during the limited-visiblity lasercom experiment," *Proceedings of SPIE*, vol. 3266, pp. 209–220, Jan. 1998.

[57] A. Dogandǔić and J. Jin, "Maximum likelihood estimation of statistical properties of composite gamma-lognormal fading channel," *IEEE Transactions on Signal Processing*, vol. 52, pp. 2940–2945, Oct. 2004.

[58] S. M. Kay, *Fundamentals of Statistical Signal Processing: Estimation Theory*. Upper Saddle River: Prentice Hall, 1993.

[59] E. L. Lehmann, *Elements of Large-Sample Theory*. New York: Springer-Verlag, 1999.

[60] D. R. Pauluzzi and N. C. Beaulieu, "A comparison of snr estimation techniques for the awgn channel," *IEEE Transactions on Communications*, vol. 48, pp. 1681–1691, Oct. 2000.

[61] X. Song and J. Cheng, "Performance of subcarrier intensity modulated mimo wireless optical communications," in *Proc. 26th Queen's Biennial Symposium on Communications*, Kingston, ON, Canada, May 2012, pp. 5–9.

[62] X. Song, M. Niu, and J. Cheng, "Error rate of subcarrier intensity modulation for wireless optical communication," *IEEE Communications Letters*, vol. 16, pp. 5–9, Apr. 2012.

[63] A. J. Viterbi, "Convolutional codes and their performance in communication systems," *IEEE Transactions on Communications Technology*, vol. 19, pp. 751–772, Oct. 1971.

[64] J. G. Proakis and M. Salehi, *Digital Communications*, fifth ed. New York: McGraw-Hill, 2007.

[65] M. K. Simon and M.-S. Alouini, *Digital Communication over Fading Channels: A Unified Approach to Performance Analysis*, first ed. New York: John Wiley & Sons, 2000.

[66] E. Malkamäki and H. Leib, "Evaluating the performance of convolutional codes over block fading channels," *IEEE Transactions on Information Theory*, vol. 45, pp. 771–781, Mar. 1999.

[67] H. E. Gamal and A. R. Hammons, "On the design of algebraic space-time codes for mimo block-fading channels," *IEEE Transactions on Information Theory*, vol. 49, pp. 151–163, Nov. 2003.

[68] J. A. Greco, "Design of the high-speed framing, fec, and interleaving hardware used in a 5.4km free-space optical communication experiment," *Proceedings of SPIE*, vol. 7464, pp. 746409–1–746409–7, Aug. 2009.

[69] E. Bayaki, R. Schober, and R. Mallik, "Performance analysis of mimo free-space optical systems in gamma-gamma fading," *IEEE Transactions on Communications*, vol. 57, pp. 3415–3424, Nov. 2009.

Appendices

Appendix A: The CF and MGF od lognormal pdf

The CF of a RV I is the Fourier transform of its pdf, $f_I(I)$, and it is defined by

$$\Phi_I(\omega) = \int_{-\infty}^{\infty} f_I(I) \exp(j\omega I)\, dI \tag{A.1}$$

or

$$\Phi_I(\omega) = \mathrm{Re}[\Phi_I(\omega)] + j\mathrm{Im}[\Phi_I(\omega)] \tag{A.2}$$

where $j^2 = -1$. In (A.2), $\mathrm{Re}[\cdot]$ and $\mathrm{Im}[\cdot]$ denote the real and imaginary parts, respectively. Both can be written, respectively, as

$$\mathrm{Re}[\Phi_I(\omega)] = \int_0^{\infty} f_I(I) \cos(\omega I)\, dI \tag{A.3}$$

and

$$\mathrm{Im}[\Phi_I(\omega)] = \int_0^{\infty} f_I(I) \sin(\omega I)\, dI. \tag{A.4}$$

Using (3.15), one can approximate (A.3) as

$$\begin{aligned} &\mathrm{Re}[\Phi_I(\omega)] \\ &\approx \int_0^{\infty} \frac{I^v \exp(-I/c)}{c^{v+1}} \sum_{n=0}^{\infty} \delta_n L_n\left(v, \frac{I}{c}\right) \cos(\omega I)\, dI \\ &= \frac{1}{c^{v+1}} \sum_{n=0}^{\infty} \delta_n \int_0^{\infty} I^v \exp(-I/c) L_n\left(v, \frac{I}{c}\right) \cos(\omega I)\, dI. \end{aligned} \tag{A.5}$$

Substituting (3.16) into (A.5), one has

$$\begin{aligned}\mathrm{Re}[\Phi_I(\omega)] \approx & \frac{1}{c^{v+1}} \sum_{n=0}^{\infty} \delta_n \sum_{k=0}^{n} \frac{(-1)^k \Gamma(\alpha)}{k!(n-k)!\Gamma(\alpha-k)} \\ & \times \int_0^{\infty} I^v \exp(-I/c) \left(\frac{I}{c}\right)^{n-k} \cos(\omega I)\, dI \\ = & \sum_{n=0}^{\infty} \delta_n \sum_{k=0}^{n} \frac{(-1)^k \Gamma(\alpha)}{k!(n-k)!\Gamma(\alpha-k)(1+c^2\omega^2)^{\frac{\alpha-k}{2}}} \\ & \times \cos((\alpha-k)\arctan(c\omega))\end{aligned} \tag{A.6}$$

where $\alpha = v+n+1$. In deriving the last equality of (A.6), an integral identity [51, eq. 3.944(6)] has been used.

Similarly, substituting (3.15) and (3.16) into (A.4) and using an integral identity [51, eq. 3.944(5)], one obtains

$$\begin{aligned}\mathrm{Im}[\Phi_I(\omega)] \approx & \sum_{n=0}^{\infty} \delta_n \sum_{k=0}^{n} \frac{(-1)^k \Gamma(\alpha)}{k!(n-k)!\Gamma(\alpha-k)(1+c^2\omega^2)^{\frac{\alpha-k}{2}}} \\ & \times \sin((\alpha-k)\arctan(c\omega)).\end{aligned} \tag{A.7}$$

The approximate CF is then found to be

$$\begin{aligned}\Phi_I(\omega) \approx & \sum_{n=0}^{\infty} \delta_n \sum_{k=0}^{n} \frac{(-1)^k \Gamma(\alpha)}{k!(n-k)!\Gamma(\alpha-k)(1+c^2\omega^2)^{\frac{\alpha-k}{2}}} \\ & \times [\cos((\alpha-k)\arctan(c\omega)) + j\sin((\alpha-k)\arctan(c\omega))].\end{aligned} \tag{A.8}$$

Using an integral identity [51, eq. 3.326(2)], one can obtain the MGF as

$$M_I(s) \approx \sum_{n=0}^{\infty} \delta_n \sum_{k=0}^{n} \frac{(-1)^k \Gamma(v+n+1)}{k!(n-k)!(1-sc)^{v+n-k+1}}. \tag{A.9}$$